THE USE OF AIRCRAFT MEASUREMENTS TO DETERMINE TRANSPORT, DISPERSION AND TRANSFORMATION RATES OF POLLUTANTS EMITTED FROM OIL SANDS EXTRACTION PLANTS IN ALBERTA

AOSERP Report 133

Alberta
ENVIRONMENT
Research Management Division
14th Floor, Standard Life Centre
10405 Jasper Avenue,
Edmonton, Alberta, Canada
T5J 3N4

ALBERTA OIL SANDS ENVIRONMENTAL RESEARCH PROGRAM
RESEARCH REPORTS

These research reports describe the results of investigations funded by the Alberta Oil Sands Environmental Research Program. This program was designed to direct and co-ordinate research projects concerned with the environmental effects of development of the Athabasca Oil Sands in Alberta.

A list of research reports published to date is included at the end of this report.

Enquiries pertaining to the reports in the series should be directed to:

Research Management Division
Publications Office
14th Floor, Standard Life Centre
10405 Jasper Avenue
Edmonton, Alberta
T5J 3N4

(403) 427-3946

The Use of Aircraft Measurements to Determine Transport, Dispersion and Transformation Rates of Pollutants Emitted from Oil Sands Extraction Plants in Alberta

AOSERP Report 133

This report may be cited as:

Cheng, L., A. Davis, E. Peake, and D. Rogers. 1987. The use of aircraft measurements to determine transport, dispersion and transformation rates of pollutants emitted from oil sands extraction plants in Alberta. Prep. for Alberta Environment, Research Management Division by Atmospheric Sciences Department, Alberta Research Council and Kananaskis Centre for Environmental Research, University of Calgary. AOSERP Report 133. 117 pp.

THE USE OF AIRCRAFT MEASUREMENTS TO DETERMINE TRANSPORT, DISPERSION AND TRANSFORMATION RATES OF POLLUTANTS EMITTED FROM OIL SANDS EXTRACTION PLANTS IN ALBERTA

by

L. CHENG[1]
A. DAVIS[1]
E. PEAKE[2]
D. ROGERS[1]

[1]Atmospheric Sciences Department
Alberta Research Council

[2]Kananaskis Centre for Environmental Research
University of Calgary

for

Research Management Division
Alberta Environment

AOSERP Report 133

1987

This report is made available as a public service. The Department of Environment neither approves nor disagrees with the conclusions expressed herein, which are the responsibility of the authors.

TABLE OF CONTENTS

		Page
LIST OF TABLES		vi
LIST OF FIGURES		viii
ABSTRACT		xi
ACKNOWLEDGMENTS		xii
1.	INTRODUCTION	1
2.	EXPERIMENT PROCEDURES, INSTRUMENTATION AND CALIBRATION	4
2.1	Experimentation Procedure	4
2.2	INTERA/ALBERTA RESEARCH COUNCIL Instrumentation Aircraft	6
2.3	Real Time Calculation and Displays	7
2.4	Aerosol and Gas Sampling Manifold	8
2.5	Filter Samples of Aerosols and Gases	10
2.6	Gas Sampling Instruments	10
2.6.1	Sulphur Dioxide	12
2.6.2	Nitrogen Oxides	15
2.7	Instrument Calibration	17
2.8	Deducing Horizontal winds	24
3.	DESCRIPTION OF PLUME TRANSPORT AND PLUME DISPERSION	26
4.	CONVERSION OF SULPHUR DIOXIDE TO PARTICULATE SULPHATE	41
5.	CONVERSION OF NITRIC OXIDE TO NITROGEN DIOXIDE	71
6.	EVOLUTION OF ICE PARTICLES NUCLEATED IN PLUMES	85
6.1	Case of December 15, 1983	87
6.2	Case of December 17, 1983	92
6.3	Discussion	97
7.	CONCLUSIONS AND RECOMMENDATIONS	102
8.	REFERENCES	106

LIST OF TABLES

		Page
1.	Gas Sampling Instrument Specifications	13
2.	Calibration of Flows in the Monitor Labs SO2 Calibrator on 1983 December 16	18
3.	Calibration of the Meloy Laboratories Model SA 285E Sulphur Dioxide Analyzer on 1983 December 13	19
4.	Calibration of Ranges in the Meloy Laboratories Model SA 285E Sulphur Dioxide Analyzer	20
5.	Calibration of the Monitor Labs 8840 NO_x Analyzer for Test of Linearity	21
6.	Calibration of the Monitor Labs 8840 NO_x Analyzer on 1983 December 08	22
7.	Calibration of the Monitor Labs 8840 NOX Analyzer on 1983 December 16	23
8.	Mean Wind Speed and Direction, Number of Plume Penetrations, Distance of Last Plume Penetration, Mean Sulphur Dioxide Concentration of Last Pass, and the Maximum Distance at Which Sulphur Dioxide Was Detected for Study Days During All Three Phases of the Project .	28
9.	Potential Temperature Gradient and Environmental Turbulence at Plume Level on Plume Study Days	32
10.	Equations and Correlation Coefficients for Horizonal Plume Dispersion	40
11.	Geometric Mean Diameter and the Variance with Respect to Volume and Surface for the Accumulation Mode Plume (Syncrude) Aerosols Measured on 1983 March 28	46
12.	Geometric Mean Diameter and the Variance with Respect to Volume and Surface for the Accumulation Mode Plume (Syncrude) Aerosols Measured on 1983 March 29	47
13.	Geometric Mean Diameter and the Variance with Respect to Volume and Surface for the Accumulation Mode Plume (Syncrude) Aerosols Measured on 1983 March 30	48
14.	Geometric Mean Diameter and the Variance with Respect to Volume and Surface for the Accumulation Mode Plume (Syncrude) Aerosols Measured on 1983 March 31	49

Continued ...

LIST OF TABLES (CONCLUDED)

		Page
15.	Geometric Mean Diameter and the Variance with Respect to Volume and Surface for the Accumulation Mode Plume (Syncrude) Aerosols Measured on 1984 June 07	50
16.	Geometric Mean Diameter and the Variance with Respect to Volume and Surface for the Accumulation Mode Plume (Syncrude) Aerosols Measured on 1984 June 08	51
17.	Geometric Mean Diameter and the Variance with Respect to Volume and Surface for the Accumulation Mode Plume (Syncrude) Aerosols Measured on 1984 June 11	52
18.	Geometric Mean Diameter and the Variance with Respect to Volume and Surface for the Accumulation Mode Plume (Suncor) Aerosols Measured on 1984 June 11	53
19.	Geometric Mean Diameter and the Variance with Respect to Volume and Surface for the Accumulation Mode Plume (Syncrude) Aerosols Measured on 1984 June 12	54
20.	Summaries of Dilution Rate, Aerosol Volume Production Rates for Various Aerosol Size Ranges and the Conversion Rate of SO_2 to SO_4 Determined by the Excess Aerosol Volume Production Method	64
21.	Sulphur Dioxide, Particulate Sulphate and SO_2 to SO_4 Conversion Rates as a Function of Distance from the Source and Plume Age as Determined by Chemical Analysis for December 1983	66
22.	Sulphur Dioxide, Particulate Sulphate and SO_2 to SO_4 Conversion Rates as a Function of Distance from the Source and Plume Age as Determined by Chemical Analysis for June 1984	68
23.	NO to NO_2 Conversion Rates for the Nine Plume Studies .	80

LIST OF FIGURES

		Page
1.	Schematic Aerosol and Gas Sample Flow Diagram	9
2.	Empirical Transfer Function for Meloy Labs SA 285E Sulphur Dioxide Analyzer	14
3.	Empirical Transfer Function for Monitor Labs 8840 Nitrogen Oxides Analyzer	16
4.	Flight Path of Research Aircraft on 1984 June 12 (12:13:30 - 13:50:30Z)	27
5.	Cube Root of the Turbulence Energy Dissipation Rate Versus Distance for the Suncor Plume on 1984 June 11	33
6.	Sounding of Potential Temperature and Relative Humidity for 1984 June 06	35
7.	Sulphur Dioxide Concentration Profiles for Six Plume Passes on 1983 December 20	36
8.	Observed Horizontal Standard Deviations for Plume Penetrations on 1983 December 13	38
9.	Typical Plume and Ambient Air Aerosol Number Distributions Observed on 1984 June 11 for the Suncor Stack	42
10.	Typical Plume and Ambient Air Aerosol Surface Area Distributions Observed on 1984 June 11 for the Syncrude Stack	43
11.	Typical Plume and Ambient Air Aerosol Volume Distributions Observed on 1984 June 11 for the Syncrude Stack	44
12.	Plume Mean Sulphur Dioxide Concentration as a Function of Plume Travel Time for the Syncrude Plume Measured on 1984 June 11	57
13.	Plume Aerosol Total Volume Concentrations for Particles Smaller than 0.3 μm, 0.3<D<1.0 μm and 0.1<D<3.0 μm as a Function of Plume Age for the Syncrude Plume Measured on 1984 June 11	59

Continued ...

LIST OF FIGURES (CONTINUED)

		Page
14.	Excess Aerosol Volume Productions for Particles Smaller than 0.3 um, 0.3<D<1.0 um and 0.1<D<3.0 um as a Function of Plume Age in the Syncrude Plume on 1984 June 11	60
15.	Gas-to-Particle Conversion Rate of Sulphur Dioxide to Sulphate as Determined from Particles Smaller than 0.3 um, 0.3<D<1.0 um and 0.1<D<3.0 um as a Function of Plume Age for the Syncrude Plume on 1984 June 11 .	63
16.	Cross-sectional Profiles of NO and NO_2 Measured from the Syncrude Plume 3.1 and 5.4 Kilometres Downwind on 1984 June 11	73
17.	Cross-sectional Profile of NO_2/NO Ratio Measured at 3.1 and 5.4 Kilometres Downwind from the Syncrude Stack on 1984 June 11	74
18.	Cross-sectional Profile of Cube Root of the Turbulent Energy Dissipation Rate Measured at 3.1 Kilometers Downwind from the Syncrude Stack on 1984 June 11	77
19.	Mean NO/NO_x Ratios verus Plume Travel Time for the Syncrude Plume Measured on 1984 June 11	79
20.	Plume Mean Cube Root of the Turbulent Energy Dissipation Rate verus Plume Travel Time for the Syncrude Plume Measured on 1984 June 11	82
21.	NO to NO_2 Conversion Rate verus the Cube Root of the Turbulent Energy Dissipation Rate	83
22.	Correlation of Total Concentrations of Cloud Droplets and Aerosol Particles	86
23.	Vertical Profiles of Temperature and Relative Humidity Observed on 1983 December 15	88
24.	Vertical Cross-section Plot of Segment-averaged Parameters Measured at Various Altitudes and Downwind Distances of the Plume on 1983 December 15	90
25.	Ice Crystal Size Distributions Measured at Selected Locations of the Gaseous Plume on 1983 December 15 ..	91
26.	Vertical Profiles of Temperature and Relative Humidity Observed on 1983 December 17	93

Continued ...

LIST OF FIGURES (CONCLUDED)

		Page
27.	Ice Crystal Size Distributions Measured at Selected Locations of the Gaseous Plume on 1983 December 17 ..	94
28.	Total Concentration of Aerosols Averaged at the Plume Centreline at Similar Downwind Distances from the Suncor and Syncrude Stacks	96
29.	Plume Cross Sectional Averaged Size Distributions of Aerosols Emitted from the Syncrude and Suncor Plants Measured at Approximately the Same Downwind Distances at Plume Centreline	99

ABSTRACT

A field program study was conducted to determine the transport, dispersion, and transformation of sulphur and nitrogen oxides emitted from oil sands extraction plants in the Fort McMurray area. Measurements using the Intera/Alberta Research Council research aircraft were made under cold winter conditions during the months of March and December 1983 and warm summer conditions during June 1984.

Sulphur dioxide emissions were detected as far as 90 km downwind from the source stack. Comparisons between the observed horizontal dispersion parameters and those of the Pasquill-Gifford stability classes show their rates of change with distance were similar, although observed values were slightly higher than predicted ones.

The rate of transformation of SO_2 to SO_4 was determined to be 0% to 2.81% h^{-1} in the winter and 0% to 8.66% h^{-1} in the summer. Higher summer values are attributed to greater solar irradiance. Excess aerosol volume productions suggest that heterogeneous conversion may be appreciable under certain meteorological conditions and close to the emission source.

The conversion rate of NO to NO_2 varied considerably, hour to hour. Its range changed from 0.2% to 21.4% min^{-1}. The rate was positively correlated with turbulent mixing. The chemical reaction is controlled by the concentration of ozone entrained from the environment into the plume by turbulence.

During cold winter conditions (below -25°C), ice crystals nucleated in the gaseous plume, grew to precipitation size. They were observed falling out of the plume to the earth's surface. This snow-out phenomenon was present only in the emission plume within about 10 km of the stack.

ACKNOWLEDGEMENT

The authors would like to acknowledge the contributions to the field experiments, the chemical analysis and research aircraft software and data analysis by the staff of Intera Technologies Ltd., Kananaskis Centre, and Alberta Research Council. Thanks also go to Ms. K. Finstad and Prof. E. Lozowski of the University of Alberta for their participations in Phase 1 of this study.

Consultations with and suggestions from Dr. S. Krupa of the University of Minnesota have been very helpful and are gratefully acknowledged.

The authors also gratefully acknowledge the interest in this work by Dr. M. English of the Alberta Research Council and the staff of the Research Management Division of Alberta Environment, in particular, Ms. B. Magill and Dr. H. Sandhu.

Numerous suggestions, which led to improvements of the final form of this report, from Mr. R. Angle of Alberta Environment are gratefully appreciated.

The research project was jointly funded by Alberta Environment and the Alberta Research Council.

1. INTRODUCTION

As many as 23 different sulphur compounds have been identified in the troposphere with sulphur dioxide and particulate sulphates constituting the most abundant sulphur species.

Sulphur is emitted into the atmosphere by non-biogenic, biogenic and anthropogenic sources. Biogenic sources contribute primarily reduced sulphur species such as hydrogen sulphide. Anthropogenic sources emit mainly sulphur dioxide. Non-biogenic sources such as sea sprays and volcanoes contribute some sulphate and sulphur dioxide, but their contributions are small, perhaps one to two percent of the global sulphur budget. Anthropogenic sources represent 30 to 45 percent of the total sulphur budget (Cullis and Hirschler 1980; Moller 1984a,b; Friend 1973; Granat et al. 1976). Stationary sources such as power plants account for about 99 percent of this (U. S. Environment Protection Agency 1979).

Sulphur dioxide may be deposited close to the source or transported hundreds of kilometers depending upon the characteristics of the source and meteorological conditions. During transport it may undergo a variety of homogeneous (gas with gas) and heterogeneous (gas with particle) reactions and be converted to particulate sulphates (Calvert et al. 1978; Bielke and Gravenhorst, 1978). The rate of conversion varies from approximately 0 to 6% h^{-1} in point source plumes (Hobbs et al. 1979; Forest and Newman 1977; Gillani et al. 1977; Whitby et al. 1978; Cantrell et al. 1978) and up to 10% h^{-1} in urban plumes (Alkezweeny and Powell 1977). Much of this conversion appears to proceed during the daylight hours only.

The initial products of sulphur dioxide reactions, H_2SO_4, NH_4HSO_4, $(NH_4)_3H(SO_4)_2$ and $(NH_4)_2SO_4$ are hygroscopic and may act as cloud condensation nuclei. By this mechanism sulphate may be incorporated in rainfall and deposited on the surface. In addition gas-phase sulphur dioxide may be "pseudochemically absorbed" by precipitation (Hales 1978) and sulphur dioxide in hydrometeors may react to form sulphate and subsequently precipitate to the ground. These processes describe the major pathways for wet removal of

atmospheric sulphur compounds; wet deposition as distinct from dry deposition which is the direct deposition of gaseous sulphur dioxide on non-hygroscopic particles.

The aforementioned processes vary considerably in magnitude and relative importance, and are influenced by such factors as source characteristics, physical and chemical climatology, and topography. Because of the significant influence of these properties on the sulphur dioxide transport-transformation-removal mechanisms, pollutant sources of concern and interest have to be evaluated on a case by case basis under a variety of weather conditions.

In recent years, several studies have been conducted to investigate the physics and chemistry of point source plumes through the use of instrumented aircraft (Fryer et al. 1978; Gillani 1978; Hegg and Hobbs 1980; Hobbs et al. 1979; Husar et al. 1978). These studies have been largely confined to the rate and mechanism of oxidation of sulphur dioxide and particulate analysis. Recently, the scope has been broadened by the observation of an apparent increase in ozone concentration within the plume boundaries at some distance downwind (Lusis et al. 1978; Miller et al. 1978; Davies et al. 1974). Since ozone formation is intimately related to the chemistry of oxides of nitrogen, this has prompted renewed attention to the determination of their plume behaviour (Leahey et al. 1983), in particular the NO_2/NO ratio (Hegg et al. 1977).

In Alberta, field studies of the dispersion characteristics and chemical reactions of pollutants emitted by power plants via aircraft measurements have been performed only on a limited basis (Davison et al. 1977; Davison and Grandia 1979; Lusis et al. 1978; Bottenheim 1982). The paucity of information on the behaviour of plumes from major Alberta sources led to the present study.

In January 1983, the Alberta Research Council, jointly with Alberta Environment, initiated a three phase project to obtain aircraft measurements of stack emission characteristics in the Athabasca Oil Sands area. Field experiments for Phase 1 were

conducted during a seven-day period from 1983 March 26 to 1983 April 01. Phase 2 experiments were carried out from 1983 December 12-20 and Phase 3 experiments from 1984 June 06-12.

The main objectives of the study were:

1. To determine the transport and dispersion of SO_2 and NO_x emitted in the Alberta Oil Sands Environmental Research Program (AOSERP) area;
2. To determine the transformation of SO_2 to SO_4, and NO to NO_2 in the AOSERP area; and
3. To determine the redistribution, and rates of removal of pollutants from the atmosphere, by clouds and precipitation in the AOSERP area.

Because of a lack of suitable clouds in the vicinity of the experiment area no cloud studies were conducted. Therefore, the objective of determining the redistribution and rates of removal of pollutants from the atmosphere by clouds and precipitation was not achieved.

In this report, the experimental procedures, the instrumentation and calibrations are described in Chapter 2. General descriptions of the plume transport and plume dispersion are presented in Chapter 3. Conversion rates of sulphur dioxide to particulate sulphate are given in Chapter 4. Transformation of nitric oxide to nitrogen dioxide is shown in Chapter 5. Evolution of ice particles nucleated in the plume are discussed in Chapter 6. Summaries, conclusions and recommendations are given in Chapter 7.

2. EXPERIMENT PROCEDURES, INSTRUMENTATION AND CALIBRATIONS

This chapter describes the experimental procedures, the INTERA/ALBERTA RESEARCH COUNCIL instrumented aircraft, the air quality instrumentation, and calibration procedures. Measurements of meteorological state parameters, air motion, aircraft position, cloud and aerosol particles and air quality were obtained with a variety of airborne instruments.

2.1 EXPERIMENTAL PROCEDURE

In order to address the three objectives of the project, two different experimental procedures were used. One was specified for plume studies and the other for cloud studies. The objectives of the plume studies were to determine the plume dispersion, plume transport and the plume physics and chemistry. The cloud studies were to investigate cloud physics, cloud chemistry and pollutant removal mechanisms. Since no suitable clouds occurred in the vicinity of the experiment area during any of the three phases of the field experiment, the experiment procedures for the cloud studies will not be presented.

Precipitators inside the main stacks of oil sands extraction plants collect most of the particles but some particles and gases are emitted. The precipitator is rapped at regular intervals of about fifteen to twenty minutes, depending upon the plant operations, to allow the collected particulates to fall away. Most of the trapped aerosols fall as a lump or cake but some can break off and are carried out the stack with the exit gas. This can be seen as a "puff" emitted from the stack every time the precipitators are rapped. The puffs are visible for about one kilometer as they move downwind from the stack.

Photochemical transformation of sulphur dioxide to sulphate aerosols is known to be only of the order of a few percent per hour in direct sunlight. The approach of sampling at a fixed distance from the source cannot provide sufficient information to calculate conversion rates when emissions are not steady, unless a great number of samples are collected. The limited amount of

airborne sampling time would restrict the number of samples collected downwind from the stack. Changes in atmospheric conditions which may occur within a short time period can also add to the uncertainty of results. Following a single puff or parcel of air, the so-called Langrangian approach, is likely to give the best chance of detecting the very low gas-to-particle conversion rate.

Plume depth is fundamentally controlled by mixing and travel time (distance from stack). Buoyancy produces mixing at close range and wind shear at long range. Ambient turbulence contributes to mixing throughout and can be indicated by the atmospheric instability. During every research flight an atmospheric sounding was taken by the research aircraft upwind of the oil sands extraction plant which was to be studied. Estimates of direction of transport, plume height, and plume depth were made using the real time on-board display of the atmospheric sounding which usually terminated at about 2500 m above ground, depending on the atmospheric instability of the day.

After the background sampling was completed, one or two passes were made orthogonal to the wind direction at the plume altitude over the stack to initiate ground and air reference homing pointers to the aircraft data system. The aircraft then flew perpendicular to the direction of transport and intercepted the same, as indicated by the homing pointer, air parcel at various altitudes and distances from the stack for plume cross section measurements. The various altitudes were necessary because a vertical pointer had not been developed for the study. Thus, in post flight analysis, the plume centreline level could be determined from the measurements obtained at various altitudes. The measurements continued downwind until the plume was no longer detectable or distinguishable from the background concentration, or as long as aircraft fuel permitted. Another sounding was then made so that changes in atmospheric conditions could be documented. Aerosol and gas samples with sampling durations of 20 to 30 minutes

were collected during the orthogonal traverses for post flight laboratory chemical analyses.

2.2 INTERA/ALBERTA RESEARCH COUNCIL INSTRUMENTED AIRCRAFT

The aircraft used is a Cessna 441 Conquest: pressurized twin turboprop, gross weight 9900 pounds, ceiling 31000 feet, stall speed 90 kn, and normal cruise speed for cloud studies 150 kn (max cruise 292 kn). The aircraft is fully de-iced and certified for flying into known icing conditions. The aircraft carries full dual navigation and communication radios and a Bendix weather avoidance radar.

Measurements of static and total pressure are made at the aircraft nose and belly (below the fuselage and near the center of gravity). Static pressure is also measured near the tail. An inertial navigation system (INS) is located near the center of gravity. The INS is a Litton LTN-76 with accessories for computing true air speed and horizontal winds, independent of the onboard data system. Air motion sensing 0.8 m ahead of the aircraft's nose is accomplished with a boom-mounted Rosemount 858AJ probe which measures total, static and two axis differential pressures. Flow angles (sideslip and attack) are deduced from the differential pressures. At the belly, a pitot-static tube is mounted beside some of the cloud physics instruments.

Cloud physics instruments are located in two places: at the belly and on the escape door (just aft of the copilot and above the wing). Cloud microphysics instrumentation on the escape door consists of a Cambridge dew point sensor (cooled mirror type), a Rosemount total temperature sensor (platinum resistance wire), a Johnson-Williams hot wire liquid water content probe, a platinum wire reverse flow temperature sensor (National Center of Atmospheric Research, NCAR, design), an inlet for a gas and aerosol sampling manifold, and a cloud water collector for warm or supercooled clouds. Four probes from Particle Measuring Systems are located at the belly location. They are:

1. ASASP - Active Scattering Aerosol Spectrometer Probe

(aerosols 0.1 to 3 μm), which did not function properly during the December 1983 field study (possibly because of the below -25 °C temperatures);

2. FSSP - Forward Scattering Spectrometer Probe (cloud droplets 0.5 to 47 μm);
3. 2D-C - Two Dimensional Optical Array Spectrometer Probe (ice crystals, 25 to 800 μm); and
4. 2D-P - Two Dimensional Optical Array Spectrometer Probe (hydrometeors, 0.2 to 6.4 mm).

Data from the instrumentation are managed by a computer based data system consisting of three LSI 11/23 microprocessors, Winchester and floppy disc storage, a streaming tape drive and CAMAC modular interface. The computers manage data acquisition, recording and real time calculations. Real time display on four video monitors provides information to the mission scientist, pilot and data system operator. Data analysis is normally performed on ground-based VAX 11/750 and 11/780 computers, but some playback and output is possible with the on-board computers.

2.3 REAL TIME CALCULATIONS AND DISPLAYS

Calculations are made by the data system in real time and displayed for use by the pilot and mission scientist. The displays include:

1. Tabulated values of thermodynamic parameters;
2. Particle images from 2D probes;
3. Size distribution histograms from FSSP and ASASP probes; diagnostic information on parameters selected by the system operator;
4. A strip chart showing the most recent seven minutes of data for SO_2 concentration, temperature, liquid water content, cloud droplet concentration and ice particle concentration;
5. A graphical atmospheric sounding (temperature and dew point versus pressure); and
6. A homing pointer display.

Most display values are updated once per second.

The homing pointer is an important feature that is used extensively for cloud and plume studies because it provides the relative position of the aircraft and particular ground locations or particular air parcels. When a homing sequence is initiated, the computer begins adding the direction and distance the aircraft has travelled and also calculates the resultant return vector to the same point. For ground reference points, the INS ground speed and true heading are used. For air reference points, the true airspeed and magnetic heading are used. Up to ten points of mixed types can be tracked simultaneously. The computer system display allows the aircraft to make repeated penetrations of the same air parcel which is drifting with the wind. The homing pointer has been tested and proved to be very accurate under relatively weak shear conditions.

2.4 AEROSOL AND GAS SAMPLING MANIFOLD

An aerosol and gas sampling system on the research aircraft is used for a variety of measurements. The system consists of several components as shown in Figure 1. Air flows continuously at approximately 370 L/min^{-1} through the large diameter (2 cm) stainless steel tubing. Two sampling ports on the tubing are flush-mounted, and two are reverse flow type, to ensure separation of particles larger than approximately 3 μm diameter from the sample air when dichotomous sampling is desired. All valves on the sampling manifold are 6 mm bore stainless steel ball valves, which offer no restriction or particle losses. Some sample air (40 L/min^{-1}) enters a metal bellows pump and is pressurized to slightly above cabin pressure for the SO_2 and NO_x instruments. The time required for air to pass through the pump and tubing is estimated at 0.3 second, calculated from the instantaneous measurements of aerosol concentration, delayed sulphur dioxide measurments and calibration data.

Airflow to the filter samples passed through reverse flow ports and total mass flow was measured by either a Tylan Model FM 362 flow meter, connected to the data system, or by a Sierra

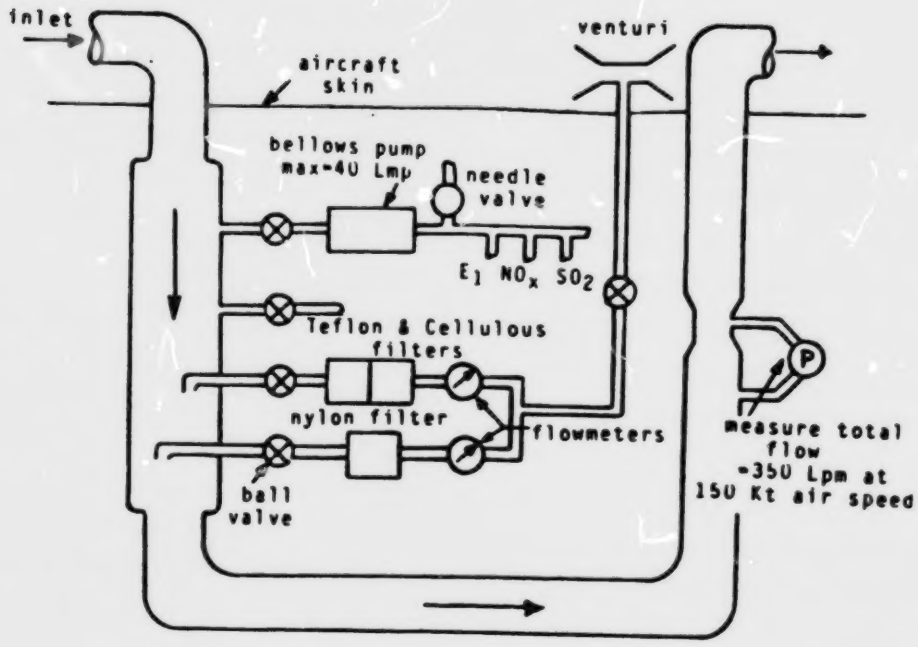

Figure 1. Schematic aerosol and gas sample flow diagram in the system used on research aircraft.

Instruments Model 715 which was monitored by the system operator. The Sierra Instrument flow meter was also connected to the data system during the Phase 3 field experiment. Suction for filter samples was provided by a venturi.

2.5 FILTER SAMPLES OF AEROSOLS AND GASES

Tubing and filter holders made of TFE (Teflon) were chosen for their chemical inertness. Each filter holder contained two filters, and three different configurations were used: a 2.0 μm Teflon filter to collect particulate nitrate and sulphate followed by a 1.0 μm nylon filter to collect nitric acid; a second filter holder contained a cellulose filter to collect particulate sulphate followed by a cellulose filter treated with triethanolamine to adsorb sulphur dioxide (allowing gaseous SO_2 : particulate SO_4 ratios to be determined); and a third holder with a single formaldehyde treated filter to collect HSO_3^-. Three complete series of filters were loaded into the nine filter holders at the airport so that the complete filter packs could be changed in flight without handling the filters. In the March 1983 field experiment, the nylon filter to collect nitric acid was not installed. To ensure chemical purity, all filters were pre-extracted with deionized, distilled water.

2.6 GAS SAMPLING INSTRUMENTS

During the March 1983 sampling period sulphur dioxide measurements were made whereas during December 1983 and June 1984 both sulphur dioxide and nitrogen oxides were measured. Instruments were selected for compatibility with the aircraft system, sensitivity, and especially rapid time response. Some modifications were performed to enhance the time response characteristics.

Instrument lag time and response time are critical parameters in the monitoring of atmospheric pollutants from an aircraft. A one second delay typically will result in the apparent displacement of the plume by 70 meters, furthermore a plume close to its sources may be less than 200 meters wide.

Air pollutant analyzers, because of inherent lags and response time, will not produce an exact record of a varying pollutant concentration. Corrections must be made to allow for delays in instrument response and lag times providing a more accurate analysis of true variations in air quality. A linear system should have its own unique transfer function (which is the response of the system to an unit impulse excitation). From this transfer function, the system's response to an arbitrary input can be determined. The development of such a transfer function usually involves the use of Laplace transforms. If the input function is denoted by Y(t) and the output function by S(t), where t=0 is the time that the input function is applied, it has been shown that the system can be expressed by the governing equation (Mage and Noghrey, 1979):

$$S(t) = Y(t)A(0) - \int_0^t Y(T)\frac{d}{dT}A(t-T)\,dT \qquad (2.1)$$

where A(t) is the response to a unit step function, i.e., A(t) is the output S(t) produced when Y(t)=0 for t<0 and Y(t)=1 for t≥0, and T a dummy variable used for the convolution integration. For a system without systematic bias, Eq.(2.1) can be simplified as:

$$S(t) = \int_0^t Y(t-T)C(T)\,dT \qquad (2.2)$$

where

$$C(T) = \frac{d\,A(T)}{dT} \qquad (2.3)$$

is the transfer function of the system. The analytical solution to the convolution integral of Eq.(2.2) is quite involved, and a finite

difference numerical method may be used to approximate the solution. The latter was adopted to deconvolute the actual SO_2 and NO_x concentrations from the instrumental data.

2.6.1 Sulphur Dioxide

SO_2 was measured with a Monitor Labs 8450 sulphur dioxide monitor in March 1983 but this was replaced by a faster response Meloy Labs SA 285E sulphur dioxide analyzer for the December 1983 and June 1984 sampling periods. Both instruments are of the flame photometric type. The air sample is burned in a hydrogen flame and the intensity of a sulphur line emission is measured by a thermally stabilized photomultiplier tube. The instruments require an external supply of pressurized pure hydrogen gas. The electrical output of the photomultiplier tube is linearized to provide a signal proportional to sulphur dioxide concentration in the range of 0 to 1000 ppb. The manufacturer's specifications for both instruments are given in Table 1.

Sample airflow in the Meloy Labs SA 285E sulphur dioxide analyzer was modified to improve the time response characteristics for aircraft use by removing the hydrogen sulphide scrubber. The resulting transfer function was determined during a calibration period by differentiating the response to a step change in SO_2 calibration gas. This function for the Meloy Labs SA 285E is shown in Figure 2. It represents the response of the instrument with 1 Hz sampling rate to a delta input of 100%. Notice that the response is delayed by three seconds and has a rise time to 95% of around 7 seconds, so it is considerably faster than the manufacturer's specifications (30 to 300 seconds). This function was used to deconvolute the measurements taken during research flights in Phase 1 and Phase 2. However, the correction using this function does not include the delay and spreading of the signal caused by the bellows pump and piping. Because, as shown earlier, the response of the pump and piping system is much faster compared to that of the instrument, the correction using only the transfer function of the instrument should account for the greatest part of the signal

Table 1. Gas sampling instrument specifications.

	SULPHUR DIOXIDE		NITROGEN OXIDES
make	Monitor Labs	Meloy Labs	Monitor Labs
model	8450	SA 285E	8840
range (ppb)	0 - 500	0 - 1000	0 - 10000
noise (ppb)	1.0	0.5	1.0
minimum detectable (ppb)	4.0	1.0	1.0
zero stability	2.5 ppb day^{-1}	4 ppb day^{-1}	0.4% full scale day^{-1}
span stability	5.0 ppb day^{-1}	2.0% full scale day^{-1}	1.0% full scale day^{-1}
linearity	1%	1%	1%
lag time (sec)	< 10	< 5	3
rise time to 95% (sec)	45	30 to 300	180
sample flow (mL min^{-1})	118	240	700
signal output (volts)	0 - 5	0 - 10	0 - 10
power (watts)	500	250	320
auxiliary equipment	regulated hydrogen @ 20 psi	regulated hydrogen @ 45 psi	vacuum pump

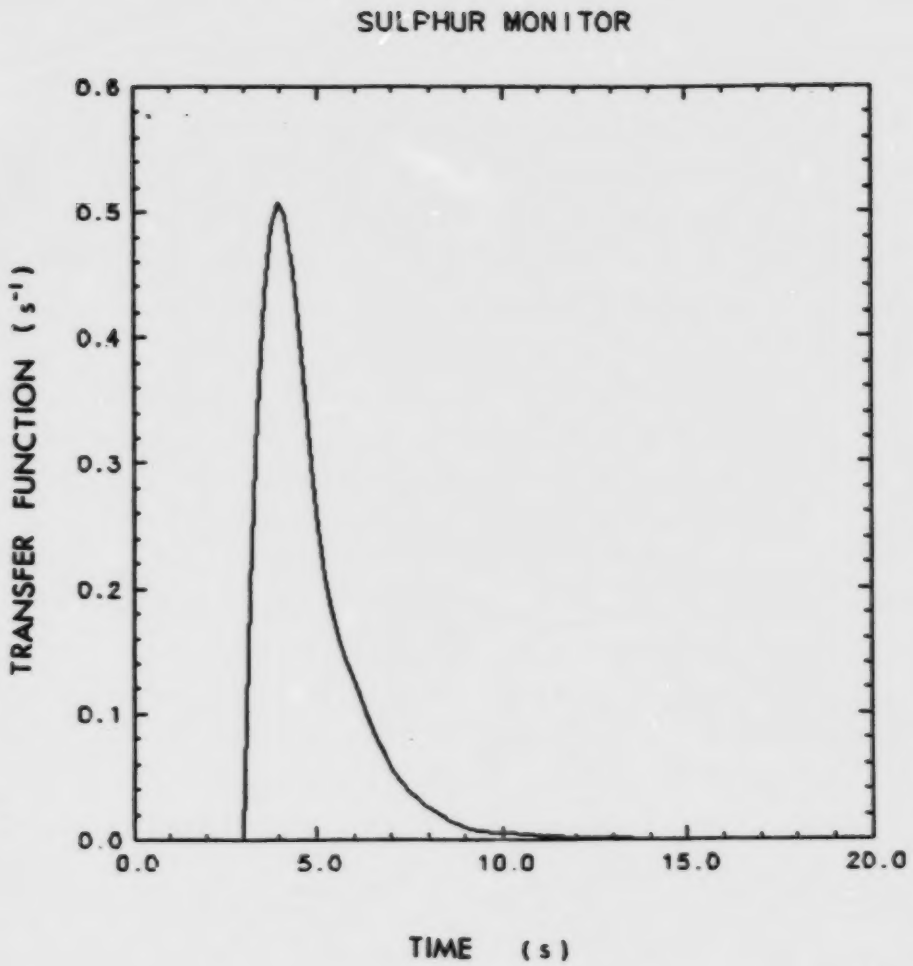

Figure 2. Empirical transfer function for Meloy Labs SA 285E sulfur dioxide analyzer. Response to unit Delter function input at time zero.

spreading. In Phase 3, when the sampling rate of the instrument was increased to 10 Hz, another transfer function was derived in a manner similar to that above but the pump and piping used was taken into account in the correction.

2.6.2 Nitrogen Oxides

NO and NO_x were measured with a Monitor Labs Nitrogen Oxides Analyzer Model 8840. It is a dual channel chemiluminescent type instrument. The concentrations of NO and NO_x are simultaneously measured in two reaction chambers. Sample air is divided into two paths, one leading through an NO_2-to-NO converter and then to a reaction chamber, and the other going directly to a reaction chamber. Each portion of the sample reaches the reaction chambers almost simultaneously, and the difference in the two channels' readings is NO_2. The electrical output voltage is linearly proportional to concentration from 0 to 10 ppm. The manufacturer's specifications are given in Table 1.

The instrument was modified to enhance its time response characteristics for aircraft use by replacement of an orifice thereby increasing the sample flowrate. The transfer function was determined during a calibration period by differentiating the response to a step change in NO calibration gas. This function is shown in Figure 3. It represents the response of the instrument with 1 Hz sampling rate to a delta input of 100%. Notice that the response is delayed by one second and has a rise time to 95% of approximately 4 seconds, so it is considerably faster than the manufacturer's specifications (180 seconds). This function was used to deconvolute the measurements taken during research flights in Phase 1 and Phase 2. The discussion concerning the correction using the instrument response given in the section on the SO_2 analyzer also applies here. In Phase 3 another transfer function suitable for 10 Hz sampling rate and also accounted for the signal spreading by the pump and piping was used.

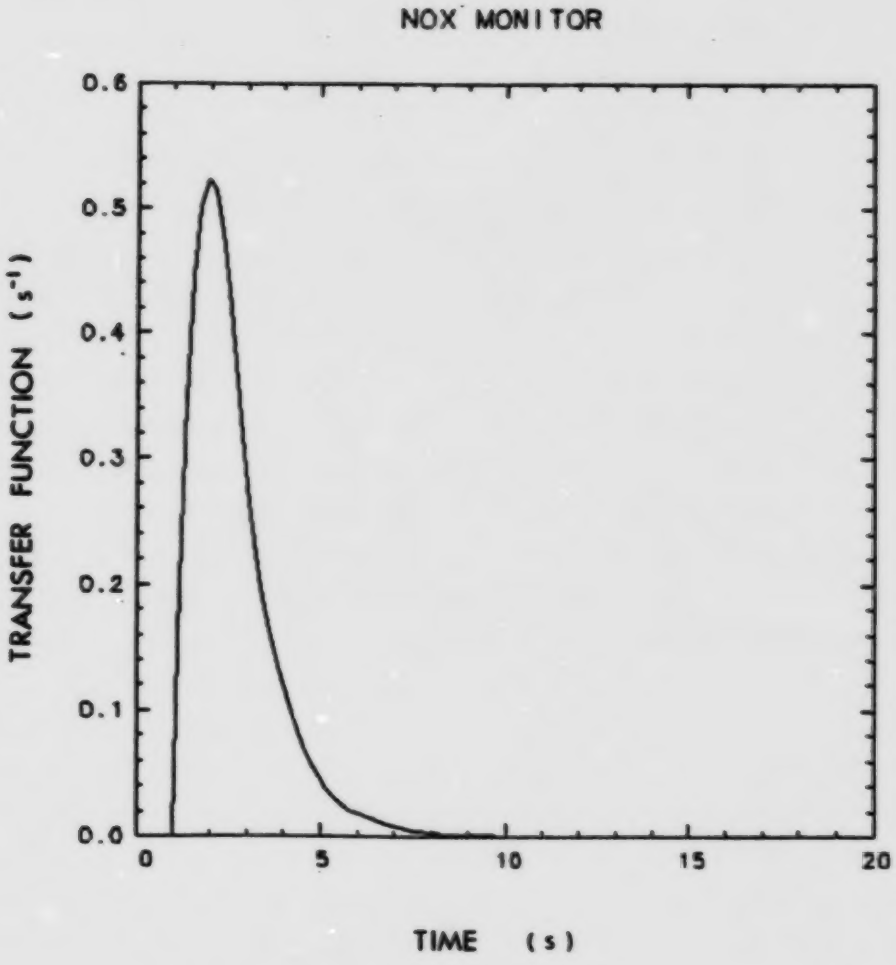

Figure 3. Empirical transfer function for Monitor Labs 8840 nitrogen oxides analyzer. Response to unit Delter function input at time zero.

2.7 INSTRUMENT CALIBRATION

The SO_2 and NO_x analyzers were calibrated daily with a five point calibration. For the SO_2 monitor, a Monitor Labs 8500 calibrator, carrying a permeation device traceable to a National Bureau of Standard (NBS) of 123 ng of SO_2 per minute, was used in March 1983. Three calibrators were used to generate standards of known concentration in December 1983 and June 1984. These included: (1) a Monitor Labs Model 8500 calibrator with a permeation tube producing 123 ng of SO_2 per minute; and two calibrators built by Alberta Environment; (2) one producing 1540 ng SO_2 per minute; and (3) another producing 1585 ng SO_2 per minute. Flow through the calibration systems were measured with a Teledyne-Hastings Model HBM-1 494 bubble flow meter. All flows were corrected for temperature, pressure and vapour pressure effects which affected the flows by approximately 5%, as shown in Table 2. The Columbia Scientific Industry (CSI) Meloy Model SA 285E SO_2 analyzer was found to give stable readings reproducible to $\pm$5%, as shown in Table 3. The major source of error was not the instrument itself, but the calibration systems which were subject to fluctuations in the permeation rate of SO_2 caused by minor temperature changes. The calibrators built by Alberta Environment showed less variation than the Monitor Labs calibrator. Little evidence of drift or changes in the sensitivity of the analyzer was found over the lifetime of the project. For example, on December 13, a 61 ppb standard, produced 1248 computer counts when the instrument was operated on the 100 ppb range and, on December 15, 1157 counts (7% less) were recorded for the same conditions. The instrument was also linear between ranges as shown in Table 4.

The Monitor Labs Model 8840 Analyzer was calibrated using a CSI Model 1800 flow dilution system with an NBS traceable standard NO gas. Zero grade air was used in the flow dilution system. The flow dilution system was calibrated against the Teledyne-Hastings bubble flow meter. The analyzer was linear over the entire NO concentration range to 1000 ppb, and no change in sensitivity was found during the field program (see Tables 5, 6,

Table 2. Calibration of flow in the monitor labs SO_2 calibrator. 1983 December 16. Flows corrected at 25°C at a pressure of 760 mm of mercury and for water vapour pressure.

Rotameter Setting	Volume (mL)	Time (minutes)	Flow (mL min^{-1})	Corrected Flow (mL min^{-1})
7.35	1000	0.531 0.530	1880	1780
8.35	1000	0.473 0.473	2110	2000
4.00	500	0.513 0.513	975	940
4.30	500	0.477 0.476	1050	995
2.35	500	0.419	477	452
2.50	200	0.369	542	514
6.10	500	0.325 0.321	1550	1470
3.40	200	0.252 0.254	790	750

Table 3. Calibration of the Meloy Labs Model SA285E sulphur dioxide analyzer. 1983 December 13. Relationship between concentration of SO_2 and computer counts.

SO_2 (ppb)	Meter[a] (mv)	Computer (count)	ppb/mv	ppb/count	Calibrator
26.4	160	323	0.166	0.0817	ML[b]
50.0	285	573	0.175	0.0872	ML
104	600	1248	0.173	0.0833	ML
105	640	1323	0.164	0.0794	
144	890	1830	0.162	0.0787	

[a] 1000 ppb = 1000 mv
0.168 $\pm$ 0.007 ppb/mv
0.0821 $\pm$ 0.0034 ppb/count

[b] Monitor Labs

Table 4. Calibration of ranges in the Meloy Labs Model SA285E sulphur dioxide analyzer.[a]

Scale (ppb)	Millivolt Output (mv)
100	720
500	144
1000	72

[a] Monitor is linear within ranges $\pm$ 1.0 mv.

Table 5. Calibration of the Monitor Labs 8840 NO_x analyzer. Test of linearity at low concentrations[a] (diluter NO flow fixed, dilution air change).

NO/Air Ratio (corrected)	NO (ppb)	Millivolt Output (1.0 ppb scale)	ppb/mv
1.73/4870	33	39	0.85
1.73/3750	43	51	0.84
1.73/2470	66	75	0.88
1.73/1250	130	150	0.87

[a] The monitor is linear at low concentrations, (ie. ppb/mv = 0.86 $\pm$ 0.02 ppb/mv).

Table 6. Calibration of the Monitor Labs 8840 NO_x analyzer. 1983 December 08.

NO/Air Ratio (corrected)	NO[a] (ppb)	Meter Reading (mv) NO	NO_2	NO_x	Scale (v)
zero air	0	0	0	0	0.050
48.5/4870	936	1140	-4	1130	1.000
37.5/4870	724	871	-4	867	1.000
26.0/4870	500	595	0	586	1.000

[a] Ratio of actual NO concentration to meter reading 0.83 $\pm$ 0.01 (ppb/mv)

Table 7. Calibration of the Monitor Labs 8840 NO_x analyzer. 1983 December 16. Installed in aircraft, computer hooked up.

NO/Air Ratio (corrected)	NO_x (ppb)	Meter[a] (mv on 1.0 ppm scale)	Computer (counts)	ppb/count[b]
zero air	0	0	0	ND[c]
13.4/4850	260	300	237	1.097
26.0/4850	504	565	461	1.093
37.5/4850	727	840	700	1.039
43.6/4850	845	990	842	1.004

[a] ppb/mv 0.86 $\underline{6}$ 0.03

[b] ppb/count 1.06 $\pm$ 0.04

[c] No Data

and 7). Gas phase titration showed the NO and NO_2 channels of the instrument to be well balanced. Instrument response was 1.06 $\pm$ 0.04 ppb per computer count on the 1000 ppb range.

2.8 DEDUCING HORIZONTAL WINDS

The horizontal wind is the vector difference between the motion of the aircraft with respect to the air (true airspeed) and the motion of the aircraft with respect to the ground (ground speed). True airspeed is measured at two locations of the aircraft, the tail and the belly. Ground speed is measured with the INS at the plane's center of gravity. The airspeed and ground speed vectors can be subtracted to obtain an estimate of the horizontal wind.

This technique had limited success during the field experiment because of the following:

1. There were often light winds which are poorly estimated as being the difference between two large vectors;
2. The nose boom, tail and belly locations are in a region of airflow that is disturbed by the aircraft; and
3. Corrections for second-order effects were not applied (e.g., sideslip and angle of attack).

An attempt to compensate for these unknown, systematic errors was made during post hoc computer analysis of the data, and the procedure is outlined here. It was assumed that during a small time interval, the winds over a small region of space and at one elevation are constant. So that when the aircraft flies two legs, each relatively straight and level at the same elevation but different headings, the calculated winds should be identical. The computer analysis calculated the horizontal winds for these two legs and computed the vector difference between them. If the difference was larger than 0.1 m s^{-1}, an additive drift angle correction and a multiplicative true airspeed correction were computed iteratively until the winds for the two legs were the same. These corrections

were then used to adjust other data during the same flight and so to arrive at an adjusted estimate of the true wind. The adjustments were typically a factor 0.98 in true airspeed at the tail and less than one degree in drift angle. Comparisons of wind profiles from aircraft soundings with those deduced from pilot balloon soundings at Fort McMurray airport favored this correction procedure.

3. DESCRIPTION OF PLUME TRANSPORT AND PLUME DISPERSION

During the three phases of this project, twenty-three plume studies were conducted. Seven took place in the first phase, and eight in each of the second and third phases. Of these, four were in the Suncor plume, and the remainder were in the Syncrude plume.

To determine the extent of plume transport downwind both a ground and an air parcel reference point would be initiated onto the aircraft data system. When a ground reference point or an air reference point, or both, are initiated onto the data system, the direction and distance to the reference point are calculated. As the wind carried the plume downwind the aircraft would fly orthogonal passes through the plume and intercept the same air parcel at progressively farther distances away from the stack. These horizontal passes were made as close to the plume centreline as possible. Shown in Figure 4 is the flight track for June 12, 1984 of the Syncrude plume. Similar flight tracks were flown for the other plume studies. The horizontal axis shows the distance west of the Syncrude stack, while the vertical axis indicates the distance south. The numbers along side the track indicate the time in hours and minutes in coordinated universal time. The cross indicates the location of the Syncrude plant and the heavy line with the arrow shows the path of plume travel. On this day the mean wind, calculated from 28 passes at an average plume altitude of 450 metres above ground level, was from 065 degrees at 6.1 ms^{-1}. These passes through the plume extended to a distance of 41 kilometres from the stack before sulphur dioxide plume measurements became difficult to distinguish from those of the background, which on this day was 18 parts per billion (ppb).

A wide variety of winds were encountered at plume level over the course of the three phases. These winds, averaged from measurements taken during the plume penetrations, ranged from a mean of 2.0 ms^{-1} to a mean of 18.5 ms^{-1}, and originated from various directions. These are shown in Table 8 for 20 studies made during

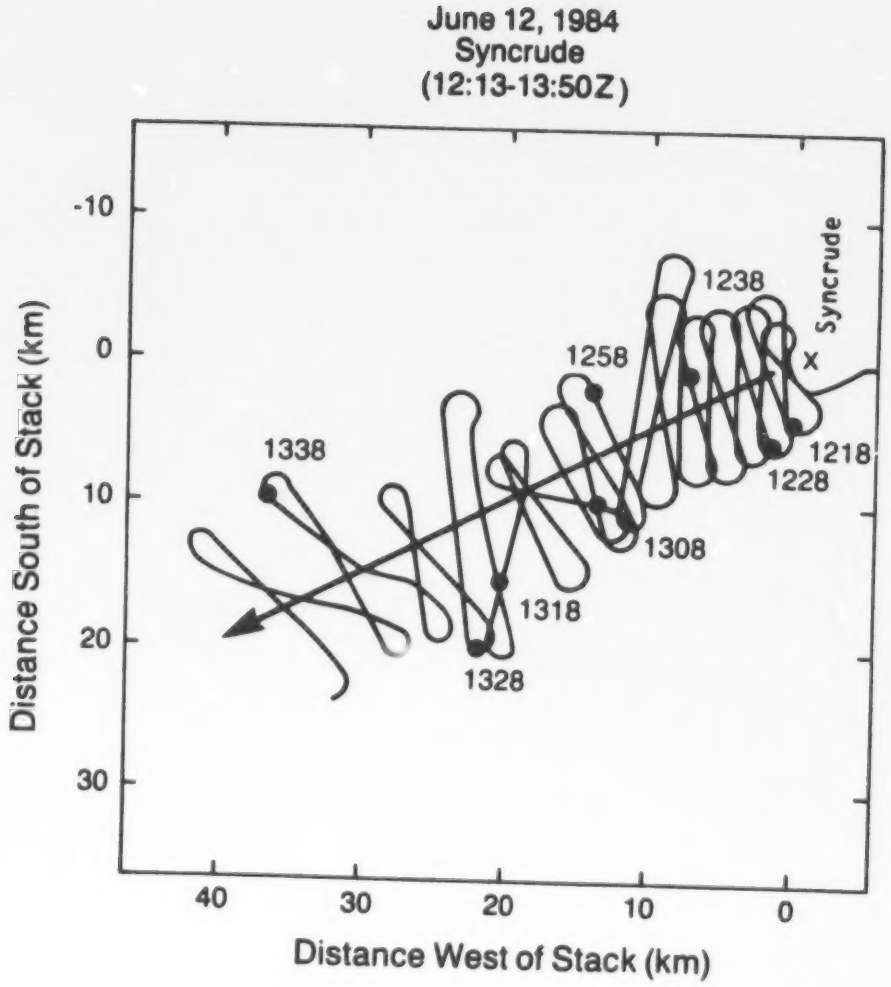

Figure 4. Flight path of research aircraft on 1984 June 12 (12:13 to 13:50Z). Numbers beside the flight path are universal coordinate times indicating the aircrafts position at that time. Horizontal and vertical axes show the distance in kilometres west and south of the Syncrude stack, which is indicated by an X.

Table 8. Plume penetration time, mean speed and direction of wind in plume, number of orthogonal plume penetrations, distance of last plume penetration, mean sulphur dioxide concentration over last pass, and the maximum distance at which sulphur dioxide was detected for study days during all three phases of the project.

DATE (yy/mm/dd)	PLUME PENETRATION TIME (local)	MEAN WIND SPEED(m/s)	MEAN WIND DIRECTION (deg)	NUMBER OF PASSES	DISTANCE OF LAST PASS (km)	MEAN SO_2 OF LAST PASS (ppb)	MAXIMUM DISTANCE (km)
83/03/28	1540 to 1725	10.5	005	13	37	42	37
83/03/29	1525 to 1740	3.1	085	6	10	80	10
83/03/30	0800 to 0950	8.0	130	10	42	11	42
83/03/31	1710 to 1905	2.1	195	0	N/A[a]	N/A[a]	96
83/12/13	1100 to 1205	18.5	010	8	20	57	21
83/12/13	1220 to 1350	11.7	015	12	37	15	37
83/12/14	1045 to 1340	2.1	330	9	3	746	45
83/12/15	1000 to 1220	2.0	265	16	45	27	45
83/12/15	1450 to 1635	5.0	025	19	32	307	32
83/12/17	1430 to 1555	7.4	345	11	17	265	27
83/12/19	1430 to 1645	4.8	330	23	71	159	71
83/12/20	1105 to 1345	6.1	345	18	68	30	68

[a]Not applicable

continued ...

Table 8. Concluded.

DATE (yy/mm/dd)	PLUME PENETRATION TIME (local)	MEAN WIND SPEED(m/s)	MEAN WIND DIRECTION (deg)	NUMBER OF PASSES	DISTANCE OF LAST PASS (km)	MEAN SO_2 OF LAST PASS (ppb)	MAXIMUM DISTANCE (km)
84/06/06	2000 to 2055	13.7	110	3	11	180	31
84/06/07	1620 to 1850	9.2	075	4	10	33	31
84/06/08	1020 to 1125	6.4	045	10	24	26	33
84/06/09	0505 to 0730	6.5	190	49	34	496	34
84/06/10	0920 to 1120	4.6	245	0	N/A[a]	N/A[a]	34
84/06/11	0545 to 0625	3.8	005	18	24	93	24
84/06/11	0700 to 0810	4.8	075	12	19	102	19
84/06/12	0620 to 0755	6.1	065	28	41	144	41

[a]Not applicable

the three phases. Also shown are the local times of plume penetrations, the number of passes made through the plume for each study, the distance downwind at which the last pass was made, the mean sulphur dioxide concentration of the last pass, and the maximum distance at which sulphur dioxide was detected on that study day. The maximum distance at which sulphur dioxide was detected occasionally exceeded the distance of the last orthogonal plume penetration. On these days, longitudinal passes along what was believed to be the plume centreline were made beyond the distance of the last orothogonal pass to collect filter samples of aerosols and gases. Orothogonal plume penetrations were not made on two flights, 1983 March 31 and 1984 June 10. On these two days the flights were flown primarily to collect samples of aerosols and gases using the filter system. Background samples of aerosols and gases were always collected upwind on flights where filter samples were gathered. The farthest distance at which the plume was detected was at 96 kilometres on 1983 March 31.

Many factors influence the transport and dispersion rate of a plume, such as winds, atmospheric stability, scavenging processes and turbulence. The transport of a plume away from its source depends primarily upon the winds at plume altitude. Strong horizontal winds with constant direction carry a plume to a farther distance from a stack than light winds given the same travel time. Changes in wind direction and speed with height can cause an enhanced lateral dispersion or a smearing of the plume. This smearing was most pronounced in the horizontal direction. On 1983 December 14, for example, the relative wind shear components orthogonal to the mean wind direction at approximately 100 metres below, at, and 100 metres above the plume centreline were 0.0093, 0.0041 and 0.0005 per second respectively. The greater shear at the plume's lower boundary resulted in a greater smearing of the plume at its lower levels compared to the upper levels. The level at which the greatest smearing took place within the plume, due to relative wind shear, varied from study to study.

Turbulence of the atmosphere acts to mix the effluent with

the surrounding air. At some point downwind from the stack the size of the dominant turbulent eddies within the plume will increase to the size found in the ambient air. Mixing of the plume with the surrounding air from this time on is then determined by ambient turbulence. This mixing eventually dilutes the plume to the point where it can no longer be distinguished from the background.

The cube root of the turbulent energy dissipation rate, ($\epsilon^{1/3}$), as suggested by MacCready (1964), of the atmosphere at plume level for most of the plume study days is given in Table 9. These cube root of the turbulent energy dissipation rates range from 0.9 $cm^{2/3}\ s^{-1}$ to 4.8 $cm^{2/3}\ s^{-1}$. It is expected that these days with stronger turbulence are also the days with the greatest dilution rates.

Initially, the plume has strong vertical components of motion from the stack exit velocity and from vertical acceleration due to buoyancy. As the plume rises the turbulence within the plume, which is generated by vertical velocity shear at the rising plume edges and by differences in thermal fields within the plume (Davison and Leavitt 1979), decreases. Plume turbulence causes entrainment of the surrounding air and subsequently reduces the plume's buoyancy. As the plume moves away from the stack the turbulence within the plume decreases until it approaches the same energy levels as that of the surrounding air. Figure 5 shows the cube root of the turbulent energy dissipation rate versus horizontal distance from one side of the plume to the other for three passes made at 1.05, 1.55 and 4.76 kilometres away from the Suncor stack on June 11, 1984. Plume width was 1440, 1520 and 6080 metres respectively. The mean cube root of the turbulent energy dissipation rates for these passes are 3.8, 3.1 and 1.6 $cm^{2/3}\ s^{-1}$ with a background rate of 1.1. During the flight the meteorological conditions at plume level remained relatively unchanged. The figure indicates that the plume turbulence decays with time until it is equivalent to the environmental turbulence.

The degree of atmospheric turbulence, which increases or decreases in three dimensions, is determined by atmospheric

Table 9. Potential temperature gradient and environmental turbulent energy dissipation rate at plume level during penetrations on plume study days.

DATE (yy/mm/dd)	TURBULENT ENERGY DISSIPATION RATE ($cm^{2/3}$ s^{-1})	POTENTIAL TEMPERATURE GRADIENT AT PLUME LEVEL (^{o}K/100 m)
83/12/13	ND[c]	+1.70
83/12/13[b]	ND	+1.50
83/12/14	ND	+1.50
83/12/15[a]	1.2	+1.40
83/12/15[b]	ND	+0.80
83/12/17	1.3	+0.70
83/12/19	1.6	+1.40
83/12/20	1.2	+0.50
84/06/06	1.0	+0.38
84/06/07	2.5	+0.02
84/06/08	4.8	0.00
84/06/09	0.9	+0.35
84/06/10	ND	+1.50
84/06/11[a]	1.1	+1.20
84/06/11[b]	1.3	+1.30
84/06/12	0.9	+1.10

[a]First flight of the day

[b]Second flight of the day

[c]No data

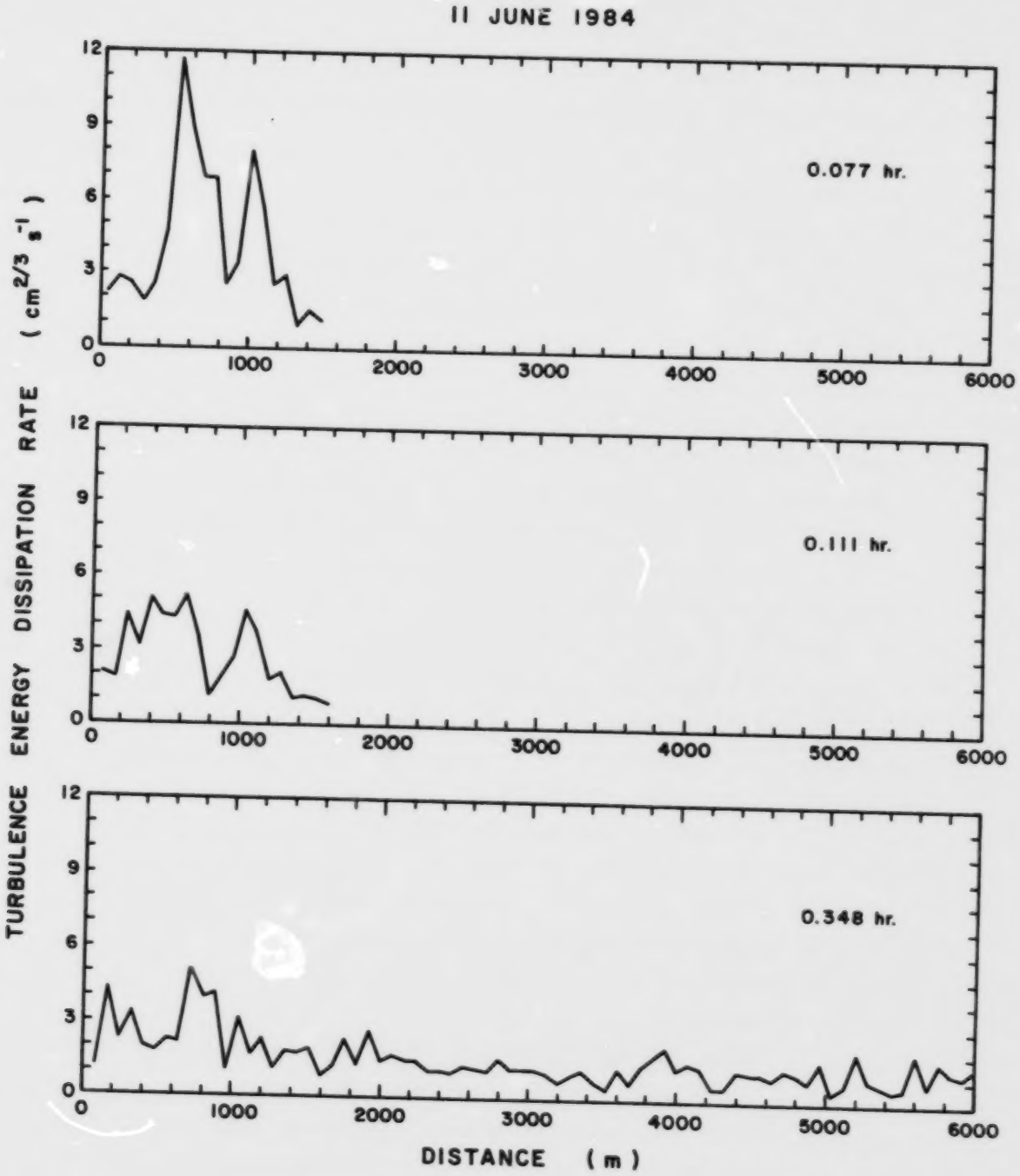

Figure 5. Cube root of the turbulence energy dissipation rate versus distance through the plume for three passes of increasing age for the Suncor plume on 1984 June 11. Zero distance marks one edge of the plume.

stability. This stability ranges from extreme instability associated with rapid mixing to extreme stability with laminar flow and negligible turbulence. An atmospheric sounding was taken upwind of the plume during each research flight to assist in the determination of plume transport and dispersion.

Figure 6 shows the potential temperature (dots), and the relative humidity (dashes) soundings for 1984 June 06. This sounding shows stable conditions from the surface to 1000 metres above ground level, a well-mixed layer from 1000 metres to 2000 metres, and stable above, to the top of the sounding at 3000 metres. Under these conditions, the sulphur dioxide plume rose to approximately 550 metres above ground level and showed little vertical mixing. If the plume had ascended into the well-mixed layer, it would have quickly dispersed vertically. The potential temperature gradient at plume level on this day showed an increase of 0.38°K/100m.

For the other days, during phases II and III, the potential temperature gradient at plume height ranged from 0.00 to +1.70°K/100m, as shown in Table 9. Although no potential temperature gradients are given for days during phase I, these days generally had stable atmospheric conditions, with the exception of 1983 March 29 which was slightly unstable. The generally stable conditions exhibited during the study periods suggest suppressed vertical dispersion. Therefore, atmospheric stability favoured long distance transport of pollutants during the three phases of the field experiments.

Plume concentration profiles were obtained from the orthogonal aircraft passes through the plume to give a cross-sectional mapping at a given plume parcel age and distance downwind of the plant. Sulphur dioxide concentration profiles, corrected for instrument response, are shown in Figure 7 for six traverses of increasing plume age on 1983 December 20. The decrease in concentration of sulphur dioxide with time is apparent.

Mean plume concentrations were calculated for each of the cross-wind passes at the plume axis line. As the plume age

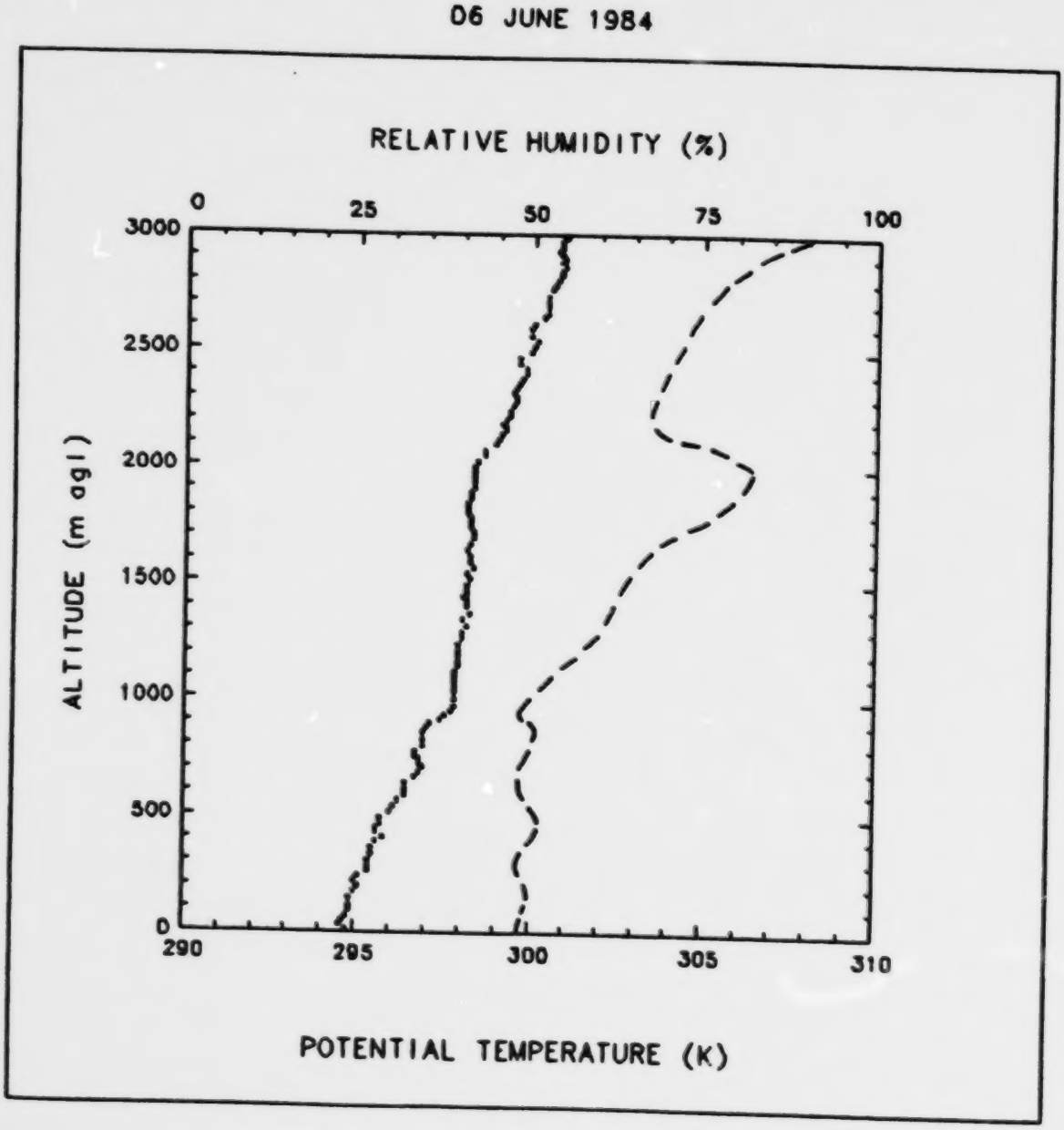

Figure 6. Atmospheric sounding upwind of plume for potential temperature (dots) and relative humidity (dashes) on 1984 June 06. Altitude is indicated as metres above ground level.

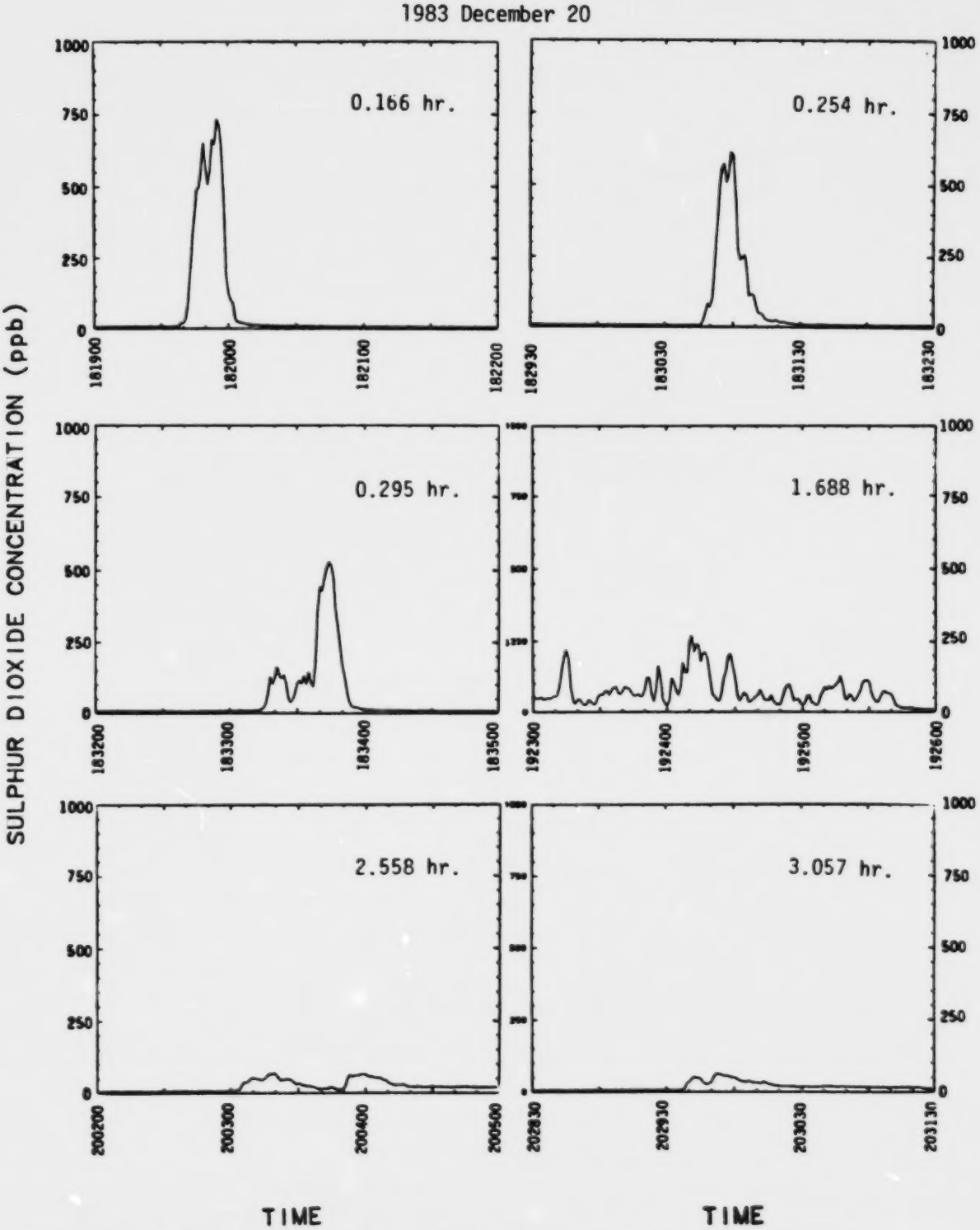

Figure 7. Sulphur dioxide concentration (ppb) profiles, corrected for instrument response, for six plume passes on 1983 December 20. The age of the plume parcel is shown.

increased, the mean sulphur dioxide concentration decreased to a value where it was no longer discernable from the surrounding air. From these mean plume concentrations a dilution rate can be obtained.

A comparison on a daily basis between the atmospheric turbulence, at time of flight, and rates of sulphur dioxide dilution suggest a general relationship between the two. Those days with higher turbulence are also the days with higher sulphur dioxide dilution. This again suggests that turbulence outside of the plume is an important factor in the overall dispersion of the plume.

The horizontal dispersion co-efficient, (δy), was computed for each traverse on the basis of the area under the sulphur dioxide concentration curve. For a Gaussian distribution, one standard deviation either side of the mean occurs at distances such that the accumulated fractions of the total area under the curve are 0.159 and 0.841 respectively. The δy values were computed using the same area criteria. By this procedure the observed concentrations were being compared with a Gaussian distribution of the same area.

Although an attempt was made to intercept the plume orthogonally on each pass, not all attempts succeeded. For such cases, the δy values calculated using the area criteria were adjusted to their orthogonal values by the cosine method. Horizontal dispersion co-efficients are functions of distance downwind, atmospheric stability and wind shear. The broad spectrum of atmospheric stabilities have been divided into six categories and are designated A, for extremely unstable, to F, for moderately stable. Each of these categories is represented by a dispersion curve which depicts horizontal plume dispersion given distance downwind. This family of curves is called the Pasquill-Gifford curves (Pasquill 1974).

For each of the plume study days a δy value was calculated for each pass at or near the plume centreline. These observed values were then compared to the empirical curves derived by Pasquill and Gifford. Plume penetrations known to be to far away from the plume centreline were not used. Shown in Figure 8 are the

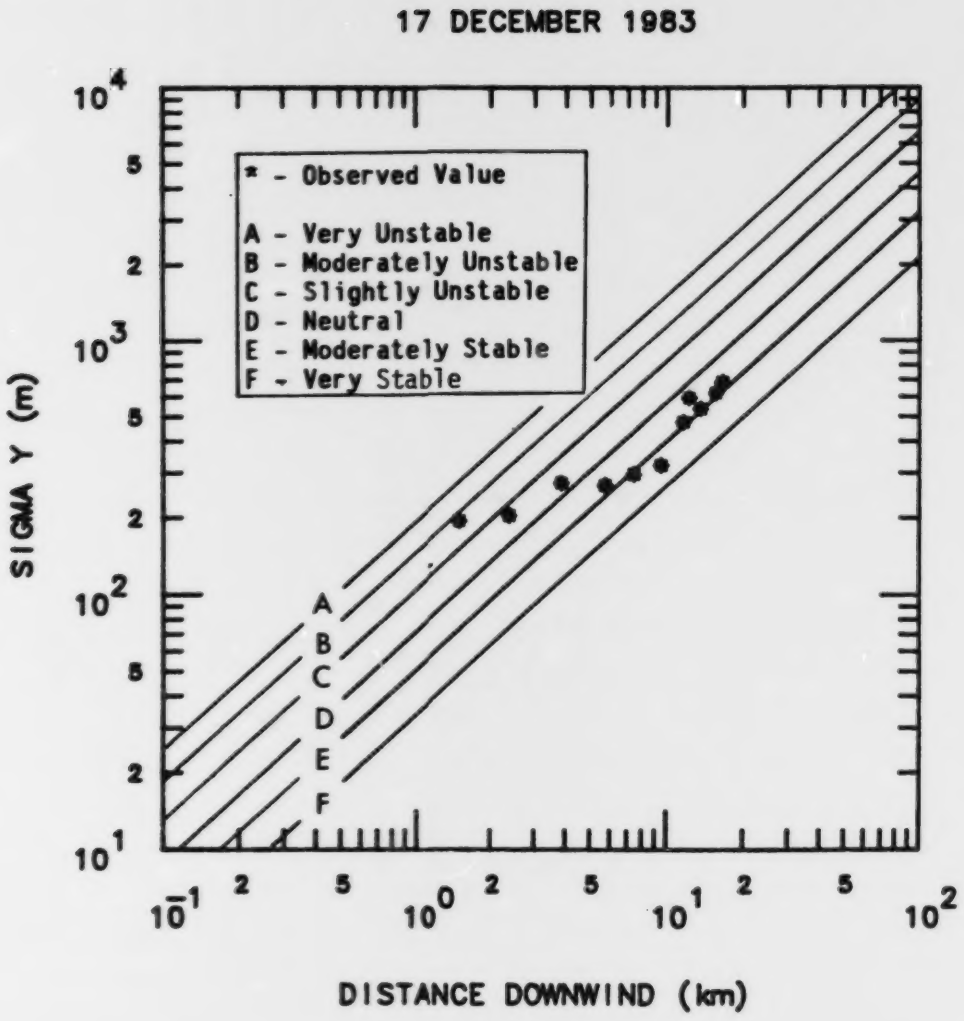

Figure 8. Observed Horizontal Dispersion Coefficients Compared to Pasquill-Gifford Curves for Plume Penetrations Made on December 17, 1983.

observed δy values for eleven Syncrude plume penetrations made within an one hour time period on 1983 December 17 as compared to the Pasquill-Gifford curves. These observed values are scattered amongst curves C to E, indicating slighlty unstable to slightly stable conditions. An atmospheric sounding completed immediately before the penetrations showed that the potential temperature gradient at plume height was +0.70°K/100m, indicating slightly stable conditions. The atmospheric soundings made immediately before and after each day's plume penetrations are representitive of the atmospheric stability for the time period of actual plume penetrations. Plume penetrations lasted from one to three hours for each of the plume studies.

Generally, observed δy values close to the stack (less than three kilometres) were greater than what the dispersion co-efficient on the Pasquill-Gifford curves would suggest. The first three values in Figure 8 indicate this greater instability in the observed values. It was also generally found that beyond twenty to forty kilometres downwind from the stack the Pasquill-Gifford curves generally overestimated the observed horizontal plume dispersion co-efficients. Davison and Leavitt found in their study on δy data that the observed δy values close to the stack were also greater than what the Pasquill-Gifford curves predicted them to be.

Observed δy values, between the high values close to the stack and those far from the stack, show close agreement in the rate of change with distance with the Pasquill-Gifford curves. However, the observed values are somewhat higher than predicted for the levels of atmospheric stability present. An equation and correlation co-efficient was calculated for each plume study day which had sufficient observed δy values after the close and far values were excluded. These are listed in Table 10. Distance downwind from the stack in kilometres is signified by d, and δy is the horizontal dispersion co-efficient in metres.

Table 10. Equations and correlation coefficients for horizontal plume dispersion.

DATE (yy/mm/dd)	EQUATION OF HORIZONTAL DISPERSION	CORRELATION COEFFICIENT
83/03/28	$\delta y = 84.70\ d^{1.0696}$	0.9694
83/03/29	$\delta y = 54.34\ d^{1.0589}$	0.9840
83/03/30	$\delta y = 26.48\ d^{1.1638}$	0.8185
83/12/13[a]	$\delta y = 116.76\ d^{0.9219}$	0.9219
83/12/13[b]	$\delta y = 59.27\ d^{0.9066}$	0.9066
83/12/14	$\delta y = 543.81\ d^{0.8035}$	0.9509
83/12/15[a]	$\delta y = 702.42\ d^{0.5013}$	0.9721
83/12/15[b]	$\delta y = 37.18\ d^{1.0092}$	0.9037
83/12/17	$\delta y = 46.02\ d^{0.9524}$	0.9541
83/12/19	$\delta y = 202.40\ d^{0.7968}$	0.9803
83/12/20	$\delta y = 209.56\ d^{0.8652}$	0.9721
84/06/08	$\delta y = 116.90\ d^{0.9491}$	0.9491
84/06/09	$\delta y = 185.91\ d^{0.1919}$	0.2855
84/06/11[a]	$\delta y = 473.47\ d^{0.5796}$	0.8250
84/06/11[b]	$\delta y = 120.35\ d^{0.8692}$	0.8692
84/06/12	$\delta y = 95.96\ d^{0.6325}$	0.8489

[a] First flight of the day

[b] Second flight of the day

Symbols: δy = Horizontal Dispersion Coefficient;

d = Distance Downwind from the stack in Kilometres.

4. CONVERSION OF SULPHUR DIOXIDE TO PARTICULATE SULPHATE

The particle size spectrum measurements were processed to give particle number (d N/d log D), particle surface area (d S/d log D) and particle volume (d V/d log D) distributions (where N, S and V are the total particle number, surface area, and volume concentrations respectively and D is the particle diameter). The particle surface area and the volume concentrations were fitted to log-normal distributions using a maximum likelihood method. Since the size range of the aerosol measurements are 0.1 to 3.0 μm, only the accumulation mode of aerosol was considered. The functions used for the fitting were:

$$\frac{dV}{d \ln D} = \frac{V}{\sqrt{2\pi} \ln vV} \exp\left[\frac{-1}{2(\ln vV)^2} (\ln \frac{D}{DVG})^2 \right]. \qquad (4.4)$$

and

$$\frac{dS}{d \ln D} = \frac{S}{\sqrt{2\pi} \ln vS} \exp\left[\frac{-1}{2(\ln vS)^2} (\ln \frac{D}{DSG})^2 \right]. \qquad (4.5)$$

Here DSG and DVG are the geometric mean diameter with respect to the surface and the volume concentrations, respectively. The geometric variances vS and vV were evaluated with respect to the surface area and volume distributions.

The number, surface and volume distributions in the accumulation mode of aerosol particles were deduced from ASASP data during horizontal plume traverses. Figures 9, 10 and 11 illustrate the results of typical plume (line) and ambient air (dot-line) aerosol size distributions. The plume measurements were obtained at a downwind distance of 3.1 km from the stack and 500 m above ground and the background values were taken upwind on 1984 June 11. The background aerosol particle size distributions observed in the Fort McMurray region generally resemble the one in Figure 9 and can be expressed approximately as a power law function of diameter, similar to the Junge distribution (Pruppacher and Klett, 1978). The plume

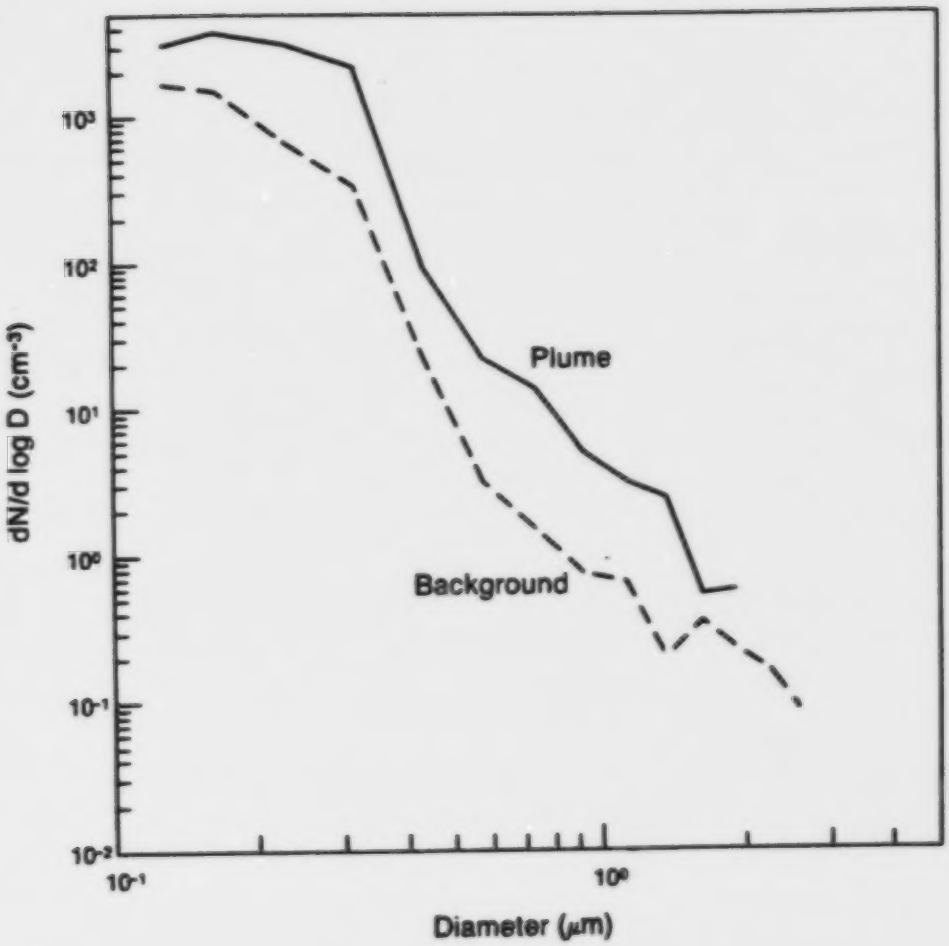

Figure 9. Typical plume (solid line) and ambient air (dashed line) aerosol number distributions observed on 1984 June 11. The plume aerosol measurements were obtained at 3.1 km downwind from the Syncrude stack and 500 m above ground level.

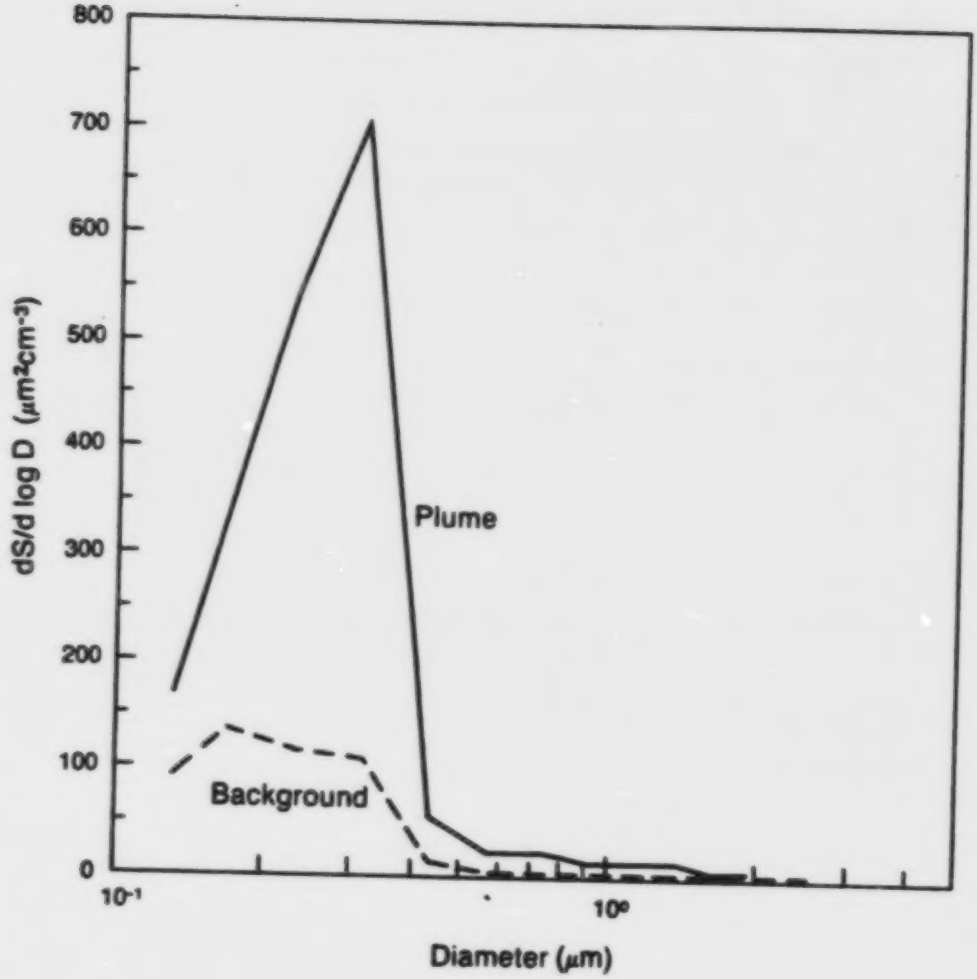

Figure 10. Typical plume (solid line) and ambient air (dashed line) aerosol area distributions observed on 1984 June 11. The plume aerosol measurements were obtained at 3.1 km downwind from the Syncrude stack and 500 m above ground level.

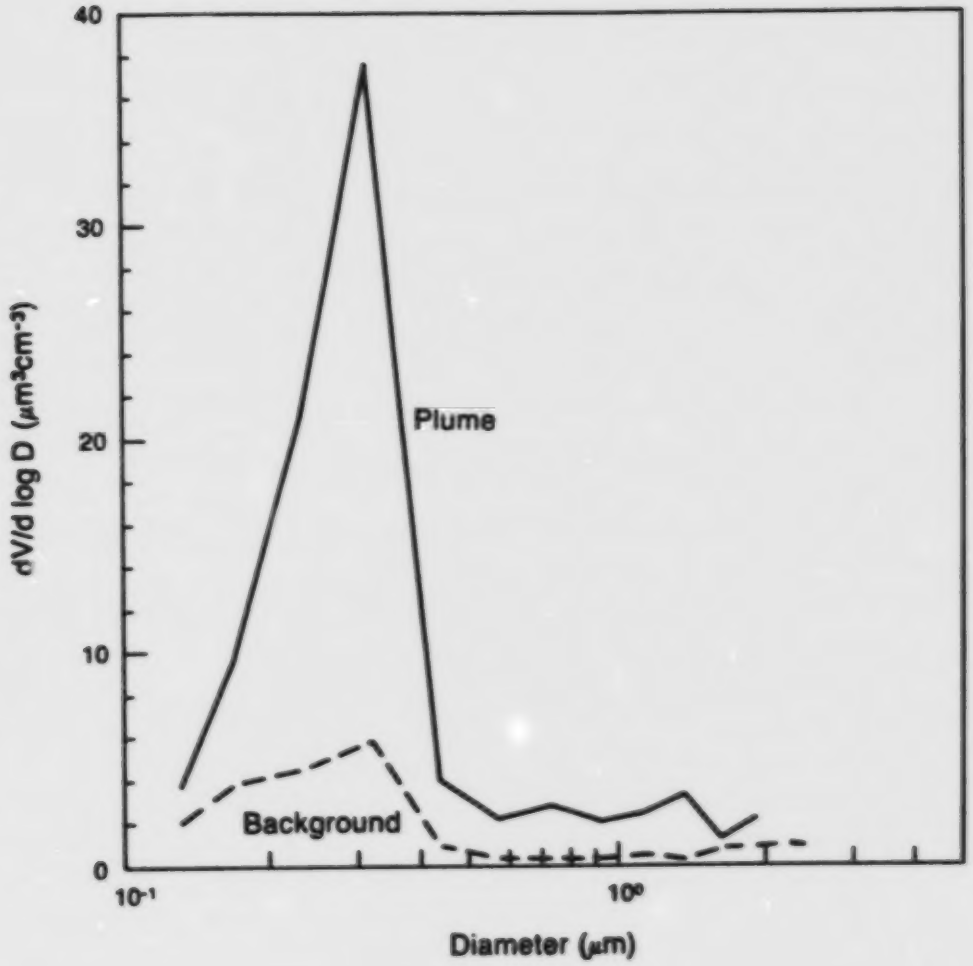

Figure 11. Typical plume (solid line) and ambient air (dashed line) aerosol volume distributions observed on 1984 June 11. The plume aerosol measurements were obtained at 3.1 km downwind from the Syncrude stack and 500 m above ground level.

aerosol size distribution usually shows a predominant maximum or point of inflection at around 0.3 μm diameter. A second maximum or point of inflection, which seems to propagate toward larger size ranges with plume travel time, also exists. Concentrations of aerosols in the plume are much larger than the ambient air, especially for the smaller size particles. As the travel time increases, the differences between the plume and background aerosol size distributions diminish because of mixing.

The background surface area distributions of the aerosol in the Fort McMurray area are similar to Figure 10. A dominant peak exists at about 0.20 μm diameter and the geometric mean diameter is around 0.25 μm. The plume aerosol surface distributions can also be expressed by a log-normal function.

The volume distributions of aerosol particles for plume and background air in the Fort McMurray area also follow the log-normal function, as reported in the literature. The geometric mean volume diameter of background aerosol is about 0.25 to 0.28 μm and the geometric mean volume diameter of the plume aerosols is larger, 0.32 to 0.39 μm. Differences in the geometric mean diameter in the surface and volume distributions between the plume and background aerosols may be due to inherent characteristics of their chemical composition. With the present instrumentation on the aircraft, the true nature of the peak cannot be explained. The evolution of the geometric mean surface and volume diameters of the plume aerosols measured on each pass of the Phase 1 and Phase 3 field experiments are summarized in Tables 11 to 19. The geometric variances, vV and vS, respectively for the surface and volume distributions are also given. The log-normal parameters for background aerosols measured on the same flight are listed in the tables. It seems that there is an overall tendency for the geometric mean sizes of the volume and surface distribution of the plume aerosols to increase rapidly to a maximum at the early plume age and decrease gradually to a more or less constant value thereafter. This suggests at least two prominant processes going on. Particle generation (by gas to particle conversion and

Table 11. Geometric mean diameter, DG, and the variance, v, with respect to volume, V, and surface, S, for the accumulation mode plume (Syncrude) aerosols measured on 1983 March 28.

Plume Age	DGV μm	vV μm	DGS μm	vS μm
Background	0.27	1.82	0.20	1.63
0.06 h	0.37	1.80	0.26	1.80
0.10 h	0.39	1.72	0.29	1.77
0.20 h	0.39	1.72	0.29	1.77
0.28 h	0.37	1.75	0.27	1.79
0.40 h	0.38	1.73	0.28	1.79
0.47 h	0.36	1.75	0.25	1.80
0.60 h	0.34	1.82	0.24	1.80
0.68 h	0.34	1.84	0.24	1.79
0.79 h	0.34	1.84	0.24	1.80
0.89 h	0.32	1.82	0.23	1.77
1.02 h	0.32	1.82	0.23	1.77
1.11 h	0.33	1.86	0.23	1.79
plume mean	0.35	1.79	0.23	1.79

Table 12. Geometric mean diameter, DG, and the variance, v, with respect to volume, V, and surface, S, for the accumulation model plume (Syncrude) aerosols measured on 1983 March 29.

Plume Age	DGV μm	vV μm	DGS μm	vS μm
Background	0.26	1.72	0.20	1.81
0.14 h	0.31	2.06	0.23	1.80
0.27 h	0.33	1.88	0.23	1.86
0.44 h	0.36	1.97	0.22	1.75
0.58 h	0.31	1.92	0.20	1.69
0.77 h	0.29	1.88	0.16	1.50
0.88 h	0.21	1.82	0.20	1.55
plume mean	0.30	1.92	0.21	1.69

Table 13. Geometric mean diameter, DG, and the variance, v, with respect to volume, V, and surface, S, for the accumulation mode plume (Syncrude) aerosols measured on 1983 March 30.

Plume Age	DGV μm	vV μm	DGS μm	vS μm
Background	0.25	1.70	0.20	1.58
0.21 h	0.29	1.97	0.19	1.75
0.35 h	0.31	1.95	0.21	1.79
0.51 h	0.30	1.90	0.22	1.77
0.62 h	0.29	1.88	0.20	1.70
0.80 h	0.28	1.86	0.20	1.75
0.92 h	0.28	1.95	0.19	1.72
1.08 h	0.26	1.88	0.19	1.65
1.21 h	0.26	1.86	0.19	1.62
1.34 h	0.25	1.79	0.19	1.62
1.47 h	0.27	1.90	0.20	1.67
plume mean	0.28	1.89	0.20	1.71

Table 14. Geometric mean diameter, DG, and the variance, v, with respect to volume, V, and surface, S, for the accumulation mode plume (Syncrude) aerosols measured on 1983 March 31.

Plume Age	DGV μm	vV μm	DGS μm	vS μm
Background	0.26	1.72	0.20	1.56
0.51 h	0.27	2.01	0.19	1.69
2.98 h	0.25	1.90	0.18	1.59
10.23 h	0.21	1.70	0.17	1.49
12.95 h	0.19	1.72	0.15	1.43
plume mean	0.19	1.70	0.15	1.43

Table 15. Geometric mean diameter, DG, and the variance, v, with respect to volume, V, and surface, S, for the accumulation mode plume (Syncrude) aerosols measured on 1984 June 07.

Plume Age	DGV μm	vV μm	DGS μm	vS μm
Background	0.29	1.32	0.24	1.20
0.03 h	0.35	1.20	0.29	1.19
0.05 h	0.34	1.16	0.29	1.17
0.07 h	0.33	1.18	0.28	1.18
0.09 h	0.34	1.23	0.28	1.20
0.10 h	0.31	1.15	0.27	1.17
plume mean	0.33	1.18	0.28	1.18

Table 16. Geometric mean diameter, DG, and the variance, v, with respect to volume, V, and surface, S, for the accumulation mode plume (Syncrude) aerosols measured on 1984 June 08.

Plume Age	DGV μm	vV μm	DGS μm	vS μm
Background	0.29	1.18	0.25	1.16
0.05 h	0.38	1.22	0.31	1.19
0.11 h	0.36	1.40	0.29	1.21
0.18 h	0.35	1.29	0.29	1.39
0.35 h	0.33	1.20	0.28	1.37
0.67 h	0.33	1.31	0.28	1.16
0.82 h	0.34	1.28	0.28	1.28
1.05 h	0.32	1.23	0.27	1.23
plume mean	0.34	1.28	0.29	1.26

Table 17. Geometric mean diameter, DG, and the variance, v, with respect to volume, V, and surface, S, for the accumulation mode plume (Syncrude) aerosols measured on 1984 June 11.

Plume Age	DGV μm	vV μm	DGS μm	vS μm
Background	0.29	1.69	0.23	1.21
0.11 h	0.32	1.32	0.26	1.16
0.20 h	0.36	1.73	0.26	1.22
0.22 h	0.35	1.55	0.26	1.20
0.31 h	0.35	1.74	0.25	1.23
0.37 h	0.30	1.26	0.25	1.16
0.66 h	0.29	1.77	0.21	1.22
0.71 h	0.30	1.52	0.23	1.21
0.78 h	0.30	1.23	0.22	1.27
1.02 h	0.30	1.57	0.22	1.21
1.13 h	0.30	1.59	0.22	1.21
1.28 h	0.29	1.48	0.22	1.20
plume mean	0.31	1.52	0.24	1.21

Table 18. Geometric mean diameter, DG, and the variance, v, with respect to volume, V, and surface, S, for the accumulation mode plume (Suncor) aerosols measured on 1984 June 11.

Plume Age	DGV μm	vV μm	DGS μm	vS μm
Background	0.28	1.34	0.23	1.18
0.08 h	0.25	1.82	0.17	1.20
0.11 h	0.28	2.19	0.18	1.23
0.35 h	0.33	2.89	0.18	1.24
0.39 h	0.29	2.44	0.18	1.24
1.16 h	0.28	2.01	0.19	1.22
1.38 h	0.29	2.25	0.19	1.23
1.50 h	0.26	1.60	0.20	1.19
1.58 h	0.29	2.13	0.19	1.23
1.74 h	0.27	1.81	0.19	1.20
plume mean	0.28	2.13	0.19	1.23

Table 19. Geometric mean diameter, DG, and the variance, v, with respect to volume, V, and surface, S, for the accumulation mode plume (Syncrude) aerosols measured on 1984 June 12.

Plume Age	DGV μm	vV μm	DGS μm	vS μm
Background	0.24	1.24	0.20	1.14
0.09 h	0.35	1.60	0.26	1.20
0.14 h	0.29	1.16	0.25	1.13
0.17 h	0.29	1.18	0.25	1.13
0.26 h	0.27	1.12	0.24	1.12
0.89 h	0.28	1.16	0.25	1.13
1.20 h	0.28	1.16	0.25	1.14
1.31 h	0.29	1.23	0.25	1.14
1.34 h	0.29	1.21	0.25	1.14
1.54 h	0.29	1.24	0.24	1.16
1.86 h	0.29	1.27	0.24	1.16
plume mean	0.29	1.23	0.25	1.14

coagulation), followed by dilution. The plume values are significantly different from those of the background. The variances of the volume and surface distributions of plume aerosols, on the other hand, do not show significant correlation with plume age and are similar to the background values.

Because of the relatively clean rural surroundings, the characteristics of the background aerosols are near constant, independent of the wind direction. The volume distributions of the aerosols in the accumulation mode show structures similar to those measured during a power plant study in St. Louis (Cantrell and Whitby 1978). Also, the geometric mean volume diameters and the geometric variances fall within the limits of the results for power plant plumes (Hobbs et al. 1979).

Gas-to-Particle (sulphur dioxide to particulate sulphate) conversion rates can be determined from the changes in the total volume of particles over the plume with travel time. The changes with time in the volume concentration V of particles in an expanding plume, assuming an expanding Lagrangian box model, is given by Hobbs et al. (1979) as:

$$\frac{dV}{dt} = \frac{-d(\ln Vp)}{dt} (V - Va) + R; \qquad (4.1)$$

where Vp is the volume of the plume, Va the volume concentration of particles in ambient air, and R is the rate of production of particle volume by the gas-to-particle conversion in a unit volume of plume. The rate of production can be obtained by solving Equation (4.1) using the finite differencing method if the dilution rate d(ln Vp)/dt is known. It should be noted that other processes, such as sedimentation and particle growth, have been ignored in the equation. The neglect of sedimentation is justified if the terminal velocities of the the particles are very small, of the range 0.0001 to 0.1 cm s^{-1}. The assumption of negligible particle growth is also acceptable because coagulation growth is relatively slow for particles from 0.1 to 10 μm in diameter with total concentrations

less than 10000 cm^{-3} (Pruppacher and Klett, 1978 and Zebel, 1966).

The dilution rate, which mainly depends upon diffusion and wind shear induced mixing, can be determined by either the downwind change in the cross-sectional area of the plume or the change in mean concentration of an inert trace species in the plume. Here, the plume sulphur dioxide is used as a tracer material. The conservation equation for the concentration of sulphur dioxide SO_2 is given as:

$$\frac{dSO_2}{dt} = \frac{-d\ (\ln Vp)}{dt} (SO_2 - SO_2a) - R - Dp; \quad (4.2)$$

where SO_2a is the background sulphur dioxide concentration and Dp is the deposition to the surface. The transformation rate of sulphur dioxide to sulphate is known to be of the order of a few percent per hour and is much smaller than the dilution rate. Thus, it can be dropped from Equation (4.2) without causing serious error in the analysis. The sulphur dioxide concentration at plume centreline is not greatly affected be dry deposition which should be the same order of magnitude as the transformation rate. Hence, the deposition term can be ignored in the equation also. Equation (4.2) can then be written as:

$$\frac{dSO_2}{dt} = \frac{-d\ (\ln Vp)}{dt} (SO_2 - SO_2a). \quad (4.3)$$

Gas-to-Particle conversion rates were calculated from Equation (4.1) using the mean plume particle volumes and dilution rates determined from Equation (4.3) with the plume sulphur dioxide concentration data.

As an example the sulphur dioxide concentration, measured by the SO_2 monitor and averaged over each plume traverse at the plume centreline level, flight on 1984 June 11 for the Syncrude plume is given in Figure 12. During the initial 0.4 hours, the peak SO_2 concentration in the plume was more than 1000 ppb, which is

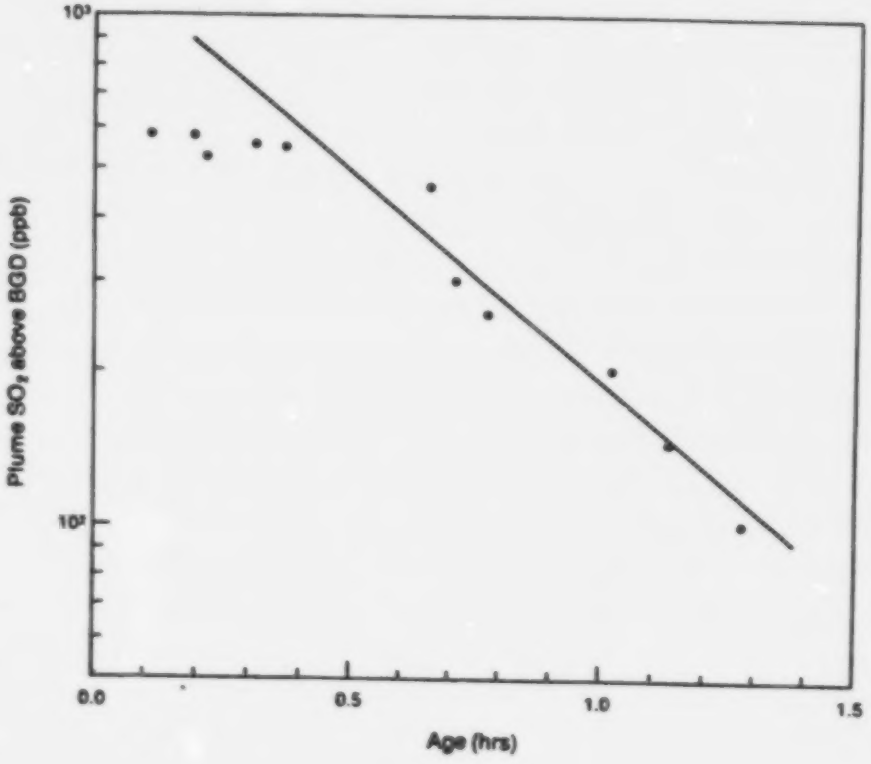

Figure 12. Plume mean sulphur dioxide concentrations as a function of plume travel time (age) for the Syncrude plume measured on 1984 June 11. BGD denotes background concentration.

above the range of the monitor on-board the research aircraft thus the mean SO_2 values reported for the early age of the plume are almost constant. Because of the range limit of the sulphur dioxide monitor, the mean sulphur dioxide concentrations for these passes were not used in the determination of the dilution rate. Using Equation 4.3 and the data points observed from travel time of 0.4 hours onward, the dilution rate was determined to be almost constant, with the value of 2.16 per hour.

The observed total volume concentrations of the plume aerosols smaller than 0.3 um, $0.3<D<1.0$ μm and $0.1<D<3.0$ μm on 1984 June 11 are shown as a function of plume age in Figure 13. The ranges are chosen for the purpose of looking for possible indication of homogeneous or heterogeneous nucleation. The dotted line is for plume aerosols smaller than 0.3 μm, the solid line for particles of $0.3<D<1.0$ μm and the dashed line for aerosols of $0.1<D<3.0$ μm. Although natural variations and measurement errors are undoubtedly present, a decline in total volume with increasing plume age is clear in all size ranges. The volume concentration of the smaller particles seems to decrease at a slower rate in the plume studied. The reduction of plume aerosol volume concentrations, which is offset somewhat by the gas-to-particle production, is due to the expansion of the plume caused by diffusion and wind shear. Similar results are obtained from other research flights.

The changes in aerosol volume due to gas-to-particle conversion during the 1984 June 11 Syncrude flight are shown in Figure 14. The dotted line is for plume aerosols smaller than 0.3 μm, the solid line for particles of $0.3<D<1.0$ μm and the dashed line for aerosol of $0.1<D<3.0$ μm. Over the plume travel time of 1.3 hours, the gas-to-particle productions of aerosol volume for particles of the size range studied decreased while the plume age increased. The volume production for particles $0.3<D<1.0$ μm was about one order of magnitude smaller than that of particles smaller than 0.3 μm. Close to the stack (travel time less than one hour) where sulphur dioxide and aerosol concentrations were high, the volume production for particles $1.0<D<3.0$ μm was comparable to that of particles smaller than 0.3 μm.

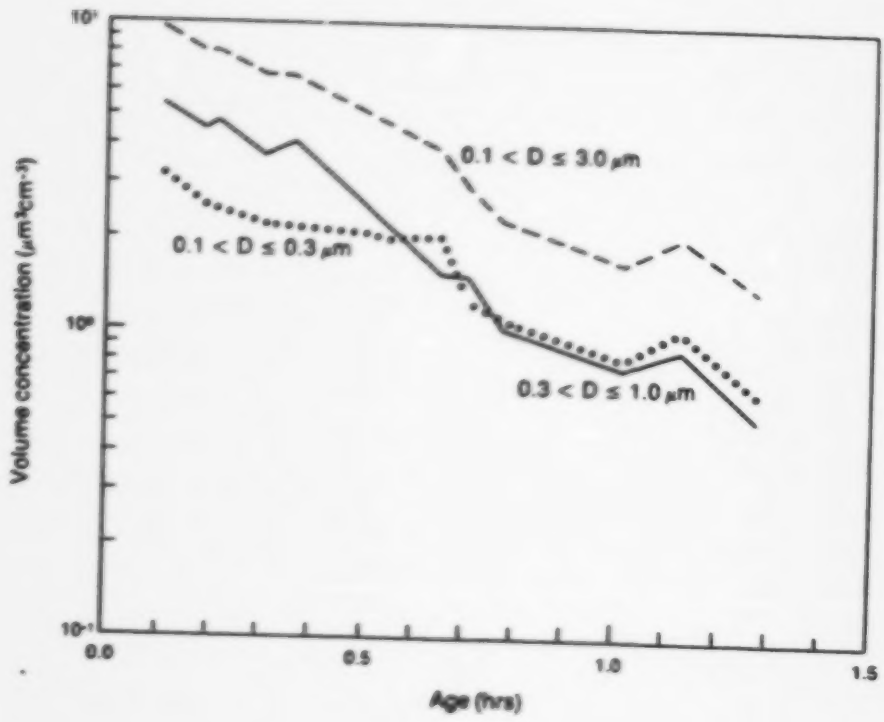

Figure 13. Plume aerosol total volume concentrations for particles smaller than 0.3 μm, 0.3<D<1.0 μm and 0.1<D<3.0 μm as a function of plume age for the Syncrude plume measured on 1984 June 11.

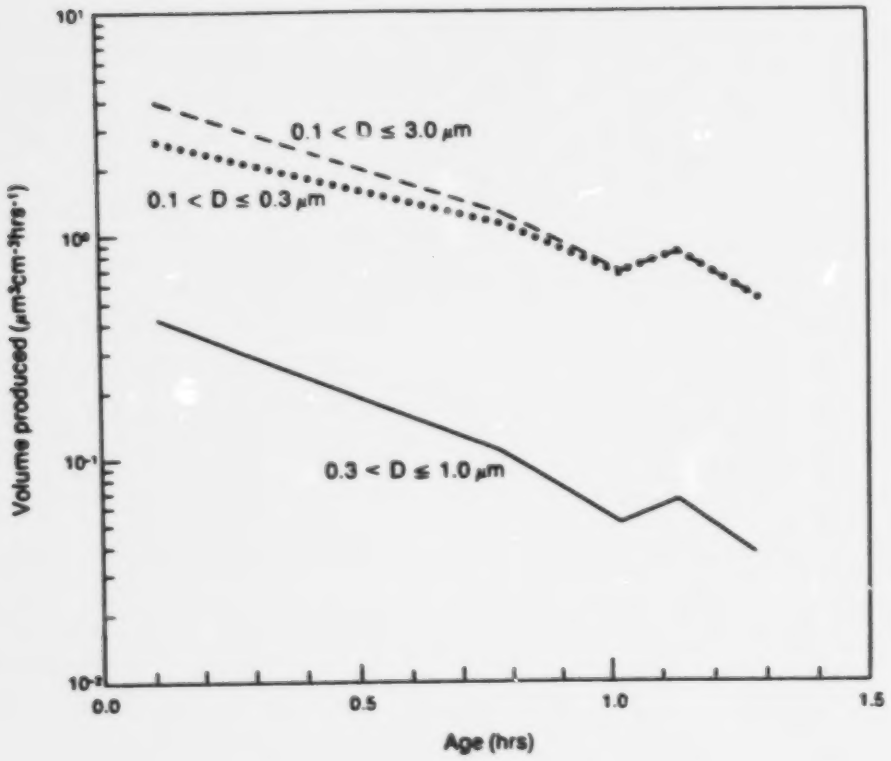

Figure 14. Excess aerosol volume productions for particles smaller than 0.3 μm, 0.3<D<1.0 μm and 0.1<D<3.0 μm as a function of plume age in the Syncrude plume on 1984 June 11.

Since homogeneous-heteromolecular nucleation (self-nucleation of two or more gaseous species without involvement of foreign bodies) will not produce particles larger than 1 μm, and coalgution is negligible for $0.1<D<10$ μm particles and total concentrations less than 10000 cm^{-3}, any increase in aerosol volume for particles larger than 1 μm is likely due to heterogeneous nucleation (nucleation of gaseous species onto a foreign body). If the excess aerosol volume products are all sulphates, the results suggest that heterogeneous conversion of sulphur dioxide to particulate sulphate may be appreciable under certain meterological conditions and close to the emission source. Heterogeneous catalysts such as vanadium, manganese and iron, associated with the surface of particles may contribute to the formation of acid droplets and surface crystals (Freiberg 1974 and Cheng et al. 1982). It has also been suggested that heterogeneous catalytic SO_2 oxidation on carbon soot particles covered with water film may be important in the generation of sulphate aerosols in the atmosphere (Benner et al. 1982 and Britton and Clarke 1980). This may probably be the reason for the significant transformation of SO_2 to SO_4 observed in winter. It might be added here that analysis of fly ash from the Syncrude chimmey showed that iron is by far the most abundant metal present (Bottenheim 1982). Similar results were obtained for other research flights of similar distance from the emission stack (plume travel time). Far from the stack the volume production rate of aerosols smaller than 0.3 μm seemed to increase or remain constant with plume age. At this distance the volume production of larger particles was reduced so as to undetectable.

The determination of the conversion rate of sulphur dioxide to particulate sulphate from the excess aerosol produced requires information on the chemical composition of the transformation product in the size range considered. Such information is not available in the present study. Ammonia is abundant in the Alberta atmosphere, therefore $(NH_4)_2SO_4$ and NH_4NO_3 may be formed by reaction with SO_2 and NH_3. This may occur in the gas phase or in the aquatic phase where SO_2 would exist as HSO_3^-.

Sulphuric acid particles can also be formed by the photo-oxidation of sulphur dioxide. Assumptions that the excess aerosol volume produced is sulphuric acid or ammonium sulphate, or combinations of the two have been made. The results are very similar. That is, the assumption that the gas-to-particle conversion product is sulphuric acid or that it is ammonium sulphate does not make a significant difference in the transformation rate calculation. As an example, the calculated gas-to-particle transformation rate for the June 11, 1984 Syncrude plume is shown in Figure 15. The dotted line is the conversion rate obtained from the excess volume production of particle smaller than 0.3 μm, and the solid line is from aerosols of $0.3<D<1.0$ μm. The conversion product of sulphuric acid is assumed for these calculations. The dashed line in Figure 15 is calculated from the excess volume production of particles $0.1<D<3.0$ μm and the assumption that the transformation product is ammonium sulphate. At plume travel times longer than 0.8 hour, as illustrated in Figure 14, significant aerosol volume production of particles was observed only for particles smaller than 0.3 μm. Note that the conversion rates obtained from the two assumptions are almost equal during this plume travel time. An apparent increase in sulphur dioxide to particulate sulphate conversion rate with plume travel time was noted in this case. Evidence of an increase in conversion rate with increasing plume age was also found by Cantrell and Whitby (1978) and an increasing rate with plume age was reported in chamber studies of SO_2 photooxidation by Kocmond et al. 1975.

The results from the field experiments are summarized in Table 20. The date and time of the measurements, plume age, dilution rate, excess volume production rates of various aerosol size ranges and gas-to-particle conversion rate of sulphur dioxide to sulphate are listed. The aerosol volume production rate for particles larger than 1 μm is comparable to that of the smaller aerosol. This is particularly apparent at short plume travel times when the particle and sulphur dioxide concentrations are large.

The conversion rates of sulphur dioxide to particulate sulphate, determined from the field measurements with the assumption

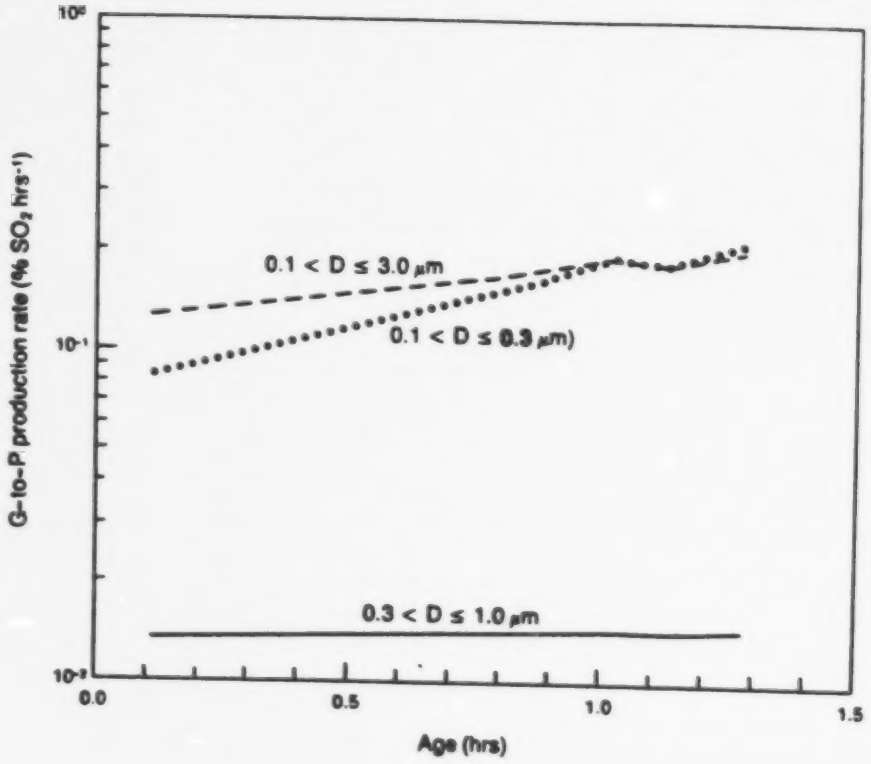

Figure 15. Gas-to-particle conversion rate of sulphur dioxide to sulphate as determined from aerosol smaller than 0.3 μm, 0.3<D<1.0 μm and 0.1<D<3.0 μm as a function of plume age for the Syncrude plume on 1984 June 11.

Table 20. Summary of the ranges of plume age at the cross-sectional traverses, the dilution rate, the aerosol volume production rates for various aerosol size intervals and the conversion rate of SO_2 to SO_4 determined by the excess aerosol volume production method.[a]

Date (dd/mm/yy)	Time (Local)	Plume age (hour)	Dilution Rate ($hour^{-1}$)	Aerosol Volume Production Rate ($um^3\ cm^{-3}\ h^{-1}$)			Conversion Rate (% h^{-1})
				$0.1<D\leq0.3$ um	$0.3<D\leq1.0$ um	$1.0<D\leq3.0$ um	
280383	1541-1726	0.06-1.11	5.70-0.73	5.90-0.18	12.4-0.18	7.33-0.20	0.49-2.81
290383	1522-1740	0.16-0.78	7.41-1.70	1.37-0.04	5.69-0.00	3.14-0.07	0.26-1.00
300383	0722-1041	0.18-1.52	3.47-1.86	0.98-0.08	0.87-0.04	1.50-0.14	0.42-0.65
310383	1710-1907	1.50-11.5	0.58-0.07	0.22-0.10	0.01-0.00	0.00-0.00	0.02-1.34
070684	1556-1750	0.03-0.10	64.6	21.83-0.57	140.42-9.25	99.92-3.16	4.70-6.01
080684	1003-1240	0.05-1.05	2.56	1.52-0.37	0.85-0.17	0.91-0.31	2.67-5.18
110684	0520-0655	0.11-1.30	2.16	2.62-0.58	0.42-0.04	0.91-0.01	0.11-0.21
110684[b]	0655-0822	0.08-1.73	1.33	4.47-1.09	0.33-0.05	1.13-0.28	0.35-0.73
120684	0559-0852	0.08-1.87	5.87-0.52	1.46-0.05	3.15-0.03	1.10-0.14	0.06-0.29

[a] Syncrude plumes

[b] Suncor plume

that the excess aerosol volume product is sulphate, varied from 0.02% to 2.81% h^{-1} during March 1983 and from 0.06% to 8.66% h^{-1} during June 1984.

The conversion rates of SO_2 to SO_4 were also calculated from results of chemical analysis of filter samples. The cellulose front filter, used to collect particulate sulphate, and the triethanolamine treated back filter, used to collected gaseous SO_2, were extracted with double distilled water using ultrasonic agitation. The extracts were analyzed by ion chromatography (Dionex 2020i) utilizing a high preformance (HPIC-AS4) separator column and a fiber suppressor column. The eluent was 0.0018 M sodium carbonate and 0.0021 M sodium hydroxide. Extracts of the triethanolamine treated filters were treated with bromine prior to ion chromatography to ensure complete oxidation of the sulphur. The ratio of the SO_4 collected on the cellulose filter to the SO_2 trapped by the triethanolamine treated filters was used to calculate the rate of conversion of SO_2 to SO_4 in the plume.

Sulphate concentrations measured in the plume during the December 1983 sampling period ranged from 0.29 $\mu g\ m^{-3}$ close to the Syncrude stack to 7.4 $\mu g\ m^{-3}$, 4.6 hours later at a distance of 35 km from the stack (Table 21). During the June 1984 sampling, sulphate concentrations ranged from 0.8 $\mu g\ m^{-3}$ near the Syncrude stack to as high as 6.9 $\mu g\ m^{-3}$, 9.8 km downwind (Table 22). On June 11, 1984 the Suncor plume was sampled. Sulphate concentrations were relatively high compared to those found in the Syncrude plume, values of 5.2 $\mu g\ m^{-3}$ at a distance of 1.8 km from the stack and 7.3 $\mu g\ m^{-3}$ at 19 km downwind were measured.

Sulphur dioxide to particulate sulphate conversion rates were low ranging from not measurable to 2.0% h^{-1} during December 1983 and from not measurable to 2.9% h^{-1} in June 1984. In general, the lowest conversion rates were found when SO_2 concentrations were highest. The conversion rates obtained from the chemical analysis of filter samples agreed reasonably well with those calculated from the excess aerosol volume productions.

Lusis et al. (1978) found conversion rates of -1.2% to

Table 21. Sulphur dioxide, particulate sulphate and SO_2 to SO_4 conversion rates as a function of distance from the source and plume age as determined by chemical analysis. December 1983.

Date DDMMYY	Time local	Mean plume travel (km)	Mean plume age (hour)	Mean SO_2 (ppb)	Mean SO_4 ($\mu g\ m^{-3}$)	Total SO_2 (as SO_4 $\mu g\ filter^{-1}$)	Total SO_4 ($\mu g\ filter^{-1}$)	Conversion rate ($\%\ h^{-1}$)
141283	1057-1026	1.0	0.2	103.5	0.29	301	7.1	ND
141283	1133-1158	33.0	4.6	49.4	5.37	221	28.5	2.0
141283	1238-1307	35.0	4.6	74.1	7.36	277	32.9	1.8
151283	1018-1044	0.6	0.0	66.7	0.45	286	4.1	ND
151283	1048-1130	24.0	1.3	32.5	0.99	219	4.5	0.5
151283	1136-1213	45.0	2.4	15.7	0.36	52	2.0	1.0
171283	1438-1514	9.3	0.3	45.2	0.68	248	5.7	ND
171283	1531-1557	26.0	1.0	81.4	4.96	342	10.1	0.9

continued....

Table 21. Concluded.

Date DDMMYY	Time local	mean plume travel (km)	mean plume age (hour)	mean SO_2 (ppb)	mean SO_4 ($\mu g\ m^{-3}$)	total SO_2 (as SO_4 $\mu g\ filter^{-1}$)	total SO_4 ($\mu g\ filter^{-1}$)	conversion rate (% h^{-1})
191283	1434-1500	3.0	0.2	198.6	3.03	359	9.1	ND
191283	1522-1543	18.0	1.3	142.3	3.50	248	7.3	0.6
191283	1559-1630	60.0	4.5	189.2	2.42	355	8.9	0.0
201283	1110-1135	3.3	0.1	49.4	2.23	199	3.9	ND
201283	1144-1206	60.0	2.5	15.7	0.64	79	2.2	0.3

Table 22. Sulphur dioxide, particulate sulphate and SO_2 to SO_4 conversion rates as a function of distance from the source and plume age as determined by chemical analysis. June 1984.

Date DDMMYY	Time local	Mean plume travel (km)	Mean plume age (hour)	Mean SO_2 (ppb)	Mean SO_4 ($\mu g\ m^{-3}$)	Total SO_2 (as SO_4 $\mu g\ filter^{-1}$)	Total SO_4 ($\mu g\ filter^{-1}$)	Conversion rate (% h^{-1})
070684	1632-1652	12.6	0.3	23.7	2.30	61	1.3	ND
070684	1724-1743	33.3	1.0	13.9	1.20	15	0.7	3.4
080684	1024-1050	6.5	0.3	33.0	1.50	80	1.1	ND
080684	1052-1129	28.3	1.2	24.5	1.10	49	1.5	1.8
080684	1133-1155	35.6	1.5	24.9	1.50	39	1.0	1.0
090684	0508-0539	5.5	0.2	104.7	3.50	720	3.3	ND
090684	0541-0618	13.3	0.6	100.0	2.80	680	3.1	0.0
090684	0619-0652	22.5	1.0	92.4	2.20	480	2.2	0.0
090684	0654-0728	30.1	1.3	135.2	3.60	815	3.8	0.0

continued.....

Table 22. Concluded.

Date DDMMYY	Time local	mean plume travel (km)	mean plume age (hour)	mean SO_2 (ppb)	mean SO_4 ($\mu g\ m^{-3}$)	total SO_2 (as SO_4 $\mu g\ filter^{-1}$)	total SO_4 ($\mu g\ filter^{-1}$)	conversion rate (% h^{-1})
100684	0925-0959	9.7	0.7	60.9	3.10	304	3.1	ND
100684	1005-1036	14.2	1.0	57.2	3.90	267	3.7	1.2
110684	0551-0625	9.8	0.7	202.4	6.90	1230	6.9	ND
110684	0627-0655	19.5	1.4	91.3	2.10	332	1.8	0.0
110684[a]	0701-0732	1.8	0.1	148.1	5.20	719	5.1	ND
110684	0737-0809	19.0	1.4	62.3	7.30	247	7.3	1.7
120684	0618-0650	5.1	0.2	47.5	0.80	214	0.8	ND
120684	0652-0723	17.6	0.7	48.3	1.10	185	1.0	0.3
120684	0724-0756	34.3	1.4	48.3	1.00	164	1.0	0.2

[a] Suncor plume

2.4% h^{-1} during February of 1977 for the GCOS (Suncor) plume and 0% (-0.2%) to 3.3% h^{-1} during June of 1977. Bottenheim (1982) studied the plumes from the two plants investigated in this report and obtained SO_2 to SO_4 transformation rates of 0% (-15.7%) to 24% h^{-1} in January, 0% (-3.5%) to 1.5% h^{-1} in March and 0% (-0.7%) to 2.6% h^{-1} in July 1980. The conversion rates obtained in the present study, hence, are not inconsistent with the earlier results. During the same season, the conversion rate apparently depends upon the time of the day. The transformation increased from early morning to a maximum at noon or early afternoon and decreased again thereafter in response to solar radiation, illustrating the importance of photochemical reactions in SO_2 to SO_4 conversion.

Based on the average SO_2 oxidation rates obtained during winter and early morning flights, Lusis et al. (1978) concluded that there was no evidence for a heterogeneous SO_2 oxidation mechanism. However, contrary to the conclusion of Lusis et al., Bottenheim (1982) suggested that an iron-catalyzed oxidation mechanism in the liquid phase was responsible for the significant SO_2 to SO_4 transformation during the first hour of plume travel which was observed in the winter of 1982. In fact, conversion rates observed at close distances from the stack during the winter or early morning summer flights in 1977 by Lusis et al. were as high as those transformation rates obtained at daylight hours in the summer. Hence, the importance of the heterogeneous catalytic oxidation mechanism in the generation of sulphates in the plume close to the emission source and under certain atmospheric conditions (possibly high humidity or cold temperature, such that emitted particles may be wet) cannot be ignored.

5. CONVERSION RATES OF NITRIC OXIDE TO NITROGEN DIOXIDE

The relative amounts of NO and NO_2 strongly affect the chemistry of pollutants in the atmosphere, especially the concentration of ozone. Ratios of NO_2 to NO which exceeded 10 may lead to the formation of ozone in concentrations exceeding the Provincial Standard of 80 ppb. Thus, the rate of conversion of NO to NO_2 in the oil sands extraction plant plumes is of importance.

Previous studies of power plant plumes by Hegg et al. (1977) indicated that the NO conversion rate of NO to NO_2 is controlled by the rates at which the plume mixes with the ambient air rather than by chemical kinetics. The main chemical reaction by which high concentrations of NO are converted to NO_2 in a power plant plume is:

$$NO + O_3 \xrightarrow{k_1} NO_2 + O_2 \qquad (5.1)$$

Under the influence of sunlight, ozone may be generated by the reactions:

$$NO_2 + h\nu \xrightarrow{k_2} NO + O; \text{ and} \qquad (5.2)$$

$$O + O_2 + M \xrightarrow{k_3} O_3 + M; \qquad (5.3)$$

where the k's are rate constants.

Thus, under photochemically steady state conditions, the relationship among O_3, NO_2, and NO is given by:

$$[O_3] = \frac{k_2\,[NO_2]}{k_1\,[NO]} \; . \qquad (5.4)$$

Under winter conditions at Fort McMurray, the value of k_2/k_1 has been calculated as 11 ppb, therefore, a NO_2/NO ratio of 8 would be required to give an ozone concentration above 80 ppb

(Bottenheim et al. 1977). Under summer conditions the k_2/k_1 ratio was calculated as 16 ppb and an NO_2/NO ratio of 5 would produce 80 ppb.

The rate of conversion of NO to NO_2 was measured in the December 1983 and June 1984 field experiments. Stable atmospheric conditions during the field studies provided an unparallelled opportunity to examine the behaviour of NO in the plume and to define the processes controlling the rate of conversion to NO_2. Nitric oxide and nitrogen dioxide measurements were made once a second during each traverse of the plume by the aircaft in December 1983. The data sampling rates were increased to 10 Hz during the June 1984 period. With typical aircraft true air speed of 80 m s^{-1}, the spatial resolution of the data is 80 m in December and 8 m in June. The two channels of the NO-NO_x monitor had different lag times, resulting in an offset of 4.1 seconds between the two channels. This offset was taken into consideration during calculation of NO to NO_2 ratios.

Figure 16 shows examples of the cross-sectional profiles of NO and NO_2 in the Syncrude plume measured on June 11, 1984. Measurements were obtained from 3.1 km downwind from the stack (travel time 6.72 min) and 500 m above ground and 5.4 km (travel time 13.14 min) and 501 m above ground. The maximum values of NO and NO_2 concentrations at 3.1 km were 158 and 50 ppb, respectively. The NO and NO_2 profiles both display distinct double maxima, created by either the over-turning of the thermal buoyancy of the emission plume or the oxidation reaction of NO and O_2 to form NO_2, which is probably important initially at high NO concentration. The maximum NO and NO_2 concentrations observed at 5.4 km were 143 and 48 ppb, respectively. The double maxima characteristics of the NO and NO_2 concentrations disappear from the earlier pass illustrating that the thermal buoyancy was lost.

For each pass of the aircraft through the plume the NO_2 to NO ratio was calculated on a point by point basis after corrections were made for instrument response characteristics. The NO_2/NO ratios for the two traverses presented earlier are given in

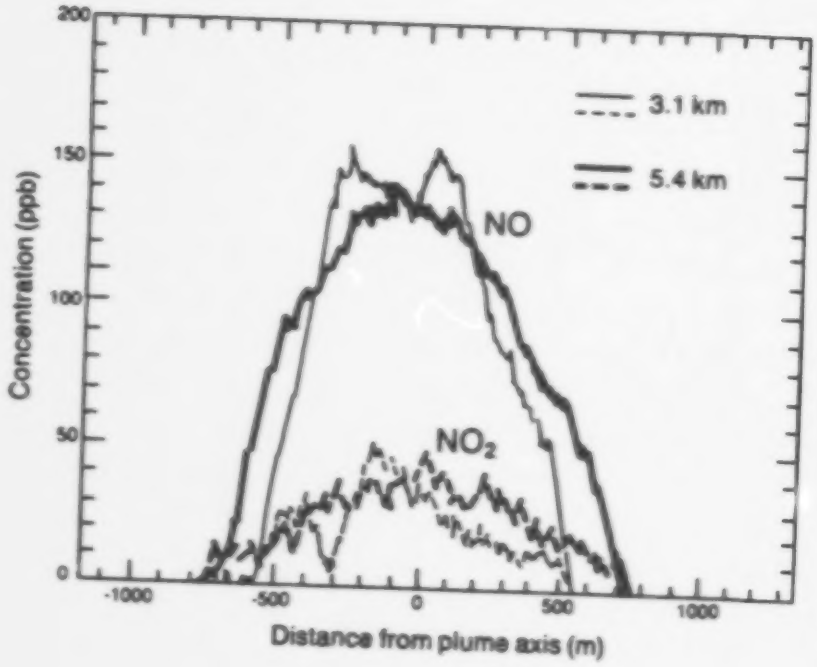

Figure 16. Cross-sectional profiles of NO and NO_2 measured at 3.1 and 5.4 km from the Syncrude stack about 500 m above ground on 1984 June 11.

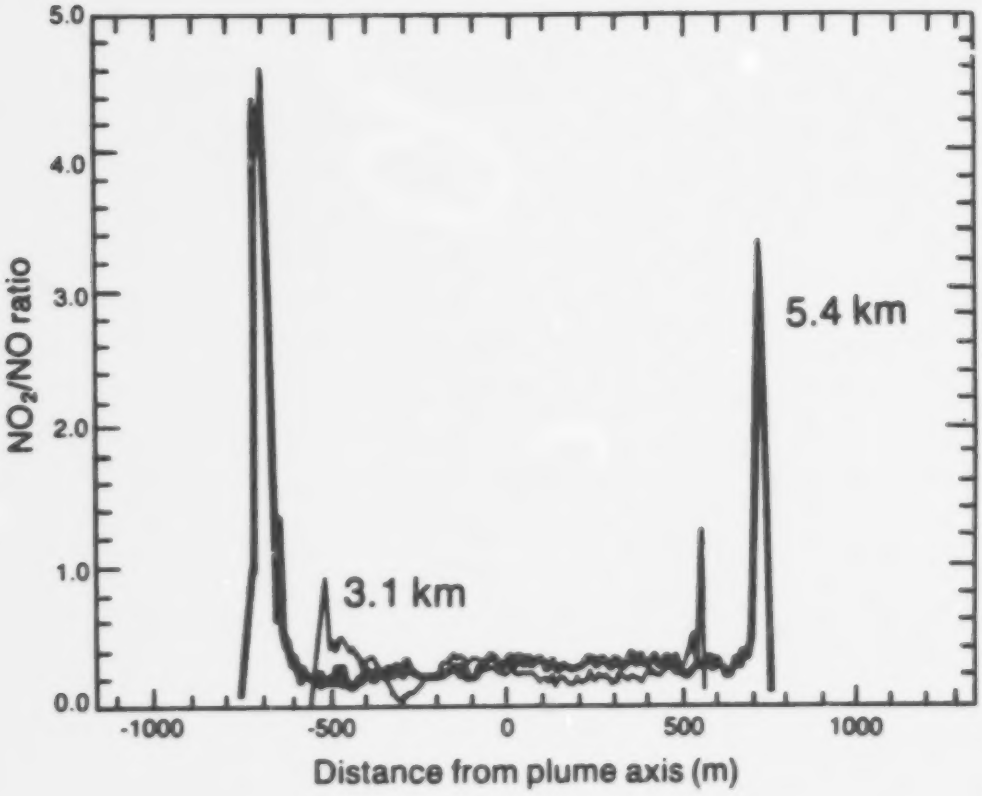

Figure 17. Cross-sectional profiles of NO_2/NO ratio measured at 3.1 and 5.4 km downwind from the Syncrude stack about 500 m above ground on 1984 June 11.

Figure 17. Both profiles show much higher NO_2/NO ratios on the outer edges than at the centre of the plume. Note that the regions of higher NO_2/NO ratio (reaction zones) are very narrow, of the order of 100 m, compared to the plume width which is of the order of 1000 m. The ratios of NO_2/NO were relatively uniform inside the plume. At the centre of the plume the NO_2/NO ratios increase only slightly from about 0.3 to 0.4. These values were significantly smaller than those predicted from theoretical parameters if photochemical equilibrium was assumed (Leahey, 1983). At the edges of the plume, the NO_2/NO ratios observed were more in keeping with the predicted values. The slightly asymmetric pattern of the NO_2/NO ratio profiles may be caused by the aircraft not flying exactly orthogonal to the plume trajectory, although great efforts were made to fly orthogonally, another explanation might be the effects of wind shear. The occurrence of high NO_2/NO ratios on the edges of the plume is in keeping with the conversion of NO to NO_2 by reaction with ozone. The reaction takes place quickly with a reaction time of about one minute. Hegg et al. (1977) considered the behaviour of a plume which is not in a photochemical steady state; that is, the plume has not been uniformly mixed with the surrounding air and ozone reacted with NO. They proposed that a diffusing plume may not be in photochemical equilibrium because the turbulent mixing time over the spatial scale of the plume may be short compared to the chemical relaxation times. Over a small enough spatial scale, the mixing times are short compared to the chemical reaction times. The relative size of this sub-scale to the plume mixing scale determines the extent to which a plume is in steady state. If the reaction is fast compared to mixing times over the scale of the plume, the reactant species become spatially segregated with the reaction occuring entirely within a relatively narrow reaction zone between the two spatial regions. The width of the reaction zone is essentially that spatial sub-scale over which the mixing time is comparable to the chemical relaxation time. The NO_2/NO ratios shown in Figure 17 clearly follow the behaviour predicted by Hegg et al. with reaction taking place on the periphery of the plume (Figure 1

in Hegg et al. 1977). The well known ozone deficits associated with power plant plumes are, in fact, manifestations of spatial segregation of reactant species. Thus, the conversion of NO to NO_2 should be confined mainly to the narrow reaction zones on the periphery of the plume. Turbulent mixing brings the converted NO_2 inside the plume and eventually produces an uniform field of NO_2/NO ratios in the centre of the plume.

The cube root of the turbulent energy dissipation rate $\varepsilon^{1/3}$ is an estimate of turbulence intensity (MacCready 1964). Turbulence measurements along the traverses displayed in Figure 16 are shown in Figure 18. The turbulent energy dissipation rate seems to be higher inside the plume than outside, because of the extra thermal buoyancy effect at early plume age. Turbulent mixing is then more intense in the centre than at the edges of the plume.

The conversion rate of NO to NO_2 was calculated for the entire plume using the method described below.

Assuming an expanding Lagrangian box model, the total rate of change of the plume mean NO_2 can be expressed as:

$$\frac{d}{dt}[NO_2] = -[NO_2]\frac{d \ln Vp}{dt} + R[NO]; \qquad (5.5)$$

where Vp is the plume volume, R is the transformation rate of NO to NO_2, and [NO] and $[NO_2]$ are the plume-averaged concentrations of NO and NO_2 respectively. The first term on the right hand side of the equation represents the dilution of NO_2 caused by an increase of plume volume due to diffusion and shear effects. The second term is the chemical conversion rate (5.1). Background concentration of NO_2 is assumed to be negligible in Equation 5.5. This assumption is acceptable according to the field measurements in the study area.

Similarly, the conservation equation for NO can be written as:

$$\frac{d}{dt}[NO] = -[NO]\frac{d \ln Vp}{dt} - R[NO]. \qquad (5.6)$$

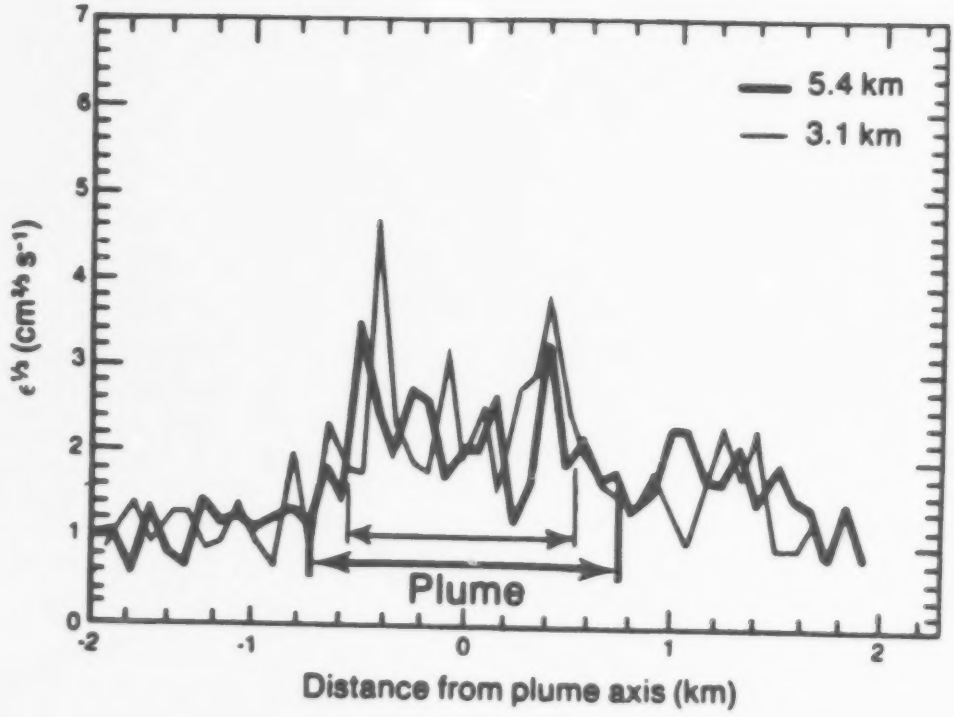

Figure 18. Cross-sectional profiles of the cube root of the turbulent energy dissipation rate measured at 3.1 and 5.4 km downwind from the Syncrude stack about 500 m above ground on 1984 June 11.

Background NO concentration is also assumed to be negligible in the above equation.

Equations 5.5 and 5.6 can be combined to eliminate the dilution rate (d ln Vp/dt) and manipulated to give the following equation:

$$\frac{d}{dt} \ln \left(\frac{[NO]}{[NO] + [NO_2]} \right) = - R. \qquad (5.7)$$

Thus, the slope of a semi-logarithmic plot of the ratio of nitric oxide to the total oxides of nitrogen against time gives the conversion rate of NO to NO_2. As an example, the measurements obtained on 1984 June 11 for the Syncrude plume are shown in Figure 19. Only data values believed to be those of the mean at the centreline of the plume were used. Note that the data points fall close to a straight line. The greater scatter found for the older age of the plume is probably due to the low NO and NO_2 concentrations which are close to the detection limit of the monitor and thus are not reliable. Least squares regression gives the slope of the line of best fit to be -1.32 h^{-1} (-2.19% min^{-1}) with a correlation coefficient of -0.95.

Using this procedure, the mean conversion at the plume centre level was determined for each plume study in Phase 2 and Phase 3 of the project. The results are summarized in Table 23. Rates varied considerably from 0.2% min^{-1} to 21.4% min^{-1}. At first glance the conversion rate of NO to NO_2 appears to depend upon the amount of sunlight. During the December 1983 field experiment the transformation rate appeared to increase with time, reaching a maximum at about noon or slightly after noon, after which it declined. During the June 1984 study period the conversion rate of NO to NO_2 was very low at dawn (0500) and increased with time. However, the suggested increases in the conversion rate of NO to NO_2 with time may be due to increased turbulence. Apparently, the transformation rate is higher in the summer than in the winter

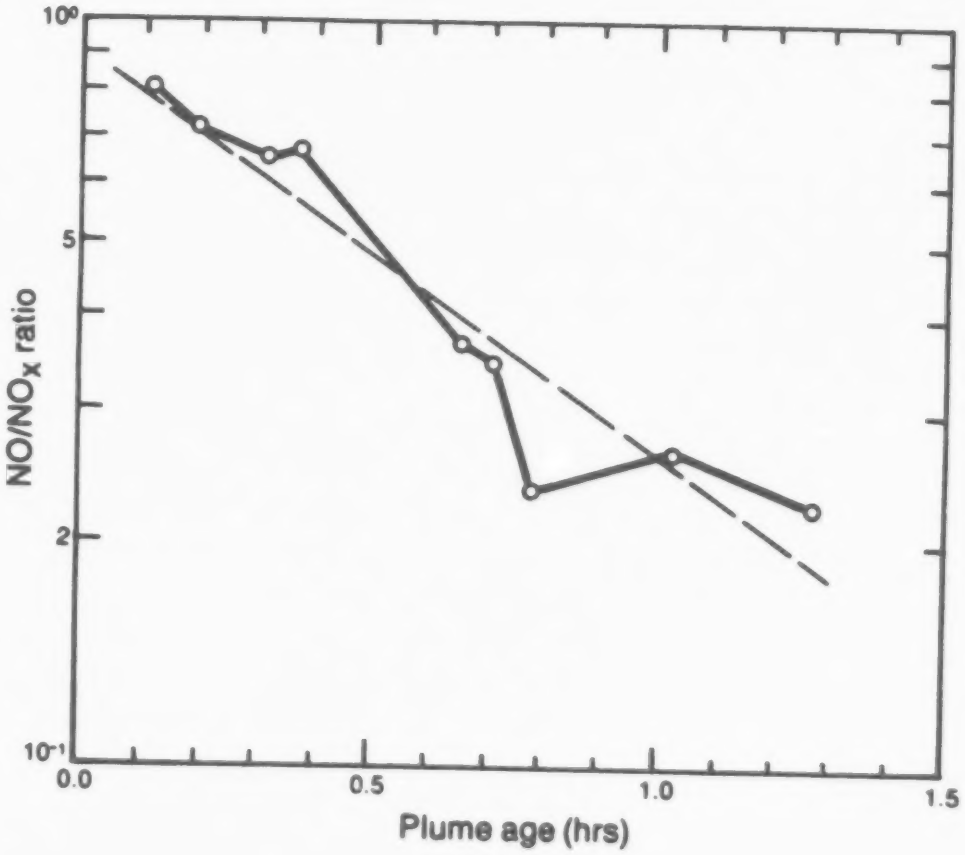

Figure 19. Mean NO/NO_x ratios as a function of travel time for the Syncrude plume measured on 1984 June 11.

Table 23. NO to NO_2 conversion rate for nine plume case studies.

Date (YYMMDD)	Time (local)	Source	Conversion Rate % min^{-1}
83/12/15	0950-1306	Suncor	1.0
83/12/17	1417-1614	Syncrude	2.4
83/12/19	1417-1647	Syncrude	1.7
83/12/20	1052-1349	Syncrude	4.1
84/06/08	1003-1241	Syncrude	21.4
84/06/09	0455-0745	Syncrude	0.2
84/06/11	0520-0655	Syncrude	0.5
84/06/11	0655-0822	Suncor	2.2
84/06/12	0559-0852	Syncrude	1.0

(possibly because of the higher sun angle or the increase in turbulent mixing).

Figure 20 gives the plume averaged turbulence $\varepsilon^{1/3}$ and the travel time of the Suncor plume measured on 1984 June 11. Close to the stack the turbulence was stronger because of the effect of thermal buoyancy. This dissipated within 0.3 hour, thereafter turbulence in the plume was the same as in the ambient air. It was shown earlier that the reaction zone is at the periphery of the plume where the turbulence has a value similar to that of the environment. If turbulent mixing is the controlling factor on the conversion of NO to NO_2 in the plume, the environmental turbulent energy dissipation rate should correlate well with the mean transformation rate of NO to NO_2.

Figure 21 shows the NO to NO_2 conversion rates and the cube root of the ambient turbulent energy dissipation rates determined for the cases studied. The inset in the figure shows one datum which does not fit into the scales in Figure 21. The turbulent energy dissipation rates are those measured outside of the plume in the surrounding air and they represent the environmental turbulence. There seems to be a direct relationship between the turbulent mixing and the NO to NO_2 conversion rate. When the turbulent energy dissipation rate is high, the transformation of NO to NO_2 is fast, or vise versa. The linear line of the conversion rates and $\varepsilon^{1/3}$ (excluding the very high NO to NO_2 conversion rate) has a slope of 4.5, with a correlation coefficient of 0.81. The regression line is shown in Figure 21 and the inset. Note that the very high conversion rate observed also lies very close to this regression line. It appears that turbulent mixing, with a minimum value of the cube root of the turbulent energy dissipation rate of about 0.78 $cm^{2/3}\ s^{-1}$, is necessary to maintain significant conversion of NO to NO_2 in the plume. This suggests that the ozone concentrations in the near-field plume deplete almost instantaneously by oxidation of NO. Continued mixing is required to supply more ozone from the ambient air for the NO to NO_2 transformation. This should have significant influence on the

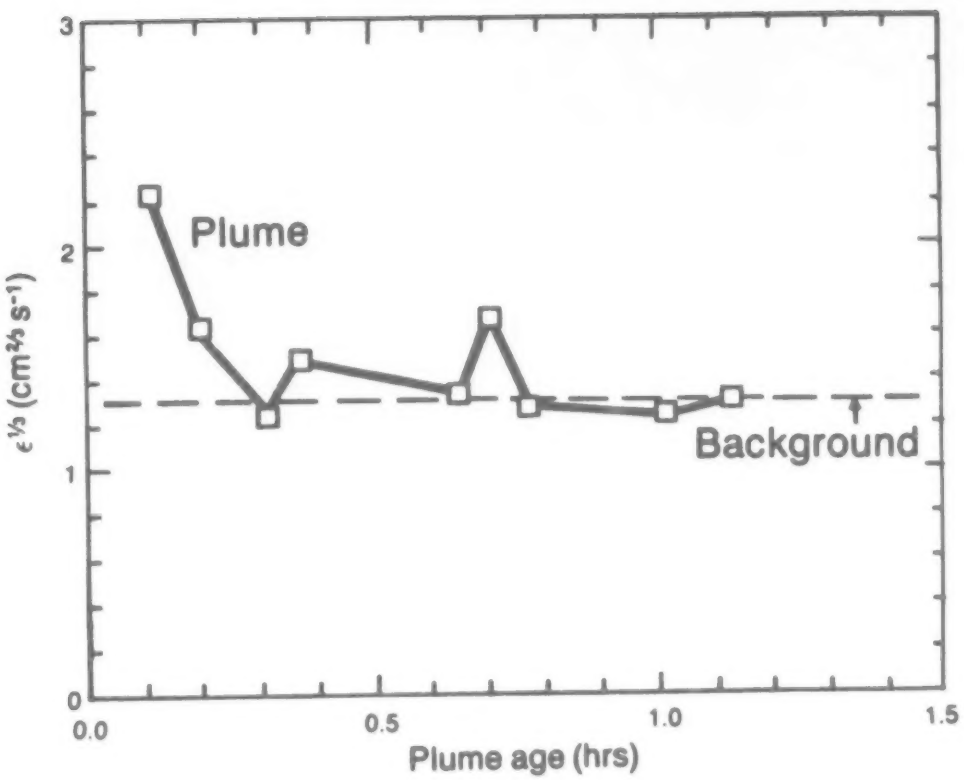

Figure 20. Plume mean cube root of the turbulent energy dissipation rate as a function of plume travel time for the Syncrude plume measured on 1984 June 11.

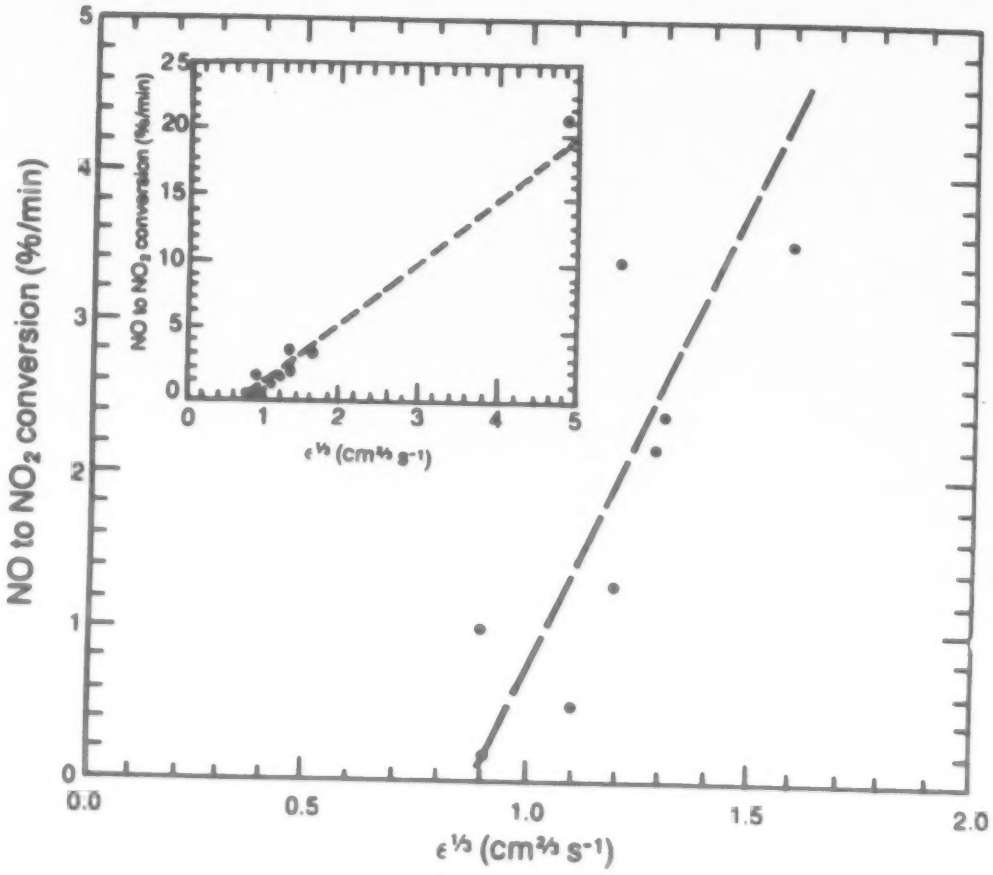

Figure 21. NO and NO_2 conversion rate as a function of the cube root of the turbulent energy dissipation rate.

modelling of plume nitrogen chemistry in short or medium range transport of pollutants. Furthur studies with simultaneous and continuous ozone measurements are warranted.

6. EVOLUTION OF ICE PARTICLES NUCLEATED IN PLUMES

Particles emitted or produced from emission plumes of power plants are known to act as cloud condensation nuclei. In recent years, several studies have been conducted to investigate this characteristic of man-made aerosols (Whitby et al. 1978; Pueschel and Van Valin 1978; Mirabel and Katz 1974; Hegg and Hobbs 1981; Hegg et al. 1980 and Barrett et al. 1979). Nucleation of emission originated acidic aerosols to form cloud droplets plays an important role in the formation of acid precipitation, as much as absorption of trace gases by cloud and rain drops and subsequent oxidation inside the drops. Figure 22 illustrates the importance of aerosol nucleation in the formation of cloud droplets. The measurments were taken during the June 1984 field experiment, from a cloud approximately 50 km downwind from the oil sands extraction plants but quite far off the plume trajectory. The cloud was located above a strong inversion layer. The sulphur dioxide measurments inside the cloud were equal to the background value (10 ppb). It was clear that the cloud was not affected by the plant emissions. Figure 22 shows the total concentrations of cloud droplets and aerosols observed simultaneously inside the studied cloud. Note that the total concentration of cloud droplets plus aerosols is almost constant. That is, the concentration of particles throughout this cloud was nearly constant, with particles present either as nuclei for cloud droplets or as interstitial aerosols. The production of cloud droplets results in the loss of aerosol particles. The figure shows evidence of the removal of aerosols by cloud droplet nucleation.

When ice crystals grow in a cloud of supercooled droplets, acidic aerosol particles may be removed by the processes of aerodynamic capture, thermo- and diffusio-phoresis, electrostatic capture, Brownian and turbulent diffusion, in addition to the aerosols which were scavenged, by either capture or nucleation, in the accreted cloud droplets. The occurrence of these phenomena makes studies of rainout, washout and snowout of atmospheric pollutants difficult.

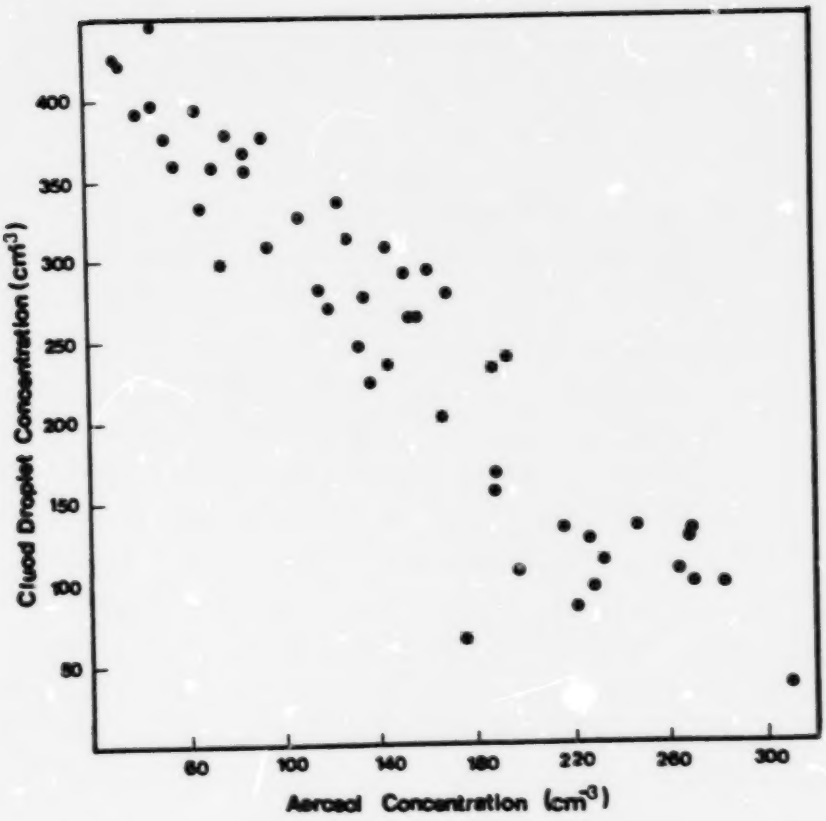

Figure 22. Correlation of total concentration of cloud droplets and aerosol particles.

Observations during the December 1983 field experiment provided an ideal natural situation for a snowout study. Hot, buoyant and moist effluent was exhausted into the frigid (below -25 °C), stable atmosphere. A liquid water cloud quickly formed in the supersaturated environment. Ice crystals nucleated and grew as the cloud cooled to the environmental temperature. The supercooled liquid water cloud evaporated to entrained dry air and to the growing crystals, such that within short distances downwind, no measurable liquid water remained. Ice crystals grew rapidly in some cases to precipitation sizes in the gaseous and aerosol plume. The ice precipitation reached the ground level near the stack, whereas the gaseous plume remained aloft and could be detected as SO_2 at great distances. Although no chemistry measurements were made for these snowout particles, the cloud physical measurments to be documented in this chapter provided some insights into the physical mechanisms which may be involved in the snowout process. Two cases, one for the Syncrude plume and the other for the Suncor plume, are presented here as examples. The two cases are chosen to illustrate the effects due to the variations in the characteristics of the two oil sands extraction plant emissions.

6.1 CASE OF 1983 DECEMBER 15

The Suncor plume (stack height 320 m msl or 107 m above ground) was studied on this flight. It was separate from the Syncrude plume for a long distance downwind because the mean wind was from the north-east at 5 m s^{-1} in the lower atmosphere. For other wind directions, the plumes may overlap. The ambient temperature at the plume levels was about -30 to -29 °C and the relative humidity with repect to ice saturation was 80 to 95%. Figure 23 shows the atmospheric sounding obtained during the period of the field experiment. The atmosphere was stable from the lowest 50 m up to 750 m above ground. A thin layer of neutral stability was capped by another stable layer which extended to the top of the sounding. Relative humidity with respect to ice was above 80% from the surface to 1200 m above ground. There was a layer of dry air

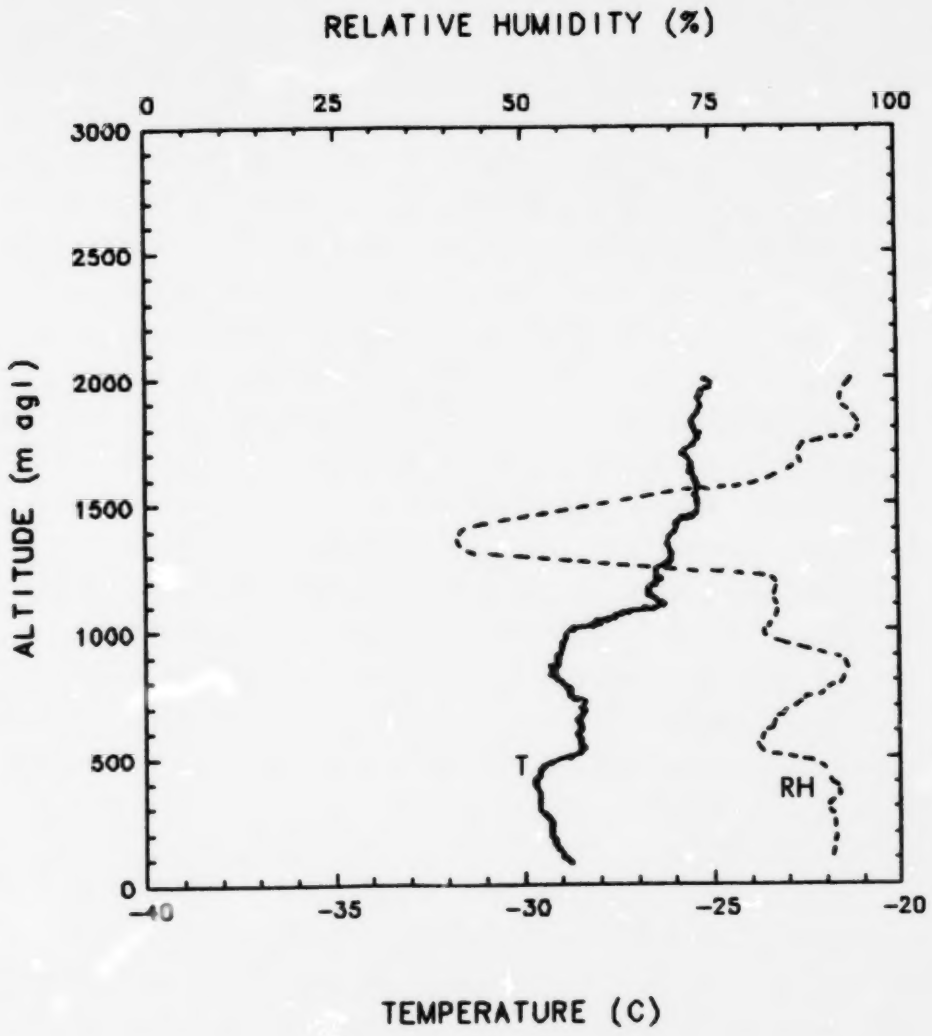

Figure 23. Vertical profile of temperature and relative humidity with respect to ice observed on 1983 December 15.

about 500 m thick located at 1000 m. Above this, the air was almost ice saturated. The atmospheric sounding was terminated at about 2000 m above ground level.

Figure 24 gives the vertical profile of the plume averaged sulphur dioxide and nitric oxide concentrations, mean diameter of ice crystals, total ice crystal concentration and maximum liquid water content in the flight segment. Values below the detection limit of the instrumentation are represented by asterisks. The maximum liquid water content measured at 480 m above ground and almost directly above the stack was 0.8 g m^{-3}, similar to the value in a summer cumulus cloud. Ice crystals nucleated rapidly in the gaseous plume and had a concentration of 27 L^{-1} over the stack. The mean size of ice particles at this location was 67 μm. The liquid water was depleted quickly and could not be detected at subsequent passes. At the plume centre level after 5 min travel time (approximately 420 m above ground and 1.7 km downwind from the stack) the ice crystal total concentration was 128 L^{-1}, with a mean size of 83 μm. Farther downwind and closer to the surface (8 km from the stack (23.4 min travel time) and 210 m above ground), the mean size of ice crystals was around 100 μm and the total concentration of ice particles was much less than upstream and above. It seems that ice crystal growth was slow in the plume. No ice crystals were detected in the gaseous plume beyond 10 km from the stack. The dashed lines in Figure 24 schematically outline the boundary of the gaseous plume and the arrow shows the extent and trajectory of the ice particle plume. Background sulphur dioxide concentration was about 7 ppb.

Figure 25 gives the ice crystal size distributions observed at the aircraft sampling locations within or below the gaseous plume. The size spectra are overlayed to show the ice crystal growth. The size distribution measured at 480 m above ground and almost directly above the stack was narrow with a maximum size of about 300 μm. The size distribution was characteristic of nucleation followed by diffusional growth process. The size distribution of ice crystals measured at 500 m above ground and

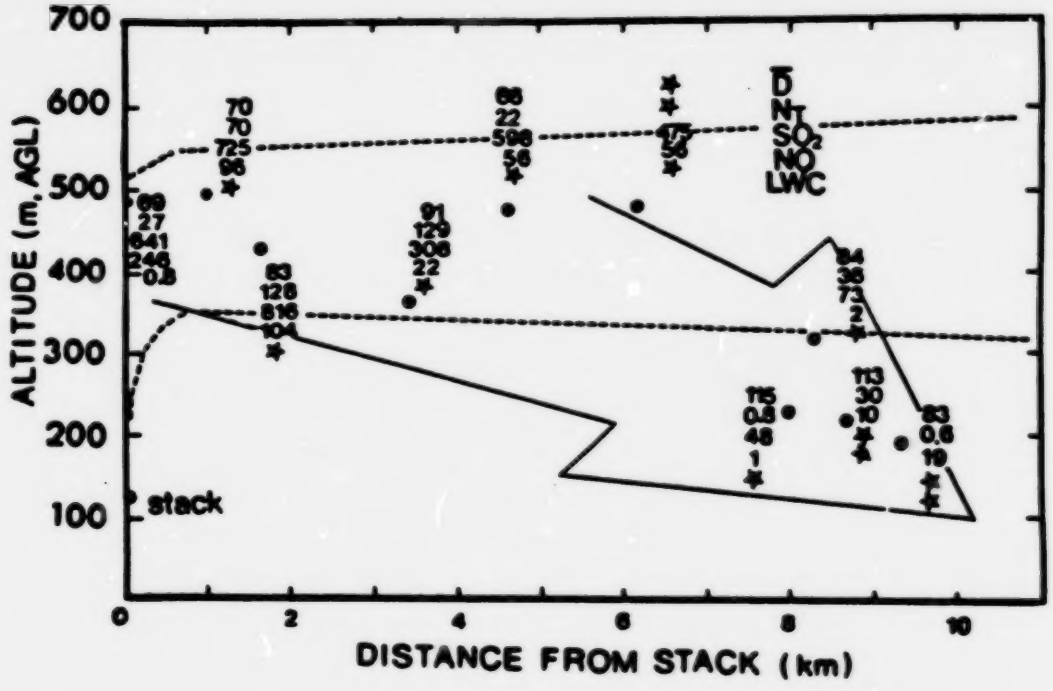

Figure 24. Vertical cross-section plot of segment-averaged mean size of ice crystals, D (μm), total ice crystal concentration, N_T (L^{-1}), sulphur dioxide, SO_2, and nitric acid, NO, concentrations (ppb), and maximum liquid water content, LWC (g m^{-1}) measured at various altitude and downwind distances of the plume on 1983 December 15. The asterisks denote undetectable values. The dots represent sampling locations. The dashed lines illustrate the gaseous plume boundaries and the arrow suggests the ice crystal trajectory.

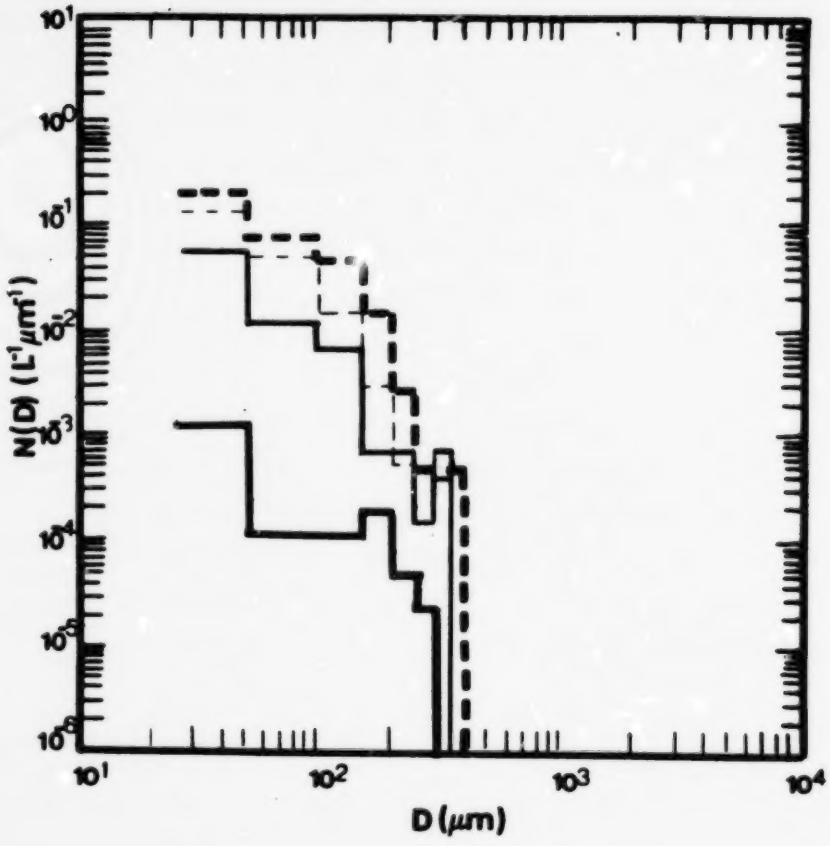

Figure 25. Ice crystal size distributions measured at selected locations of the gaseous plume on 1983 December 15. The solid line represent that obtained at 480 m above ground and almost directly above the stack, the dashed thin line at 500 m above ground and 1.0 km from the stack, the dashed thick line at 420 m above ground and 1.7 km from the stack, and the solid thick line at 190 m above ground and 9.4 km from the stack.

10 km downwind from the stack was also narrow, with a maximum size of ice crystals at about 350 μm. The liquid water droplets had evaporated by the time they reached this location. Note that initially there was a large increase in small ice crystals indicating that more ice nuclei were being nucleated. The ice crystal size distribution measured at approximately 420 m above ground and 1.7 km downstream of the stack resembled one which would have been the result of diffusional growth (Davis and Auer 1974) initiated with a narrow exponential distribution similar to the one observed upwind and above. More ice nucleation was apparent as illustrated by the increase of small ice crystals. The maximum size of ice particles detected was 450 μm. At about 190 m above ground and 9.4 km downwind from the stack, the size distribution suggests some aggregational growth and sublimation might also be important in the ice crystal evolution during this period. The maximum size detected was about 250 μm and the total concentration was 0.6 per litre. The mean size was smaller and the concentration was smaller than those measured at upstream and higher levels.

6.2 CASE OF 1983 DECEMBER 17

The Syncrude plume (stack height 373 m msl or 160 m above ground) was studied on this flight. The ambient temperature at about the plume level varied from -30 to -29 °C and the relative humidity was around 85% with respect to ice. Figure 26 shows the vertical profile of the temperature and relative humidity during this experiment. The temperature profile indicates a neutral stability in the lower atmosphere from the ground up to the base of a thick strong inversion (potential temperature vertical gradient of +6 °K / 100 m) at 800 m. The relative humidity varied between 80 and 95% from the ground up to 2000 m where the sounding was terminated. Wind speeds at the lower atmosphere were 2 to 5 m s^{-1} from the north and changed little with altitude.

Figure 27 shows a vertical profile of averaged sulphur dioxide and nitric oxide concentrations, mean size of ice crystals, total ice crystal concentration and maximum liquid water content

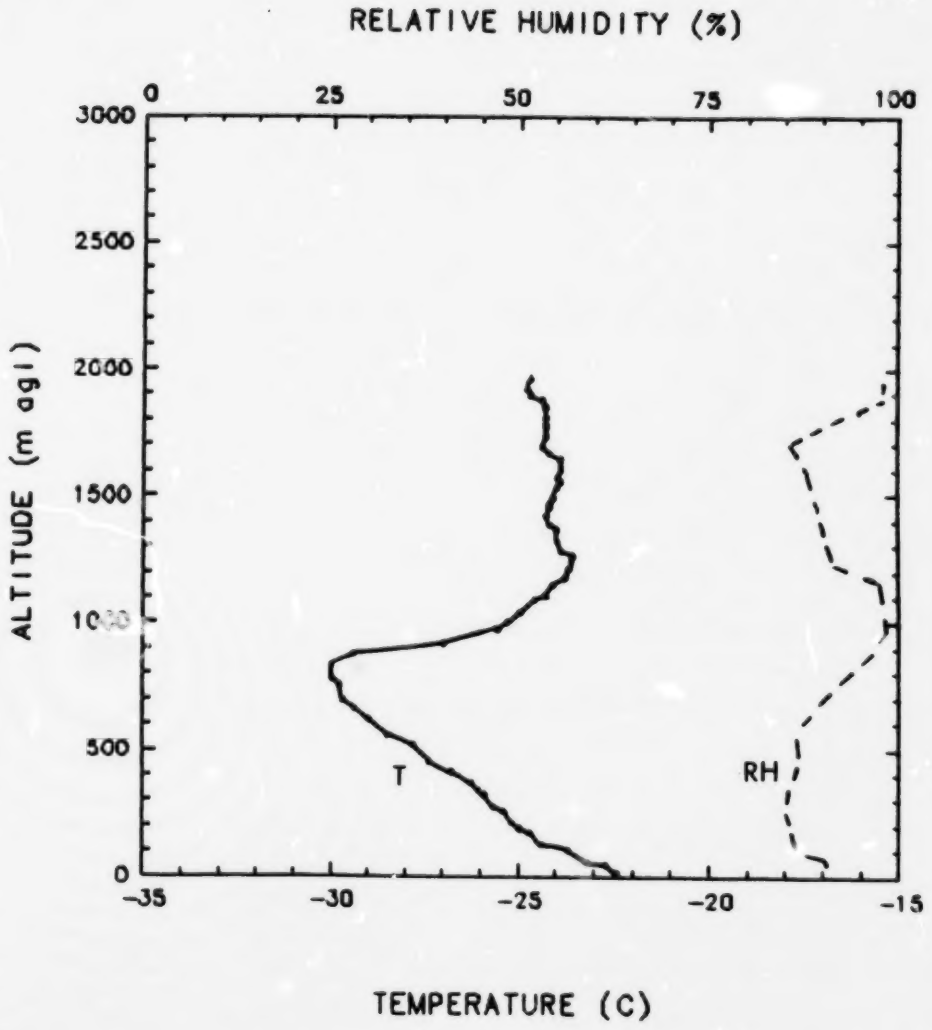

Figure 26. Vertical profiles of temperature and relative humidity with respect to ice observed on 1983 December 17.

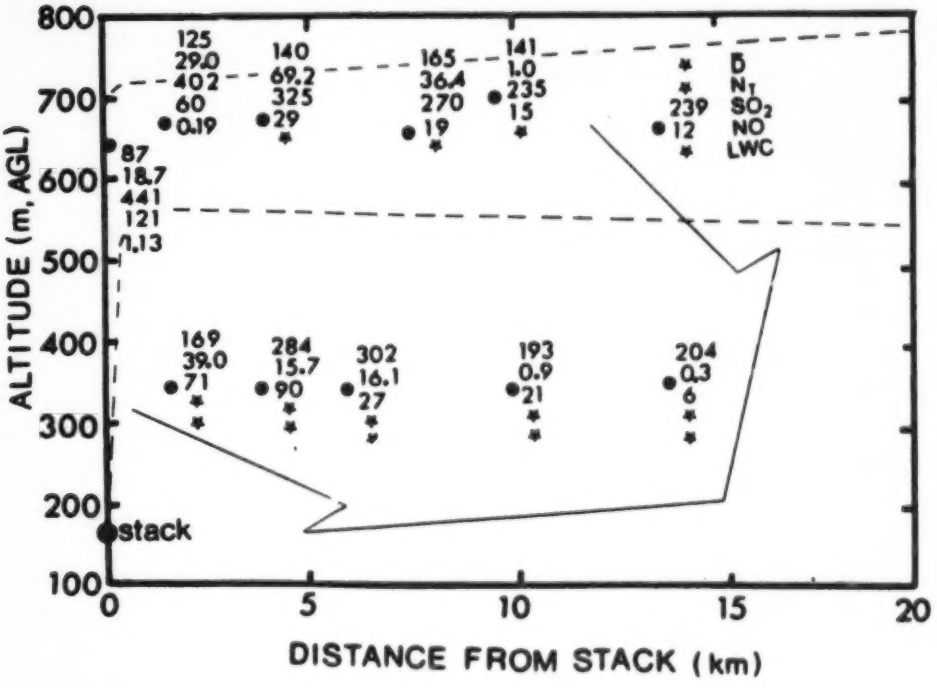

Figure 27. Vertical Cross-Section Plot of Segment-Averaged Mean Size of Ice Crystals, $\bar{D}$ (μm), Total Ice Crystal Concentration, N_T (L^{-1}), Sulphur Dioxide, SO_2, and Nitric Oxide, NO, Concentrations (ppb), and Maximum Liquid Water Content, LWC ($g\ m^{-1}$) Measured at Various Altitudes and Downwind Distances of the Plume on December 17, 1983. The Asterisks Denote Undetectable Values. The Dots Represent Sampling Locations. The Dashed Lines Illustrate the Gaseous Plume Boundaries and the Arrow Suggests the Ice Crystal Trajectory.

observed in the flight segment. The maximum liquid water content measured at 650 m above ground (approximately the plume center level) almost directly above the stack had a value of 1.13 g m^{-3}. This is equivalent to observations in summer cumulus clouds. At 1.5 km downwind and about the same altitude (3.5 min travel time), the maximum liquid water content observed was 0.19 g m^{-3} and at 2.4 km (5.3 min travel time), the maximum liquid water still had a value of 0.05 g m^{-3}. As in the 15 December case, ice crystals nucleated readily in the supercooled gaseous plume. The total concentration of ice crystals measured at 650 m above ground was 19 L^{-1}, reached a maximum of 85 L^{-1} at 2.4 km downwind from the stack and declined significantly at distances farther downwind and at the same altitude. At approximately the plume center level, the mean ice crystal size increased from 87 μm directly above the stack to 125 μm at 2.4 km downwind from the stack and increased rather slowly with travel time. Below the gaseous plume or at the lower boundary of the plume (about 350 m above ground) the total ice crystal concentration decreased, in general, as the distance from the stack increased. However, the mean ice crystal size had a maximum of 303 μm located at about 6 km from the stack (13.5 min travel time). Sulphur dioxide above background concentration level (approximately 6 ppb) was observed at this altitude, whereas nitric oxide was not detected. No ice crystal plume was detected beyond 10 km from the stack at the plume centre level, but was observed at a lower altitude (350 m) 14.2 km downwind from the stack illustrating fallout of the ice crystals. The dashed lines in Figure 27 schematically outline the gaseous plume. The envelop of ice crystal growth and fallout direction are suggested by the cross sectional analysis. Fallout trajectories are consistent with theoretical expectations for columnar and side plane crystals 100 to 1000 μm in size (Davis 1974).

Figure 28 shows the ice crystal size distributions measured at selected locations during the flight. The distributions are once again overlayed to show growth. The size distribution measured at 650 m above ground was narrow and characteristic of new

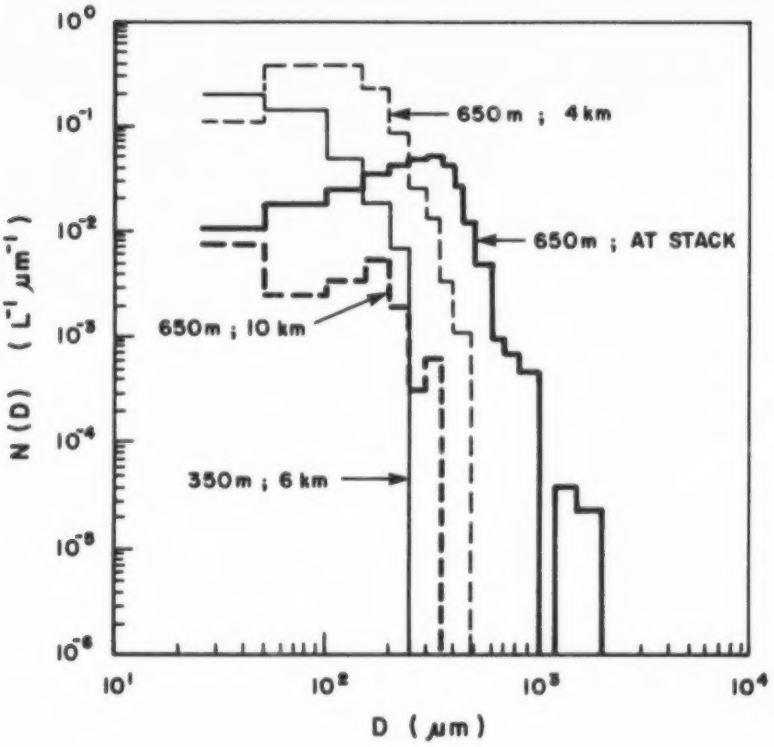

Figure 28. Ice crystal size distributions measured at selected locations of the gaseous plume on 1983 December 17. The solid line represents sampling at 650 m above ground and almost directly above the stack, the dashed thin and thick lines at the same altitude and 4 and 10 km from the stack, respectively, and the solid thick line at 350 m above ground and 6 km from the stack.

crystals formed by nucleation and a depositional growth process. The maximum ice crystal size detected was 250 μm. At approximately the same altitude but 4 km downwind from the source, the size distribution suggested diffusional growth (Davis and Auer 1974) of an initially narrow distribution similar to the one observed upwind. The maximum ice crystal size measured was about 450 μm. At 6 km from the stack and 350 m above ground, the size distribution showed some evidence of aggregational growth as indicated by the bimodal spectrum. The maximum ice crystal size measured was about 2 mm. Ice particles of precipitation size detected at this altitude should survive sublimation during fallout and reach the surface. The size distribution of ice particles measured 10 km downwind from the stack and about the plume centre level showed a narrow size range of residual crystals which were slowly precipitating and evaporating.

6.3 DISCUSSION

The observations clearly show that ice particles were nucleated soon after emission, evolved through various growth processes and fell out of the gaseous plume. However, in one case ice particles grew to precipitation size whereas in the other they did not. The temperature and relative humidity with respect to ice at the plume level were almost the same in the two cases studied. Although the environmental temperature at the stack level was warmer by about 4 °C in the Syncrude case than in the Suncor case, the emission temperatures at the stacks (about 220 °C) were much higher than the environment values. The hot effluent should have reached the plume level within a very short time so that nucleation should have taken place at this altitude, where the temperature difference between the two cases was minimal. This is probably the reason for the fact that the ice crystal concentrations at the plume centre level almost directly above the stack were approximately the same (27 L^{-1} and 19 L^{-1}) in the two cases. The different results as to snowfall on the ground may possibly be attributable to the differences in the emission characteristics of the two oil sands extraction plants. As mentioned earlier, the aerosol probe on-board

the aircraft was not functioning during the December 1983 field study. Measurements made during other phases of the field experiment illustrate marked differences in the size distributions of aerosols emitted from the Syncrude and the Suncor plants. Figure 29 shows a plot of the plume cross-sectional averaged size spectra of aerosols emitted from the two plants within a period of 90 minutes on 1984 June 11. The measurements were obtained approximately at the plume center level and at approximately the same downwind distance from the stack. The thin line represents the aerosol size distribution for the Suncor plume and the thick line that for the Syncrude plume. The aerosols emitted from the Suncor plant have much higher concentrations than those from the Syncrude plant, the difference being about one order of magnitude. Although particles emitted or produced from gaseous emissions of oil sands extraction plants have not been known to be good ice nucleating agents, some of these particles may have been activated to form ice crystals in the cases documented above.

In the Suncor plume, in which the aerosol concentrations are higher and probably the ice nuclei concentrations are higher, ice crystals grew at the expense of the evaporating supercooled liquid water content. The growth rates of these ice crystals were slow because of the greater competition for the vapour and liquid water available. Ice crystals in the gaseous plume could hardly grow to a size at which aggregational growth becomes appreciable. Ice crystals would eventually fall out of the plume at some distance from the stack, but would likely sublime before reaching the surface unless the plume height is relatively low.

In the Syncrude plume, fewer ice crystals were probably nucleated because the concentration of aerosols emitted from the stack was lower. The supply of water vapour was abundant due to less competition. Ice crystals grew rapidly to precipitation size through the depositional and aggregational process. The ice precipitation could reach the ground level near the stack, whereas the gaseous plume remained aloft.

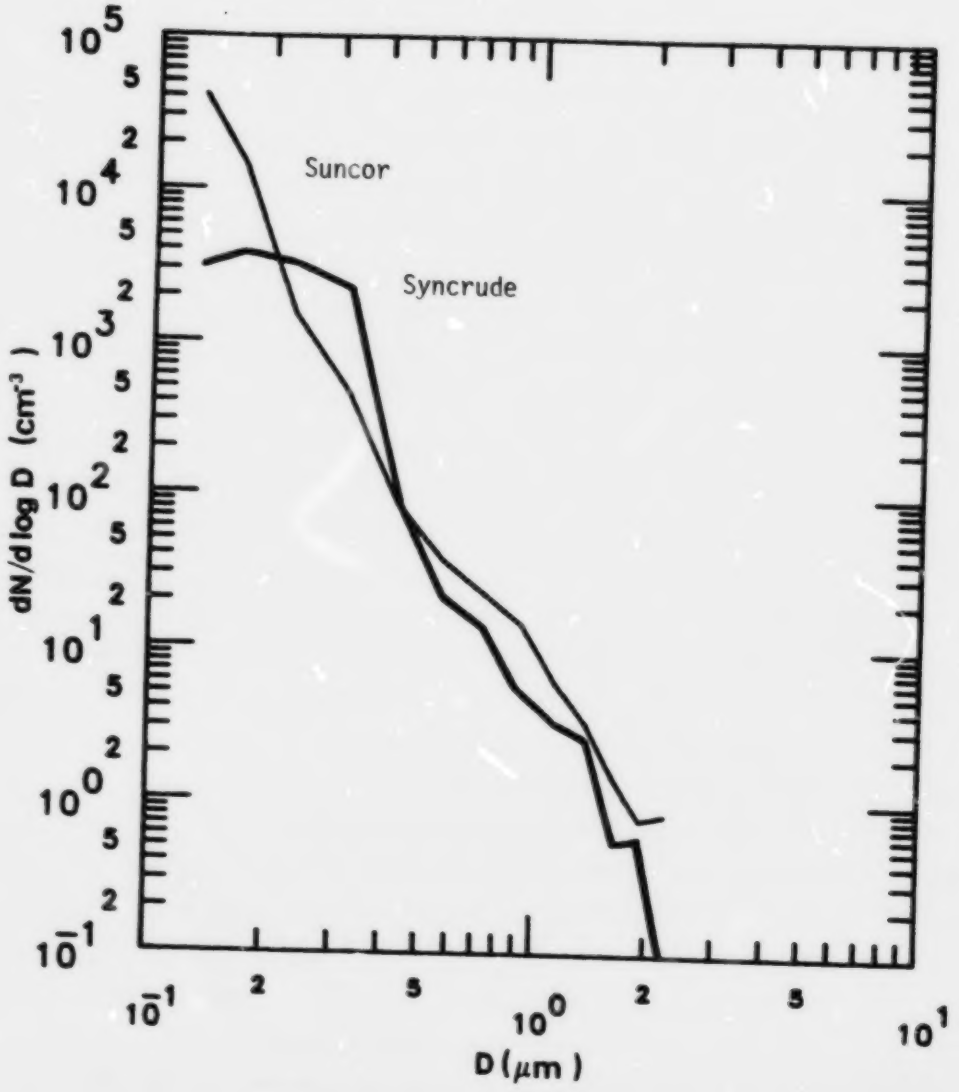

Figure 29. Plume cross-sectional averaged size distributions of aerosols emitted from Syncrude (thick) and Suncor (thin) plants measured at approximately the same downwind distance from the stacks and at the plume centreline level.

The results from the case studies demonstrate one of the important roles of anthropogenic aerosols in inadvertant weather modification. When these aerosols are vented into the cold region of a mid-latitude storm, the ice nuclei concentrations in the storm may be changed and the precipitation processes may be modified.

A number of references have been made to the in-cloud evironment as a sink of airborne aerosol particles (Slinn and Hales 1971; Hogan 1976; and Radke et al. 1980). It has been suggested that current theory fails to account for the magnitude of such scavenging (Radke et al. 1980). Most field studies thus far reported in the literature do not allow quantitative estimates of scavenging efficiency because:

1. Precipitation pollutant concentrations have not been simultaneously measured and related to pollutant concentrations in the air through which the precipitation formed; and
2. Other important meteorological and microphysical characteristics of the precipitation formation which will affect pollution scavenging are rarely reported.

Air motion, which results in cloud formation and precipitation production, transports pollutants vertically. Transported pollutants can be lifted from the lower atmosphere and suspended at higher altitudes after cloud dissipation. Thus, the effects of interaction between cloud dynamics and pollutants should be isolated when the scavenging efficiency is derived.

The observations documented in this report clearly show that ice particles fell out from the gaseous plume. The ice particles were nucleated inside the plume and underwent various evolution growth processes. The formation of a liquid water and ice cloud in the frigid and light wind conditions provides several mechanisms for scavenging the aerosol and gaseous pollutants in the plume. Besides the processes mentioned in the beginning of this chapter, it is likely that the precipitation-induced drag increased the downward deposition of pollutants (Figures 24 and 27 show that SO_2 concentrations much higher than the background value coexisted

with ice particles below the gaseous plume). Thus, for these weather conditions, there was a kind of "self-removal" process in the plume. Moreover, unlike inside cloud systems (except the stratiform type of clouds) the dynamics-pollutants interactions are relatively simple. The dispersion and advection should be the major mechanisms inside the plume. As demonstrated, other important meteorological and microphysical characteristics of the precipitation which will affect pollution scavenging can also be determined. Thus, conditions like these are ideal for a study of snowout and its effects upon pollutant concentrations. Unfortunately, when the present study was undertaken, the instrumentation aboard the research aircraft was not adequate for snowfall collection for chemical analyses and the aerosol probe did not function properly. In future studies, every effort should be made to obtain the full range of measurements that are important for snowout processes: air chemistry, precipitation chemistry, aerosol characteristics, cloud microphysics, and air motion.

7. CONCLUSIONS AND RECOMMENDATIONS

The field experiments for the jointly funded project by Alberta Environment and the Alberta Research Council, were conducted in March and December 1983 and June 1984. The objectives were to determine the transport, diffusion and transformation rates of sulphur and nitric oxides emitted from oil sands extraction plants in northern Alberta. From the analysis and interpretation of the data collected, several specific conclusions can be drawn.

One important conclusion is that these studies demonstrate that it is now technically possible to make some of the important measurements concerning air chemistry, aerosols, microphysics, and air motion from an instrumented aircraft. Factors which made the measurements obtained in these studies uniquely suited to this project include:

1. Instrumentation with a very fast response time;
2. The ability to measure most of the important parameters simultaneously;
3. The ability to follow one plume parcel for repetitive measurements.

The observed horizontal plume dispersion parameters show good agreement with the Pasquill-Gifford values for the various stability classes only as far as the rate of change with distance is concerned. The observed values were somewhat larger than those predicted by Pasquill-Gifford for the atmospheric stability present. The upward momentum and buoyancy of the hot stack emission in the relatively cold atmospheric surroundings appears to increase the initial diffusion of the plume. This leads to values of observed horizontal plume dispersion parameters, for distances relatively close to the stack, being greater than what would be expected under the prevailing atmospheric stability conditions.

The conversion rates of sulphur dioxide to particulate sulphate determined from the excess aerosol volume production technique varied from 0.02% to 2.81% h^{-1} during March 1983 and from 0.06% to 8.66% h^{-1} during June 1984. Conversion rates determined from results of the chemical analysis of filter samples ranged from

0% to 2.0% h^{-1} during December 1983 and 0% to 2.9% h^{-1} during June 1984. The range of values obtained from the two techniques in the present study seems to be compatible with earlier results and they agree relatively well with each other. The significant amounts of excess aerosol volume production of particles larger than 1.0 μm suggest that heterogeneous conversion of sulphur dioxide to particulate sulphate may be appreciable under certain conditions and close to the emission source. During the same season, the transformation rate apparantly depends upon the time of day. The conversion rate increased from early morning to a maximum at noon or early afternoon and decreased again thereafter in response to solar radiation.

The conversion rate of NO to NO_2 was determined for winter and summer conditions in the AOSERP area. Rates varied considerably from hour to hour, ranging from 0.2% to 21.4% min^{-1}. Because of the fast reaction of NO to NO_2, in the presence of ozone, the mixing times are short compared to chemical relaxation times over a small spatial scale. The transformation of NO to NO_2 takes place mainly in narrow zones at the edges of the gaseous plume. There also seems to be a direct relationshio between the turbulent mixing and the NO to NO_2 conversion rate.

The transformation of nitrogen oxides to particulate nitrate was not obtained because the amount of particulate nitrate collected was below the detection limit in all cases and little or no nitric acid was found.

A liquid water cloud quickly formed in the supersaturated environment of the emissions from the stack during the December 1983 experiment period. Ice crystals nucleated and grew as the cloud cooled to the environmental temperature. The supercooled liquid water evaporated to the entrained ambient air and growing crystals, such that within a short distance downwind, no measurable liquid water remained.

In the Suncor plume, the ice nuclei concentration seemed to be higher, and ice crystals grew at the expense of the evaporating supercooled liquid water content. The growth rates of

these ice crystals were slow because of the competition for the limited available vapour and liquid water supply. Ice particles in the gaseous plume did not grow large enough for the aggregational growth to be appreciable. However, the ice crystals eventually fell out of the plume at some distance from the stack. Some crystals sublimed before reaching the surface.

In the Syncrude plume ice crystals grew rapidly to precipitation sizes within a few kilometers from the stack and fell out of the gaseous and aerosol plume. Diffusion growth was dominant, although accretional growth may have been appreciable close to the stack where liquid water was available. The ice precipitation was observed to fall to the ground within 10 km of the stack, whereas the gaseous plume remained aloft and could be detected at a great distance from the stack.

The formation of a liquid water and ice cloud provided several mechanisms for scavenging the aerosol and gaseous pollutants in the plume. It is likely that the precipitation induced drag increased the downward deposition of gaseous emissons. Thus for these weather conditions, there was a kind of "self-removal" process in the Syncrude plume.

Based upon the experience gained during the field study and the results of the subsequent data analysis, the following specific recommendations are presented:

1. It is recommended that any models of oil sands extraction plant airborne emissions and their effects upon biological systems consider plume chemistry and deposition mechanisms and that these models be verified or tuned by field measurements.
2. It is recommended that the rates of deposition of pollutants via the "snow-out" mechanism during the winter months be investigated. This mechanism may be of prime importance in determining the short, medium, and long range transport of acid forming emissions generated by these plants.

3. In order to better understand the chemistry of nitrogen and sulphur oxides in the plumes from the oil sands plants (and thereby their effects) it is necessary to obtain a fast response ozone monitor and consideration must be given to continuous particulate nitrate and sulphate analyzers.
4. Particles emitted by the oil sands plants or generated from gaseous emissions may play an important role in the transport of pollutants and their environmental effects. It is recommended that further consideration be given to the transport of particles and the chemical composition of different size fractions with particular emphasis on metals, nitrates and sulphates.
5. For stable, light wind conditions, the plume spreads widely in the horizontal and interrupts the normal radiation balance. It is recommended that future airborne studies should address the significance of this effect.

8. REFERENCES

Alkezweeny, A.J. and D.C. Powell. 1977. Estimation of transformation rate of SO_2 to SO_4 from atmospheric concentration data. Atmos. Environ. 11:179-182.

Barrett, E.W., F.P. Parungo, and R.F. Pueschel. 1979. Cloud modification by urban pollution: A physical demonstration. Meteor. Rdsch. 32:136-149.

Benner, W.H., R. Brodzinshy, and T. Novakov. 1980. Oxidation of SO_2 in droplets which contain soot particle. Atmos. Environ. 16:1-7.

Bielke, S. and G. Gravenhorst. 1978. Heterogeneous SO_2-oxidation in the droplet phase. Atmos. Environ. 12:231-240.

Bottenheim, J.W. 1982. Plume chemistry studies during 1980 in the Athabasca tar sands area. Proc. Acid Forming Emissions in Alberta and Their Ecological Effects, 1982 March 09-12, Edmonton, Alberta. pp. 181-205.

Bottenheim, J.W., S.E. Braslavsky, and O.P. Strausz. 1977. Modelling study of seasonal effect on air pollution at $60^{o}N$ latitude. Environ. Sc. and Technol. 11:801-808.

Britton, L.G. and A.G. Clarke. 1980. Heterogeneous reactions of sulfur dioxide and SO/NO mixtures with carbon soot aerosol. Atmos. Environ. 14:829-839.

Calvert, J.G., F. Su, J.W. Bottenheim, and O.P. Strausz. 1977. Mechanisms of homogeneous oxidation of sulphur dioxide in the troposphere. Atmos. Environ. 12:197-226.

Cantrell, B.K. and K.T. Whitby. 1978. Aerosol size distributions and aerosol volume formation for a coal-fired power plant plume. Atmos. Environ. 12:323-333.

Cheng, R.J. 1982. Emissions from electric power plants and their impact on the Environment. Energy, Proceedings of First U.S.-China Conference on Energy, Resources and Environment, S.W. Yuen, ed. Beijing, China: Pergamon Press. pp. 591-598.

Cullis, C.F. and M.M. Hirschler. 1980. Atmospheric sulphur: Natural and man-made sources. Atmos. Environ. 14:1263-1278.

Davis, C.I. 1974. The ice-nucleating characteristics of various AgI aerosols. Laramie, Wyoming: University of Wyoming. 267 pp. Ph.D. Thesis.

Davis, C.I. and A.H. Auer. 1974. Use of isolated orographic clouds to establish the accuracy of diffusional ice crystal growth equations. Proceedings of Cloud Physics Conference in Tucson, Arizona. Amer. Meteor. Soc., Boston, Massachusetts. pp. 141-147.

Davis, D.D., G. Smith, and G. Klauber. 1974. Trace gas analysis of power plant plume via aircraft measurement. Science 186:733-735.

Davison, D.S. and K.L. Grandia. 1979. Plume dispersion measurements from an oil sands extraction plant, June 1977. Prep. for the Alberta Oil Sands Environmental Research Program by Intera Environmental Consultants Ltd. AOSERP Report 52. 209 pp.

Davison, D.S. and E.D. Leavitt. 1979. Analysis of AOSERP plume sigma data. Prep. for the Alberta Oil Sands Environmental Research Program by Intera Environmental Conculstants Ltd. AOSERP Report 63. 251 pp.

Davison, D.S., C.J. Fortems, and K.L. Grandia. 1977. Plume dispersion measurements from an oil sands extraction plant, March 1976. Prep. for the Alberta Oil Sands Environmental Research Program by Intera Environmental Consultants Ltd. AOSERP Report 13. 195 pp.

Flyger, J., E. Lewin, E. Lund Thomsen, J. Fenger, E. Lych, and S.E. Gryning. 1978. Airborne investigations of SO_2 oxidation in the plumes from power plants. Atmos. Environ. 12:295-296.

Forest, J. and L. Newman. 1977. Further studies on the oxidation of sulfur dioxide in coal-fired power plant plume. Atmos. Environ. 11:465-474.

Freiberg, J. 1974. Effects of relatively humidity and temperature on iron-catalysed oxidation of SO_2 in atmospheric aerosols. Env. Sci. Technol. 8:731-734.

Friend, H.P. 1973. The global sulphur cycle. Chemistry of the lower atmosphere, S.I. Rasool, ed. New York and London: Plenum Press. pp. 177-201.

Gillani, N.V. 1978. Project MISTTT: Mesoscale plume modelling of the dispersion, transformation and ground removal of SO_2. Atmos. Environ. 12:569-588.

Gillani, N.V., R.B. Husar, J.D. Husar, D.E. Patterson, and W.E. Wilson, Jr. 1978. Project MISTT: Kinetics of particulate sulfur formation in a power plant out to 300 km. Atmos. Environ. 12:589-598.

Granat, L., H. Rodhe, and R.O. Hallbery. 1976. The global sulphur cycle. Ecological Bulletin 22:89-134.

Hales, J.M. 1978. Wet removal of sulfur compounds from the atmosphere. Atmos. Environ. 12:389-399.

Hegg, D.A. and P.V. Hobbs. 1980. Measurements of gas-to-particle conversion in the plumes of five coal-fired electric power plants. Atmos. Environ. 14:99-116.

Hegg, D.A. and P.V. Hobbs. 1981. Cloud water chemistry and the production of sulfates in clouds. Atmos. Environ. 15:1597-1604.

Hegg, D.A., P.V. Hobbs, and L.F. Radke. 1980. Observations of the modification of condensation nuclei in wave clouds. J. Rech. Atmos. 14:217-222.

Hegg, D.A., P.V. Hobbs, L.F. Radke, and H. Harrison. 1977. Reactions of ozone and nitrogen oxides in power plant plumes. Atmos. Environ. 11:521-526.

Hobbs, P.V., D.A. Hegg, M.W. Eltgroth, and L.F. Radke. 1979. Evolution of particles in the plumes of coal-fired power plants - I. Deductions from field measurements. Atmos. Environ. 12:935-959.

Hogan, A.W. 1976. Aerosols of the tradewind region. J. Appl. Meteor. 15:611-619.

Husar, R.B., D.E. Patterson, J.D. Husar, N.V. Gillani, and W.E. Wilson. 1978. Sulfur budget of a power plant plume. Atmos. Environ. 12:549-568.

Kochmond, W.C., D.B. Kittelson, J.Y. Yang, and K.L. Demerjian. 1975. Study of aerosol formation in photochemical air pollution. EPA Report No. EPA-650/3-75-007.

Leahey, D.M., M.J.E. Davies, and H.A. Bambrough. 1983. Values of NO_2:NO_x observed in the exhaust plume from a turbine driven compressor installation. Atmos. Environ. 17:991-997.

Lusis, M.A., K.G. Anlauf, L.A. Barrie, and H.A. Wiebe. 1978. Plume chemistry studies at a northern Albert power plant. Atmos. Environ. 12:2429-2437.

MacCready, P.B. 1964. Standardization of gustiness values from aircraft. J. Appl. Meteor. 3:439-449.

Mage, D.T. and J. Noghrey. 1979. True atmospheric pollutant levels by use of transfer function for an analyzer system. J. Air Poll. Cont. Assoc. 22:115-118.

Miller, D.F., A.J. Alkezweeny, J.M. Hales, and R.N. Lee. 1978. Ozone formation related to power plant emissions. Science 202:1186-1188.

Mirabel, P. and J.L. Katz. 1974. Binary homogeneous nucleation as a mechanism for the formation of aerosol. J. Chem. Phys. 60:1138-1144.

Moller, D. 1984a. Estimation of the global man-made sulphur emission. Atmos. Environ. 18:19-27.

Moller, D. 1984b. On the global natural sulphur emission. Atmos. Environ. 18:29-39.

Pasquill, J. 1974. Atmospheric diffusion, 2nd ed. New York: Halstad Press. 429 pp.

Pruppacher, H.R. and J.D. Klett. 1978. Microphysics of clouds and precipitation. Holland: D. Reidel Publishing Co. 714 pp.

Pueschel, R.F. and C.C. Van Valin. 1978. Cloud nucleus formation in a power plant plume. Atmos. Environ. 12:307-312.

Slinn, W.G.N. and J.M. Hales. 1971. A re-evaluation of the role of thermophoresis as a mechanism of in and below cloud scavenging. J. Atmos. Sci. 28:1465-1471.

U.S. Congr. - U.S. EPA. 1979. Mobile source sulphur oxides. 403 pp.

Whitby, K.T., B.K. Cantrell, and D.B. Kittelson. 1978. Nuclei formation rates in a coal-fired power plant plume. Atmos. Environ. 12:313-321.

Zebel, G. 1966. Coagulation of aerosols. Aerosol Science, C.N. Davis, ed. London and New York: Academic Press. pp. 31-58.

CUMULATIVE LIST OF AOSERP PUBLICATIONS TITLES

1. AOSERP First Annual Report, 1975
2. Walleye and Goldeye Fisheries Investigations in the Peace-Athabasca Delta - 1975
3. Structure of a Traditional Baseline Data System
4. A Preliminary Vegetation Survey of the AOSERP Study Area
5. The Evaluation of Wastewaters from an Oil Sand Extraction Plant
6. Housing for the North. The Stackwall System Construction Report - Mildred Lake Tank and Pump House
7. A Synopsis of the Physical and Biological Limnology and Fishery Programs within the Alberta Oil Sands Area
8. The Impact of Saline Waters upon Freshwater Biota. A Literature Review and Bibliography
9. A Preliminary Investigation into the Magnitude of Fog Occurrence and Associated Problems in the Oil Sands Area
10. Development of a Research Design Related to Archaeological Studies in the Athabasca Oil Sands Area
11. Life Cycles of Some Common Aquatic Insects of the Athabasca River, Alberta
12. Very High Solution Meteorological Satellite Study of Oil Sands Weather: A Feasibility Study
13. Plume Dispersion Measurements from an Oil Sands Extraction Plant, March 1976
14. (No report published)
15. A Climatology of Low-Level Air Trajectories in the Alberta Oil Sands Area
16. The Feasibility of a Weather Radar near Fort McMurray, Alberta
17. A Survey of Baseline Levels of Contaminants in Aquatic Biota of the AOSERP Study Area
18 Interim Compilation of Stream Gauging Data to December 1976 for AOSERP
19. Calculations of Annual Averaged Sulphur Dioxide Concentrations at Ground Level in the AOSERP Study Area

20. Characterization of Organic Constituents in Waters and Wastewaters of the Athabasca Oil Sands Mining Area

21. AOSERP Second Annual Report, 1976-77

22. AOSERP Interim Report Covering the Period April 1975 to November 1978

23. Acute Lethality of Mine Depressurization Water to Trout-Perch and Rainbow Trout: Volume I

24. Air System Winter Field Study in the AOSERP Study Area, February 1977

25. Review of Pollutant Transformation Processes Relevant to the Alberta Oil Sands Area

26. Interim Report on an Intensive Study of the Fish Fauna of the Muskeg River Watershed of Northeastern Alberta

27. Meteorology and Air Quality Winter Field Study in the AOSERP Study Area, March 1976

28. Interim Report on a Soils Inventory in the Athabasca Oil Sands Area

29. An Inventory System for Atmospheric Emissions in the AOSERP Study Area

30. Ambient Air Quality in the AOSERP Study Area

31. Ecological Habitat Mapping of the AOSERP Study Area: Phase I

32. AOSERP Third Annual Report, 1977-78

33. Relationships Between Habitats, Forages, and Carrying Capacity of Moose Range in Northern Alberta. Part 1: Moose Preferences for Habitat Strata and Forages

34. Heavy Metals in Bottom Sediments of the Mainstem Athabasca River Upstream of Fort McMurray: Volume I

35. The Effects of Sedimentation on the Aquatic Biota

36. Fall Fisheries Investigations in the Athabasca and Clearwater Rivers Upstream of Fort McMurray: Volume I

37. Community Studies: Fort McMurray, Anzac, and Fort MacKay

38. Techniques for the Control of Small Mammal Damage to Plants: A Review

39. The Climatology of the AOSERP Study Area

40. Mixing Characteristics of the Athabasca River below Fort McMurray - Winter Conditions

41. Acute and Chronic Toxicity of Vanadium to Fish

42. Analysis of Fur Production Records for Registered Traplines in the AOSERP Study Area, 1970-1975

43. A Socio-Economic Evaluation of the Recreational Use of Fish and Wildlife Resources in Alberta, with Particular Reference to the AOSERP Study Area. Volume I: Summary and Conclusions

44. Interim Report on Symptomology and Threshold Levels of Air Pollutant Injury to Vegetation, 1975 to 1978

45. Interim Report on Physiology and Mechanisms of Air-Borne Pollutant Injury to Vegetation, 1975 to 1978

46. Interim Report on Ecological Benchmarking and Biomonitoring for Detection of Air-Borne Pollutant Effects on Vegetation and Soils, 1975 to 1978

47. A Visibility Bias Model for Aerial Surveys of Moose in the AOSERP Study Area

48. Interim Report on a Hydrogeological Investigation of the Muskeg River Basin, Alberta

49. The Ecology of Macrobenthic Invertebrate Communities in Harley Creek, Northeastern Alberta

50. Literature Review on Pollution Deposition Processes

51. Interim Compilation of 1976 Suspended Sediment Data for the AOSERP Study Area

52. Plume Dispersion Measurements from an Oil Sands Extraction Plant, June 1977

53. Baseline States of Organic Constituents in the Athabasca River System Upstream of Fort McMurray

54. A Preliminary Study of Chemical and Microbial Characteristics of the Athabasca River in the Athabasca Oil Sands Area of Northeastern Alberta

55. Microbial Populations in the Athabasca River

56. The Acute Toxicity of Saline Groundwater and of Vanadium to Fish and Aquatic Invertebrates

57. Ecological Habitat Mapping of the AOSERP Study Area (supplement). Phase 1

58. Interim Report on Ecological Studies on the Lower Trophic Levels of Muskeg Rivers within the AOSERP Study Area

59. Semi-Aquatic Mammals: Annotated Bibliography

60. Synthesis of Surface Water Hydrology

61. An Intensive Study of the Fish Fauna of the Steepbank River Watershed of Northeastern Alberta

62. Amphibians and Reptiles in the AOSERP Study Area

63. Analysis of AOSERP Plume Sigma Data

64. A Review and Assessment of the Baseline Data Relevant to the Impacts of Oil Sands Development on Large Mammals in the AOSERP Study Area

65. A Review and Assessment of the Baseline Data Relevant to the Impacts of Oil Sands Development on Black Bears in the AOSERP Study Area

66. An Assessment of the Models LIRAQ and ADPIC for Application to the Alberta Oil Sands Area

67. Aquatic Biological Investigations of the Muskeg River Watershed

68. Air System Summer Field Study in the AOSERP Study Area, June 1977

69. Native Employment Patterns in Alberta's Athabasca Oil Sands Region

70. An Interim Report on the Insectivorous Animals in the AOSERP Study Area

71. Lake Acidification Potential in the AOSERP Study Area

72. The Ecology of Five Major Species of Small Mammals in the AOSERP Study Area: A Review

73. Distribution, Abundance, and Habitat Associations of Beavers, Muskrats, Mink, and River Otters in the AOSERP Study Area, Northeastern Alberta

74. Air Quality Modelling and User Needs

75. Interim Report on a Comparative Study of Benthic Algal Primary Productivity in the AOSERP Study Area

76. An Intensive Study of the Fish Fauna of the Muskeg River Watershed of Northeastern Alberta

77. Overview of Local Economic Development in the Athabasca Oil Sands Region Since 1976

78. Habitat Relationships and Management of Terrestrial Birds in Northeastern Alberta

79. The Multiple Toxicity of Vanadium, Nickel, and Phenol to Fish

80. History of the Athabasca Oil Sands Region, 1890 to 1960s. Volume I: Socio-Economic Development; Volume II: Oral History

81. Species Distribution and Habitat Relationships of Waterfowl in Northeastern Alberta

82. Breeding Distribution and Behaviour of the White Pelican in the Athabasca Oil Sands Area

83. The Distribution, Foraging Behaviour and Allied Activities of the White Pelican in the Athabasca Oil Sands Area

84. Investigations of the Spring Spawning Fish Populations in the Athabasca and Clearwater Rivers Upstream from Fort McMurray: Volume I

85. An Intensive Surface Water Quality Study of the Muskeg River Watershed. Volume I: Water Chemistry

86. An Observational Study of Fog in the AOSERP Study Area

87. Hydrogeological Investigation of the Muskeg River Basin, Alberta

88. Ecological Studies of the Aquatic Invertebrates of the AOSERP Study Area of Northeastern Alberta

89. Fishery Resources of the Athabasca River Downstream of Fort McMurray, Alberta: Volume I

90. A Wintertime Investigation of the Deposition of Pollutants around an Isolated Power Plant in Northern Alberta

91. Characterization of Stored Peat in the Alberta Oil Sands Area

92. Fisheries and Habitat Investigations of Tributary Streams in the Southern Portion of the AOSERP Study Area: Volume I

93. Fisheries and Aquatic Habitat Investigations in the Mackay River Watershed of Northeastern Alberta

94. A Fisheries and Water Quality Survey of Ten Lakes in the Richardson Tower Area, Northeastern Alberta. Volume I: Methodology, Summary, and Discussion

95. Evaluation of the Effects of Convection on Plume Behaviour in the AOSERP Study Area

96. Service Delivery in the Athabasca Oil Sands Region since 1961

97. Differences in the Composition of Soils under Open and Canopy Conditions at Two Sites Close-In to the Great Canadian Oil Sands Operation, Fort McMurray, Alberta

98. Baseline Condition of Jack Pine Biomonitoring Plots in the Athabasca Oil Sands Area: 1976-1977

99. Synecology and Autecology of Boreal Forest Vegetation in the AOSERP Study Area

100. Baseline Inventory of Aquatic Macrophyte Species Distributions in the AOSERP Study Area

101. Woodland Caribou Population Dynamics in Northeastern Alberta

102. Wolf Population Dynamics and Prey Relationships in Northeastern Alberta

103. Analysis of the Leisure Delivery System 1972-1979, with Projections for Future Servicing Requirements

104. Review of Requirements for Air Quality Simulation Models

105. Approaches to the Design of a Biomonitoring Program Using Arthropods as Bioindicators for the AOSERP Study Area

106. Meteorological Factors Affecting Ambient SO_2 Concentrations near an Oil Sands Extraction Plant

107. Small Mammal Populations of Northeastern Alberta. Volume I: Populations in Natural Habitats

108. Small Mammal Populations of Northeastern Alberta. Volume II: Populations in Reclamation Areas

109. Symptomology and Threshold Levels of Air Pollutant Injury to Vegetation, 1979-1980

110. Physiology and Mechanisms of Airborne Pollutant Injury to Vegetation, 1979-1980

111. Ecological Benchmarking and Biomonitoring for Detection of Airborne Pollutant Effects of Vegetation and Soils

112. A Study of Human Adjustment in Fort McMurray. Volume I: Field Study and Results

113. A Laboratory Study of Long-Term Effects of Mine Depressurization Groundwater on Fish and Invertebrates

114. Aquatic Biophysical Inventory of Major Tributaries in the AOSERP Study Area. Volume I: Summary Report

115. Report on an Ecological Survey of Terrestrial Insect Communities in the AOSERP Study Area

116. An Assessment of Benthic Secondary Production in the Muskeg River of Northeastern Alberta

117. Development of a Chemically Reactive Plume Model for Application in the AOSERP Study Area

118. Alberta Oil Sands Environmental Research Program, 1975-1980. A Summary Report

119. Airshed Management System for the Alberta Oil Sands Area. Volume I: A Gaussian Frequency Distribution Model

120. Airshed Management System for the Alberta Oil Sands Area. Volume II: Meteorological Data

121. The Metabolism of Selected Organic Compounds by Microorganisms in the Athabasca River

122. Soil Inventory of the AOSERP Study Area

123. Circulation of Water and Sediment in the Athabasca Delta Area, 1981

124. Airshed Management System for the Alberta Oil Sands Area. Volume III: Validation and Sensitivity Studies

125. The 1981 Snowpack Survey in the AOSERP Study Area

126. Modelling Topographic Effects on Winds in the Alberta Oil Sands Area

127. Alberta Oil Sands Environmental Research Program Annual Report for the Fiscal Year 1981/82

128. A Comparative Study of Benthic Algal Primary Productivity in the AOSERP Study Area

129. Athabasca Oil Sands Precipitation Chemistry Studies: 1976-1979 and 1981

130. Climatological Analysis of Recent Data from the Athabasca Oil Sands Area

131. Annual Report 1982/83. Alberta Oil Sands Environmental Research Program

132. Annual Report 1983/84. Alberta Oil Sands Environmental Research Program

133. The Use of Aircraft Measurements to Determine Transport, Dispersion, and Transformation Rates of Pollutants Emitted from Oil Sands Extraction Plants in Alberta